Improving mechanical properties of a magnesium alloy by severe plastic deformation

Michal Gzyl

This thesis is submitted to the Department of

Design, Manufacture and Engineering Management

University of Strathclyde

For the degree of Doctor of Philosophy

Glasgow, 2014

Table of contents

4

Acknowledgements

I would like to express my sincere gratitude to my supervisor, Dr Andrzej Rosochowski, for his guidance and fruitful discussions, which led to the successful completion of this thesis. I am also very grateful to Dr Rosochowski and to my second supervisor, Dr Paul Wood, for securing funds necessary for running experiments and presenting obtained results at international conferences. Financial support from Carpenter Technology Corporation is kindly acknowledged.

Additionally, I would like to acknowledge the contributions of my colleagues from our research group and from other Universities. I am very grateful to:

- Dr Raphael Pesci from ENSAM-Arts et Métiers ParisTech, Metz, France for conducting texture measurements and running *in situ* tensile tests in SEM chamber during my stay in Metz in June 2012;
- Mr Jawad Qarni from Advanced Forming Research Centre, University of Strathclyde for developing controlling system for the screw press and his support with technical issues with the hydraulic press;
- Dr Evgenia Yakushina from Advanced Forming Research Centre, University of Strathclyde for giving me training on the polishing machine and taking some of the SEM pictures presented in Section 5.4.1;
- Dr Lech Olejnik from Warsaw University of Technology, Poland for preparation of the conversion coating for magnesium alloy and discussions about the role of friction in metal forming;
- Mr James Gillespie from Advanced Materials Research Laboratory, University of Strathclyde for his help with carrying out mechanical tests;
- all of the people who contributed to development of the I-ECAP experimental rig, i.a. Dr Malgorzata Rosochowska, Dr Lech Olejnik, Mr Jawad Qarni, Mr Mohammad Salamati.

Finally, I would like to give my sincere thanks to my wife, Ewelina, for her love, patience, and understanding. I would also like to thank my parents and all my family for their support.

Abstract

Magnesium alloys are very promising materials for automotive and aerospace applications due to their low density. The market of medical implants (e.g. temporary orthopaedic and cardiovascular implants) is another field of possible applications of magnesium alloys since they can completely dissolve within human body without causing any major health issues. Unfortunately, magnesium alloys have been well-known from their low formability at room temperature and poor corrosion resistance. The aim of the current work was to improve mechanical properties of a magnesium alloy by incremental equal channel angular pressing (I-ECAP). The goal of the process is to refine grain structure of a continuous bulk metallic billet without changing its dimensions. In the current work, the most popular wrought magnesium alloy AZ31B was subjected to I-ECAP for the first time to confirm potential of the method for industrial production of innovative lightweight materials. The process window was determined on the basis of I-ECAP experiments conducted with various process parameters (temperature, processing route, initial grain size of the alloy). Additionally, various microstructural characterization methods, including *ex situ* and *in situ* analyses, were incorporated in this work to show a relation between the grain size and the deformation mechanisms occurring in the alloy. It was found that mechanical properties of AZ31B can be tailored to a specific application by using different process parameters. It was shown that yield strength can be increased from 165 MPa to 290 MPa when temperature of I-ECAP is reduced to 150 °C. Moreover, room temperature ductility of the produced material can exceed 40% when a combination of I-ECAP and subsequent heat treatment is applied. The results of the work confirmed that I-ECAP could be considered as the useful method for producing advanced lightweight metallic materials with a potential for industrial applications.

Chapter 1
Introduction

1.1. Research motivation

A high demand for lightweight structural elements in various industries has drawn interest of many researchers to magnesium, which is one of the lightest metals with density 1.74 g/cm^3. Although magnesium was discovered at the beginning of 19th century, it was not used for structural components due to its high chemical reactivity leading to low corrosion resistance. However, high specific strength of magnesium, defined as a ratio of yield stress to density, was crucial at the beginning of 20th century when materials for aviation applications were sought. For example, magnesium alloys were used extensively in military aircrafts during the Second World War. However, the interest in magnesium alloys subsided after the war due to economic and technological reasons and emphasis was put on development of aluminium alloys (Friedrich and Mordike, 2006).

Nowadays, the need for reducing fuel consumption of cars, due to environmental and economic reasons, encouraged the automotive sector to seek new lightweight materials. Due to the low formability of magnesium alloys at room temperature the main focus was put on cast parts, e.g. gear box housing and intake manifold. However, interior parts, e.g. steering wheel, seat elements, inner door panel, were also manufactured from wrought alloys (Schumann and Friedrich, 2006). Additionally, some on-board devices in modern aircrafts are also made of magnesium alloys. However, low corrosion resistance significantly reduces a potential of magnesium parts to be used for external components in cars and aircrafts (Froes et al., 2006).

The market of medical implants is another field of possible applications of magnesium alloys since magnesium completely dissolves within human body without causing any major health issues and its excess can be removed with urine. Therefore, it is a promising material for temporary orthopaedic (Steiger et al., 2006) and cardiovascular implants (Zartner et al., 2006). Such devices can support broken bone until it rebuilds itself and dissolve when the process of tissue healing is finished. This eliminates the requirement for removing remaining implants by a second surgical procedure. Cardiovascular stents are not removed from a blood vessel after implantation due to a high risk of medical complications. However, after a few years they can cause health problems, especially for young patients whose blood vessels are expanding as they grow. Therefore, a controlled dissolution of a cardiovascular stent after healing period is highly demanded. Unfortunately, an excessive corrosion rate of the current magnesium alloys within human body limits their use in the medical sector and a solution to this problem is extensively sought by researchers. Recent studies have shown that grain refinement resulted in improvement of corrosion resistance of some magnesium alloys (Jiang et al., 2009). Combination of extrusion and ECAP led to break-up and redistribution of Mg–Zn and Zn–Zr intermetallic precipitates in ZK60 alloy, which improved corrosion resistance, measured by electrochemical experiments and immersion tests in NaCl (Orlov et al., 2011). It opens a very promising future prospect for biodegradable metallic implants.

Mechanical properties of metallic materials can be tailored by modifying their grain structure; particularly, strength can be increased significantly by reducing grain size. Such modification can be introduced by imposing a very large plastic deformation to

a material. As a result, properties obtained after processing are usually remarkably improved, comparing to the initial state. Thus, heavy components can be replaced with parts made of low-density materials without decreasing their load capacities. Accordingly, grain size strengthening can be classified as another technique for reducing weight of structural components.

A combination of two presented approaches, using low-density materials and modification of grain structure by applying large strain, could be an effective method of producing lightweight metals and alloys with improved mechanical properties. It has been already shown that improved ductility and/or strength at ambient temperature can be achieved in magnesium alloys through severe plastic deformation (SPD) without changing billet dimensions (Mukai et al., 2001; Ding et al., 2008). Additionally, formability at elevated temperatures can be also significantly enhanced due to superplastic properties of fine-grained materials (Figueiredo and Langdon, 2009a). However, the most of SPD methods have not left research laboratories since they are not able to process continuous billets.

The approach based on simple shear deformation applied in incremental steps proposed by Rosochowski and Olejnik (2007), called incremental equal channel angular pressing (I-ECAP), makes production of fine- and ultrafine-grained metals possible on industrial scale. Nevertheless, I-ECAP has been never applied to magnesium alloys and its effects on microstructure and mechanical properties are unknown. On the other hand, literature reports on conventional equal channel angular pressing (ECAP) are encouraging as they show that it could be an effective method

of improving mechanical properties of magnesium alloys (Mukai et al., 2001; Ding et al., 2008; Figueiredo and Langdon, 2009a).

1.2. Aims and goals of the research

As it was explained in the previous section, magnesium alloys are very promising materials for automotive, aerospace and medical sectors due to their low density and high biocompatibility with human organism. Additionally, methods of SPD can improve their mechanical properties and corrosion resistance, which can expand the field of potential applications. The current work was focused on overcoming the problem of low productivity of conventional SPD processes, which restricts opportunities for a large-scale production of magnesium alloys with improved properties. Therefore, the aim of the thesis was to show that I-ECAP can be successfully used to improve mechanical properties of AZ31B magnesium alloy. Additionally, the work was aimed at investigating a relationship between the structure and the mechanical properties of the alloy with various grain sizes. The following objectives were defined to achieve the stated aims:

1. To determine window of allowable processing parameters for I-ECAP of AZ31B magnesium alloy.
2. To investigate effects of process variables on material properties.
3. To study *ex situ* microstructural features of coarse- and fine-grained magnesium alloy subjected to tension and compression.
4. To obtain fine-grained metal sheets by combination of I-ECAP and upsetting.

5. To investigate fracture mechanism *in situ* in coarse- and fine-grained magnesium alloy subjected to tension.

1.3. Organisation of the thesis

The thesis is composed of the following eight chapters:

Chapter 1 presents the motivation, aims, objectives and organisation of the thesis.

The current state-of-the-art in the field of ultra-fine grained metals and alloys is presented in **Chapter 2**. The chapter gives a brief explanation of polycrystalline nature of metals, a role of grain boundaries and some advantages arising from grain refinement. The concepts of equal channel angular pressing (ECAP) and incremental equal channel angular pressing (I-ECAP) as methods for producing ultrafine-grained materials are introduced. Additionally, the most important aspects of ECAP of magnesium alloys, including grain refinement mechanism, process variables and the effects of processing parameters on material properties, are described.

Chapter 3 describes the equipment used to conduct experiments and its general principles of operation. The microstructural and mechanical characteristics of the used materials are also shown in this chapter.

The formability of magnesium alloy during I-ECAP is studied in **Chapter 4**. A diagram showing the relation between minimum allowable processing temperature and grain size is plotted in this chapter using results of the conducted I-ECAP experiments and the selected literature data. An effect of processing route on billet

shape and fracture mechanism is studied through experimental work and numerical analysis.

Chapter 5 presents a relation between process variables and obtained microstructures and mechanical properties. Effects of temperature and processing route of I-ECAP on mechanical properties, grain size and texture of AZ31B magnesium alloy are investigated. Microstructure characterisation of tensioned and compressed coarse- and fine-grained samples is performed in order to determine a dominating deformation mechanism. The tension-compression yield stress asymmetry of coarse- and fine-grained materials is also studied. Additionally, the effect of heat treatment after I-ECAP on grain size and mechanical properties is investigated. Finally, a numerical model is developed to verify if microstructure evolution during subsequent passes of ECAP/I-ECAP can be predicted using equations usually used to simulate dynamic recrystallisation.

A method of producing fine-grained magnesium alloy sheets by I-ECAP followed by upsetting was presented in **Chapter 6**. Microstructure evolution in coarse- and fine-grained samples subjected to tension was observed *in situ* in order to investigate a grain size effect on the fracture mechanism. Additionally, FE simulations of microstructure evolution were performed to support interpretation of experimental results.

The conclusions from the results and discussions presented in Chapters 4-6 were gathered in **Chapter 7**. The chapter also includes the contribution of the thesis to knowledge enhancement, a list of accompanying publications and recommendations for the future work.

Chapter 2

Grain refinement of magnesium alloys by severe plastic deformation (SPD) – state of the art.

A literature review in the field of ultra-fine grained (UFG) metals and alloys is presented in this chapter. In Section *2.1. Motivations for grain refinement,* a brief explanation of the polycrystalline nature of metals, the role of grain boundaries and some advantages related to grain refinement are included. In Section *2.2. Producing nanostructured materials,* various approaches for producing nanomaterials are described. This section also introduces the definitions of batch and continuous severe plastic deformation processes (SPD). The concepts of equal channel angular pressing (ECAP) and incremental equal channel angular pressing (I-ECAP) are introduced in Section *2.3 Principles of equal channel angular pressing (ECAP) and its incremental variant (I-ECAP)* as the experimental part of the present work was done using the latter method. Section *2.4. Formability of magnesium alloys* demonstrates how microstructural features of magnesium alloys influence their formability; the origin of low ductility at room temperature is also explained. Finally, Section *2.5. Equal channel angular pressing of magnesium alloys* gathers the most important aspects of ECAP of magnesium alloys, including grain refinement mechanism, process variables and the effects of processing parameters on material properties.

2.1. Motivations for grain refinement

2.1.1. Polycrystalline structure of metals

Metals and their alloys are polycrystalline materials; it means that they are made up of grains with different crystallographic orientations (Fig. 2.1). Crystallographic misalignment and different chemical composition (in case of alloys) between neighbouring regions give rise to formation of grain boundaries. Therefore, grain boundary could be considered as a defect in crystalline structure. Depending on the misorientation angle between grains, the high angle grain boundaries (HAGB) and low angle grain boundaries (LAGB) can be distinguished. Grain boundaries with misorientation angle greater than 15° are usually treated as HAGB (Mishin et al., 2003).
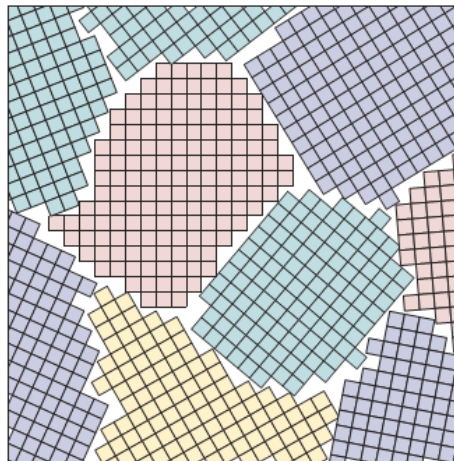
Fig. 2.1. Schematic illustration of polycrystalline structure of metals. Image was taken from work by Dobrzanski (2002).

Grain size is a significant parameter which determines macro-scale mechanical properties of metals. A relation between material yield strength (σ_y) and mean grain size d is described by Hall-Petch equation (Hall, 1951; Petch, 1953):

$$\sigma_y = \sigma_0 + k_y d^{-1/2} \tag{2.1}$$

where: σ_0 – friction stress opposing dislocation motion, k_y – constant of yielding. According to equation (2.1), strength is increasing along with grain refinement. This relation was confirmed experimentally for mild steel (Hall, 1951), copper (Sanders et al., 1997), aluminium (Sato et al., 2003), and titanium (Wang et al., 1993). However, experimental results obtained for copper with grain size smaller than 25 nm showed that yield stress did not follow equation (2.1) and plateaued after reaching a critical value (Sanders et al., 1997; Masumura et al., 1998). Although some exceptions from Hall-Petch equation were reported, it can be concluded that most of metals follow this relation. Especially transition from coarse-grained (CG) to fine- and ultrafine-grained (UFG) structure usually results in a significant strength increase.

2.1.2. *Ultra-fined grained (UFG) metals*

Ultra-fined grained (UFG) metals are usually defined as polycrystals with the mean grain size smaller than 1 μm. The microstructure of such metal should be also homogenous and dominated by equiaxed grains. Moreover, majority of grain boundaries should be HAGB to ensure unique properties (Valiev et al., 2000). Nevertheless, a definition of UFG material can also take into account microstructural changes during deformation. Cheng et al. (2003) classified metals into nanocrystalline, ultrafine-grained, and conventional ones on the basis of deformation mechanism map for face centre cubic (fcc) metals, as shown in Fig. 2.2. Thus, ultrafine grain regime can be described as dominated by dislocation-based plasticity (>30 nm) with predominance of unit dislocations (< 1 μm).
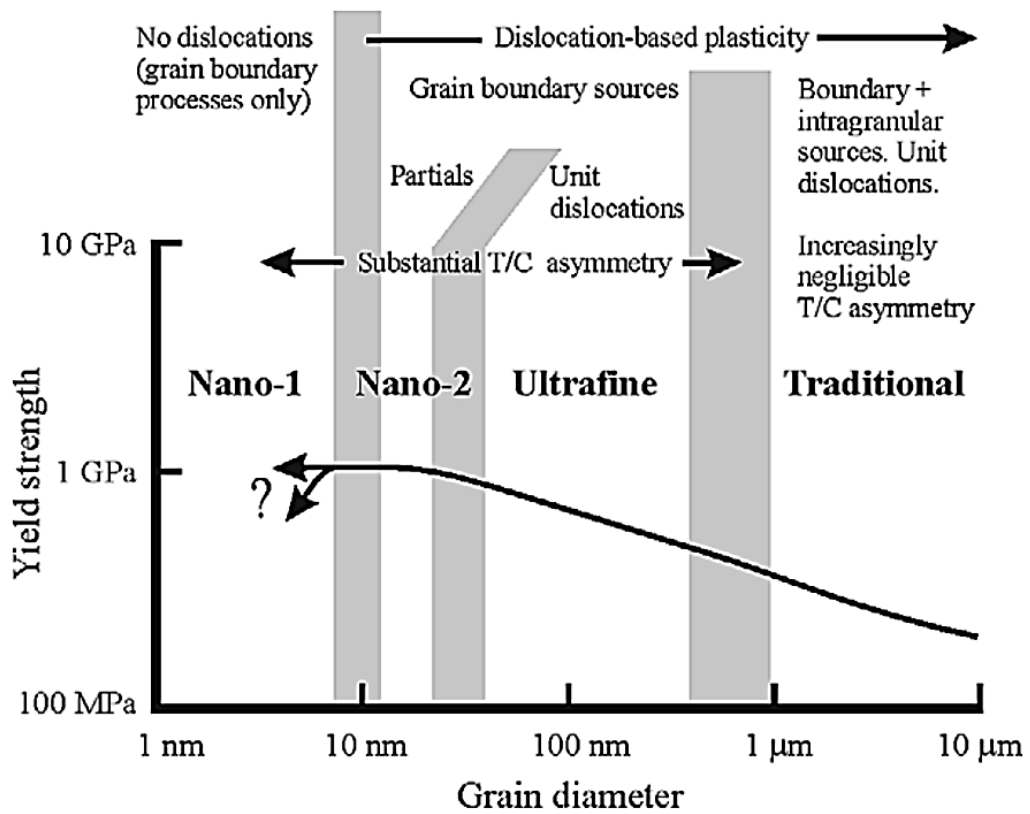
Fig. 2.2. Deformation mechanism map for fcc metals. Image was taken from the work by Cheng et al. (2003).

2.1.3. Advantages of UFG materials and their applications

According to Hall-Petch equation (2.1), reducing grain size below 1 μm enables improvement of metals' strength. Indeed, aluminium (Horita et al. 2001), titanium (Stolyarov et al., 2001) and copper (Valiev et al., 2002) exhibited significant yield stress increase at room temperature due to a grain refinement. Moreover, superplasticity in nanostructured metals and alloys can be achieved at temperatures and/or strain rates lower than in conventional CG materials (Langdon, 2013).

Dental implants made of pure titanium (Fig. 2.3) with the grain size of 150 nm were shown to have higher strength than widely used coarse-grained Ti-6Al-4V-ELI

(Valiev et al., 2008). Yield stress of Ti Grade 4 was improved in this study from 530 MPa to 1200 MPa. It shows that modification of grain structure can lead to development of metals and alloys with extraordinary mechanical properties without changing their chemical composition. Therefore, an addition of alloying elements, e.g. aluminium, can be avoided, which reduces a risk of harmful ions release. Additionally, it has been also shown that UFG titanium exhibits faster integration with a surrounding tissue. Experiments revealed that attachment and growth rate of pre-osteoblast cells are improved on the surface of nanostructured titanium substrates (Faghihi et al., 2007).

Fig. 2.3. Dental implants made of nanostructured Ti. Image was taken from the work by Valiev et al. (2008).

Aerospace industry takes advantage of UFG Ti-6Al-4V titanium alloys in superplastic forming (SPF) of aircraft panels. SPF enables manufacturing complex shape parts in only one operation. However, the process requires high temperatures and low strain rates, e.g. forming temperature could be as high as 900 °C and it could take 2 hours to obtain final shape of a part. By using UFG Ti-6Al-4V alloy, process

temperature was lowered to 775 °C and forming time was also reduced significantly, which led to remarkable improvement of process efficiency. Although additional manufacturing operations are required to obtain UFG material, the total cost of a final part produced by SPF could be reduced (Comley, 2004).

Besides its influence on mechanical properties, microstructure of material also becomes relevant when the size of a produced component is comparable to its grain size. Therefore, fine- and ultrafine-grained materials are believed to have a large potential for micro-manufacturing. Rosochowski et al. (2007) produced miniature cups by backward extrusion from CG and UFG aluminium 1070. The force needed to process UFG aluminium at room temperature was obviously higher due to the strengthening effect of grain boundaries. However, flow distribution was more uniform and SEM images clearly showed that surface quality, especially on the cup's edge, was much better comparing to the cup obtained from CG aluminium. Additionally, hardness was higher in the case of UFG cup and its distribution was more uniform.

The grain size effect on surface quality of compressed aluminium samples was also reported by Rosochowski et al. (2006). In this study, Rastegaev-type specimens were subjected to uniaxial compression at room temperature. The top and bottom surfaces were not in a direct contact with tools due to a separating layer of lubricant entrapped in the specimen recesses. After compression, surface roughness was measured and 3D pictures of texture evidently showed that much smoother surface was obtained in the case of UFG aluminium (Fig. 2.4). A reduction of surface roughness was also

observed in micro-milling (Popov et al., 2006) and diamond turning of optical surfaces (Osmer et al., 2007).
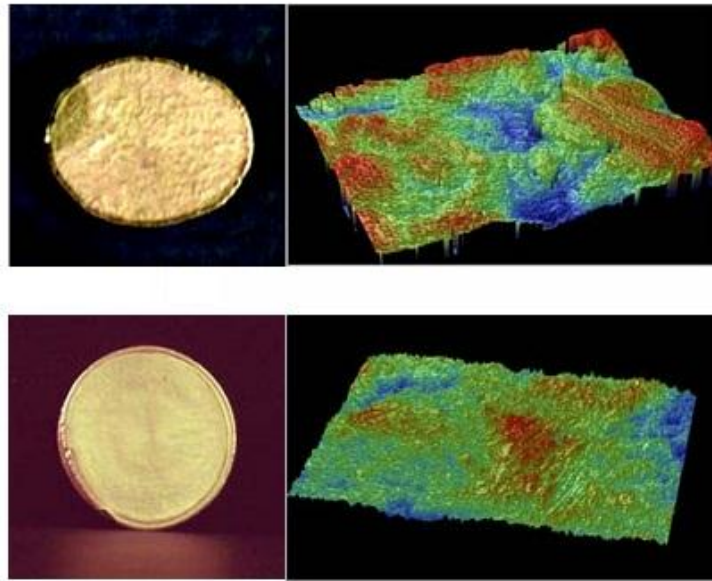
Fig. 2.4. Roughness of specimens faces for CG aluminium (upper) and UFG aluminium (lower). Image was taken from the work by Rosochowski et al. (2006).

UFG aluminium was also shown to be a suitable material for micro heat exchangers, which are relevant components of micro-electromechanical systems (MEMS). Efficiency of such micro heat exchangers can be improved by increasing the number of channels produced by microembossing. Qiao et al. (2010) compared behaviour of CG and UFG aluminium 1050 subjected to microembossing. It was concluded that replacing conventional aluminium with UFG metal improved quality of a final product.

2.2. Producing nanostructured materials

2.2.1. *Bottom-up and top-down approaches*

Nanostructured materials can be fabricated using two different approaches, which are called *bottom-up* and *top-down* techniques. In the former one, a bulk solid is formed using consolidation processes, starting from the atomic scale, through nanoscale clusters, to a final part. The top-down approach starts from a solid piece of material (usually metal or alloy) and refines its structure by using methods of structural decomposition (Koch, 2009).

Chemical synthesis of nanoscale materials is one of the most popular bottom-up techniques. The idea is based on the chemical reactions between particular atoms and molecules which lead to the formation of nanocrystalline particulates. In order to produce bulk nanostructured material, the obtained particulates require further consolidation, e.g. by compaction and sintering. This method was successfully applied by McCandlish et al. (1992) to produce ultrafine-grained WC-Co with superior mechanical properties, comparing to the CG alternative. This approach is classified as a two-step method since the stages of producing nanoparticles and their consolidation are required.

Another bottom-up technique used to produce nanocrystalline layer on a surface of metal, alloy, composite or ceramic is electrodeposition. Thick electrodeposit could be considered as a bulk nanomaterial. The main stages of the electrodeposition process are: (1) the nucleation of crystallites on a surface of substrate and (2) their subsequent growth accompanied by nucleation of new crystallites. Grain growth should be suppressed as much as possible in order to obtain a nanocrystalline grain

size. A quality of the final product depends on bath composition, bath pH, temperature, overpotential, bath additives, and direct current vs. pulse electrodeposition. Electrodeposition has been studied since 1980s and it is now used in commercial production of nanocrystalline materials (Erb, 1995).

The most popular top-down method is severe plastic deformation (SPD), which is based on the idea of microstructure refinement by applying a very large strain. The main assumption of this technique is that shape of a processed billet remains unchanged. Therefore, only the grain structure of a material is affected and a SPD process could be repeated in order to facilitate further microstructural changes. Rosochowski and Olejnik (2012) introduced the classification which distinguishes *batch* and *continuous* SPD processes. Batch processes use billets with all dimensions of the same order while continuous ones enable processing very long billets, e.g. long bars, sheets or plates.

2.2.2. Batch SPD processes

The earliest batch processes are: high pressure torsion (HPT), equal channel angular pressing (ECAP) and cyclic extrusion compression (CEC). Recently, new processes have also been developed: multiaxial forging (Ghosh, 2000), repetitive corrugation and straightening (Huang et al., 2001) and twist extrusion (Beygelzimer et al., 2002). However, they are still considered as batch processes. The overview of the most popular batch SPD processes is displayed in Fig. 2.5.
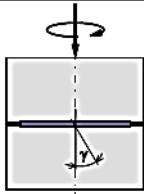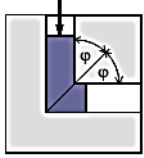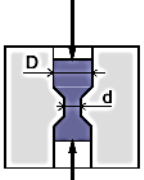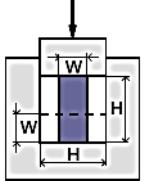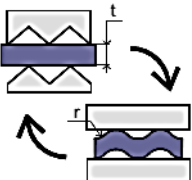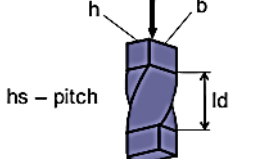
Process name and origin	Schematic representation	Equivalent plastic strain
High pressure torsion (HPT) Valiev et al. (1991)		$\varepsilon = \dfrac{tg\gamma}{\sqrt{3}}$
Equal channel angular pressing (ECAP) Segal et al. (1981)		$\varepsilon = n\dfrac{2}{\sqrt{3}}\cot\varphi$
Cyclic extrusion compression (CEC) Korbel et al. (1981)		$\varepsilon = n4\ln\left(\dfrac{D}{d}\right)$
Multiaxial forging (MF) Ghosh (2000)		$\varepsilon = n\dfrac{2}{\sqrt{3}}\ln\left(\dfrac{H}{W}\right)$
Repetitive corrugation and straightening (RCS) Huang et al. (2001)		$\varepsilon = n\dfrac{4}{\sqrt{3}}\ln\left(\dfrac{r+t}{r+0.5t}\right)$
Twist extrusion (TE) Beygelzimer et al. (2002)		$\varepsilon = 3.46\left(\dfrac{hs}{0.5\sqrt{b^2+h^2}}\right)^{-0.47}\left(\dfrac{ld}{hs}\right)^{0.55}\left(\dfrac{h}{b}\right)^{-0.56}$

Fig. 2.5. Batch SPD processes. Image was taken from the work by Rosochowski and Olejnik (2012).

In HPT, a very thin disk is compressed in a closed die by applying a very high pressure (about 6 GPa). A compressing and rotating punch provides torque by the contact friction at a punch/disk interface (Valiev et al., 1991). The method was

investigated for the first time by Bridgman (1935), who used an extremely thin disc (<0.1 mm), which was compressed freely.

Equal channel angular pressing (ECAP), invented by Segal in the 1970s (Segal, 1981), is currently one of the most popular SPD techniques. In this process, a billet is pressed through two channels of the same cross section intersected at 90°. In some cases the channel angle could be increased in order to enable processing of brittle metals, however, it decreases the level of strain. As the billet dimensions remain unchanged, the process can be repeated in order to introduce ultra-large deformation. Friction in ECAP rises significantly with billet length; therefore, only relatively short billets can be processed using this technique. ECAP was described in detail in Section 2.3.

The concept of cyclic extrusion compression (CEC) involves the cyclic flow of metal between the alternating extrusion and compression chambers (Korbel et al., 1981). In this process, the forming force is strictly dependant on friction conditions (Rosochowski, 2005). Therefore, providing very good lubrication is crucial, especially for difficult-to-work alloys.

In multiaxial forging (MF), a large strain is introduced to a billet by compression. Then, the billet is rotated, which enables repeating this operation along another axis. As a consequence, upsetting along two or three axes of the billet can be realised. A strain distribution after the first operation is non-uniform but homogenous microstructure can be obtained after several compressions along various directions (Ghosh, 2000). Repetitive corrugation and straightening (RCS) includes two operations: (1) bending of a straight billet with corrugated tools and (2) restoring the

straight shape of the billet with flat tools (Huang et al., 2001). Similarly to MF, the repetition of the process is required to obtain a large strain and homogenous microstructure. Twist extrusion (TE) is based on pressing a billet through a twisted die with the same inlet and outlet cross-sections (Beygelzimer et al., 2002). Therefore, the processed billet maintains its original shape and it can be pressed repeatedly to accumulate a large strain. Strain distribution is not uniform in the transverse direction, with the minimum strain close to the billet centre, and it cannot be homogenised by subsequent pressing.

2.2.3. *Continuous SPD processes*

A high demand for industrial application of SPD techniques encouraged researchers to focus their work on developing continuous processes, e.g. accumulative roll bonding (ARB), continuous repetitive corrugation and straightening (CRCS), ECAP-conform, continuous SPD, and incremental equal channel angular pressing (I-ECAP). The overview of the most popular continuous SPD processes is shown in Fig. 2.6.

One of the first attempts to refine microstructure of metallic sheet by plastic deformation was made by Saito et al. (1998), who used the process called accumulative roll-bonding (ARB). The sheet is cut into two pieces, cleaned, stacked and hot rolled to bond two pieces together and to reduce their thickness by 50%. This operation can be repeated until desirable strain level is reached. However, the process is limited by the manageable sheet length; therefore, it is not a truly continuous SPD method.
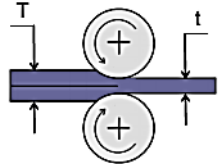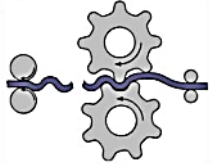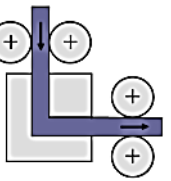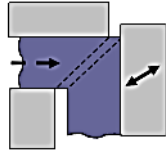
Accumulative roll bonding (ARB) Saito et al. (1998)		$\varepsilon = n \dfrac{2}{\sqrt{3}} \ln\left(\dfrac{T}{t}\right)$
Continuous repetitive corrugation and straightening (CRCS) Huang et al. (2004)		$\varepsilon = n \dfrac{4}{\sqrt{3}} \ln\left(\dfrac{r+t}{r+0.5t}\right)$
Continuous SPD (CSPD) Srinivasan et al. (2006)		$\varepsilon = n \dfrac{2}{\sqrt{3}} \cot\varphi$
ECAP-Conform (ECAP-C) Raab et al. (2004)		$\varepsilon = n \dfrac{2}{\sqrt{3}} \cot\varphi$
Incremental ECAP (I-ECAP) Rosochowski and Olejnik (2007)		$\varepsilon = n \dfrac{2}{\sqrt{3}} \cot\varphi$

Fig. 2.6. Continuous SPD processes. Image was taken from the work by Rosochowski and Olejnik (2012).

The continuous version of repetitive corrugation and straightening was invented by Huang et al. (2004). Continuous RCS (CRCS) uses a rotating corrugating tool to plastically deform a billet. The role of straightening platens, which were used in batch RCS, was taken over by rolls, which enables processing of long billets.

Continuous variants of ECAP form a large group of SPD processes. In CSPD, a billet is fed to deformation zone by set of rolls (Srinivasan et al., 2006). The friction

between the rolls and the billet should be high enough to oppose the friction on the billet-die interface and enable plastic deformation. A similar approach has been used in the continuous shear deformation process (Utsunomiya et al., 2001) and continuous confined strip shearing (Lee et al., 2001). The combination of ECAP and conform, which is a continuous extrusion process, was proposed by Raab et al. (2004). Billet feeding in this process is realised only by friction which seems to be not enough for the die with 90° angle. Therefore, the angle is usually increased in order to reduce deformation force but it also results in lowering the strain level in one pass. Moreover, high friction, which is crucial for material feeding, seems to be also a limitation of the process since it allows processing only wires and rods, and makes nanostructuring of sheets and plates virtually impossible (Segal, 2010). Incremental ECAP was invented by Rosochowski and Olejnik (2007); this process will be described in detail in Section 2.3.7.

2.3. Principles of equal channel angular pressing (ECAP) and its incremental variant (I-ECAP)

2.3.1. *Deformation by simple shear*

Severe plastic deformation (SPD) is a general term which covers all processes which involve large strain and ensure that all billet dimensions remain constant after processing. Various operations can be realised to introduce strain which implies that different modes of deformation could be active, e.g. pure and simple shear (Fig. 2.7). Segal (2002) has compared the effects of pure shear and simple shear on microstructure evolution during SPD. Pure shear was realised in his study in a central

area of samples rolled with different reductions while simple shear was developed by ECAP (originally called by him ECAE – equal channel angular extrusion).
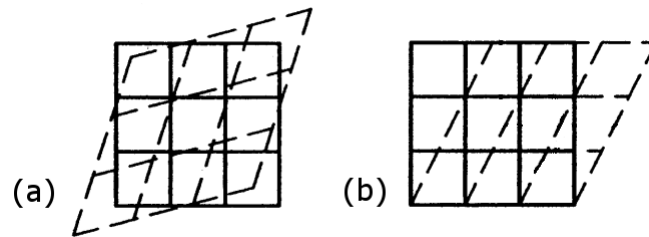
Fig. 2.7. Schematic illustration of deformation by pure shear (a) and simple shear (b). Image was taken from the work by Segal (2002)

The effect of deformation mode on texture development was studied for aluminium alloy Al0.5Cu. Texture strength was estimated by orientation distribution index (ODI), which is the root-mean-square deviation from the random orientation. In the case of rolling, the strong texture (ODI of 37) was reported for reductions within range 90-95%. For reductions greater than 95%, decrease of ODI to 10 was observed. However, it was still considered as the strong texture while ECAPed samples exhibited a much smaller ODI, measured as 7.0.

Intensity of recrystallization during deformation by pure shear and simple shear was studied on aluminium alloy Al5N2. It was shown that fully recrystallized structure could be obtained after four passes of ECAP (equivalent to total strain of 4.6). Then, rolling with reductions 68, 90, 97, and 99% was conducted which corresponded to 1, 2, 3, and 4 passes of ECAP, respectively. It was shown that bands of elongated grains were separated by segments of non-recrystallized grains even after rolling with 99%

reduction. The recrystallized part of the investigated microstructure was only 50% of the total area, comparing to 100% after four passes of ECAP.

The final conclusion from the study of Segal (2002) was drawn that simple shear can be treated as the optimal deformation mode for development of fine and equiaxed grains with high angle boundaries. Although different processing methods could be considered for simple shear deformation, ECAP is believed to be the simplest realisation which ensures relatively uniform strain distribution.

2.3.2. General concept of ECAP

A schematic illustration of ECAP is shown in Fig. 2.8. A die is made of two channels, with the same cross sections, intersecting at an angle Φ varying from 90° to 135°. A billet is machined to fit the channels and then well lubricated to reduce the pressing force. Next, the billet is pressed through the channels by a punch/plunger. Deformation by simple shear is achieved in the thin layer at the channels' intersection. It is apparent that the billet dimensions remain unchanged, which enables repetitive pressing of the same billet.
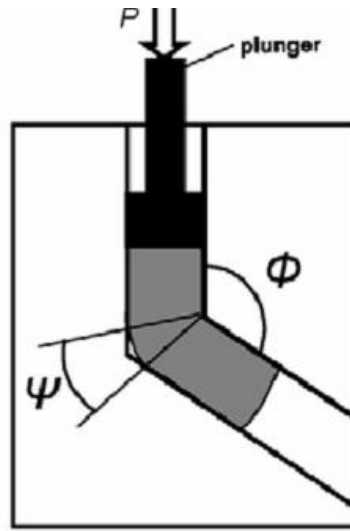
Fig. 2.8. Schematic illustration of ECAP. Image was taken from the work by Jiang and Ma (2011).

The total strain introduced in the material depends on the channel intersection angle, Φ, and the angle subtended by the arc of curvature at the point of intersection, Ψ. Iwahashi et al. (1996) performed an analysis of the single element distortion after pressing through dies with different geometry to calculate strain imposed by ECAP. They have assumed that friction effects could be neglected in this analysis; therefore, their equation gives a theoretical estimation of strain. If a multipass process is considered, equivalent strain derived for one pass should be multiplied by number of passes, n, to find the total strain ε_n:

$$\varepsilon_n = n \left[\frac{2\cot\left(\dfrac{\Phi}{2} + \dfrac{\Psi}{2}\right) + \Psi\csc\left(\dfrac{\Phi}{2} + \dfrac{\Psi}{2}\right)}{\sqrt{3}} \right].$$
(2.2)

2.3.3. Route effects in ECAP

Since the pressing through the die can be repeated, different processing routes, in terms of billet rotation between subsequent passes, can be used. Langdon (2007) distinguished four main routes: A, B_A, B_C, and C (Fig. 2.9). A billet is not rotated about its axis when route A is used. Route B_A denotes rotation through 90° about the longitudinal axis of the billet in alternate directions between each pass. Rotation through 90° is also used in case of route B_C but the billet is rotated in the same sense between passes. Finally, the billet is rotated by 180° after each pass when route C is used.
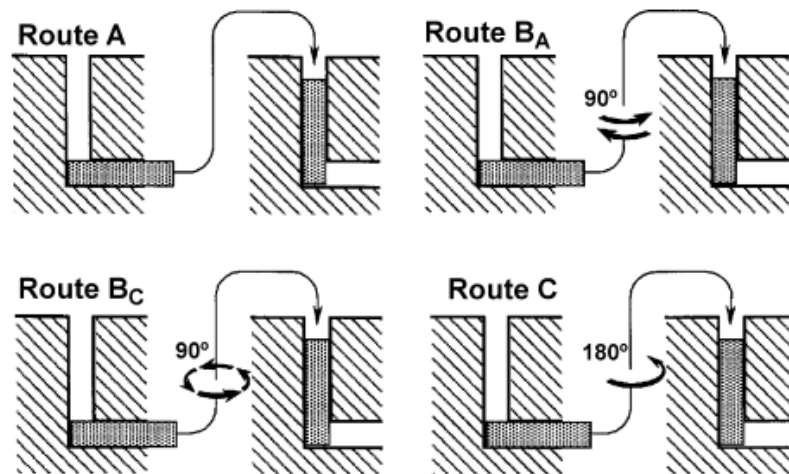
Fig. 2.9. The four processing routes in ECAP. Image was taken from the work by Langdon (2007).

Even one pass of ECAP can introduce significant microstructural changes to a material. Iwahashi et al. (1998) revealed a presence of bands of elongated grains and subgrains in ECAPed samples of pure aluminium, as shown in Fig. 2.10. Moreover, the bands lied parallel to the shearing direction, which clearly showed a relation between the deformation mode in the macro scale and the corresponding

microstructural effects. The structure formed during first pass is changed during subsequent passes and this modification is dependent on billet rotations. Therefore, the distinction between various processing routes is important as they introduce different shearing patterns to the billet.
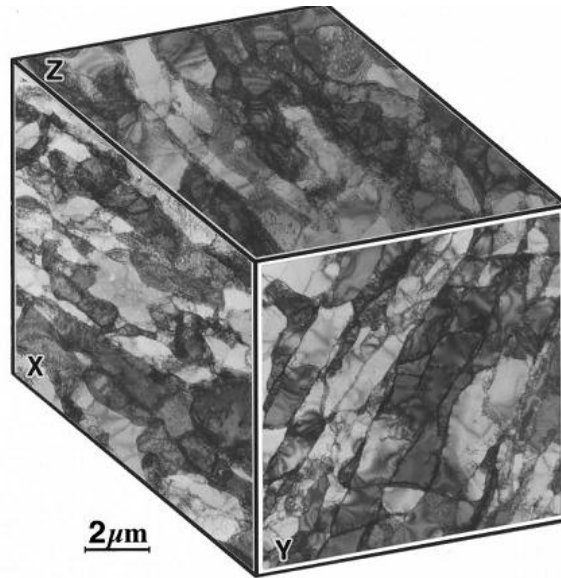
Fig. 2.10. Microstructure in pure aluminium after one pass of ECAP. Image was taken from the work by Iwahashi et al. (1998).

Segal (1995) investigated the effect of processing route on microstructure evolution by pressing pure Ni using routes A and C. The occurrence of filamentary structure after four passes via route A was revealed, which was explained by a gradual material element distortion with consecutive passes. In the same study, the periodic change of microstructure was reported for route C, where equiaxed grains were observed after even-numbered passes and elongated grains after odd-numbered passes. It was concluded that billet rotation by 180° resulted in distortion (shearing) of the material element and its subsequent restoration in the following pass.

Therefore, even number of passes is required to obtain array of equiaxed grains when route C is used.

Iwahashi et al. (1998) compared effects of processing routes A, B_C, and C on microstructure evolution in pure Al during consecutive passes of ECAP. The results obtained for routes A and C were in agreement with the work by Segal (1995); additionally, route B_C was shown to give more uniform structure than route C. It was revealed that processing with 90° rotation led to an earlier disappearance of subgrain bands (even after third pass) and formation of high angle grain boundaries (HAGB). This observation was explained by a different shearing patterns arising from the various processing routes. It was noticed that the subgrain bands were developed in route B_C along two separate and intersecting planes which led to a reasonably rapid formation of array of equiaxed grains with HAGB. The development of ultra-fine and equiaxed grains by route B_C was also achieved in pure titanium by Stolyarov et al. (2001).

2.3.4. *Model of grain refinement*

Langdon (2007) proposed a theoretical model of grain refinement in aluminium subjected to various routes of ECAP (Fig. 2.11). The formation of subgrain bands lying along shear plane was predicted after first pass. As the number of passes increases, different microstructures are developed in samples processed by routes A, B_C, and C. Shear patterns introduced in the second and fourth pass of ECAP intersect with subgrain bands arising from the previous pass in case of routes A and B_C. Bands in the sample processed by route C are aligned with shear plane since only even-

numbered passes are taken into account, accordingly to the results obtained by Segal (1995). In this case, four passes of ECAP lead only to increase of dislocation density in vicinities of grain boundaries.
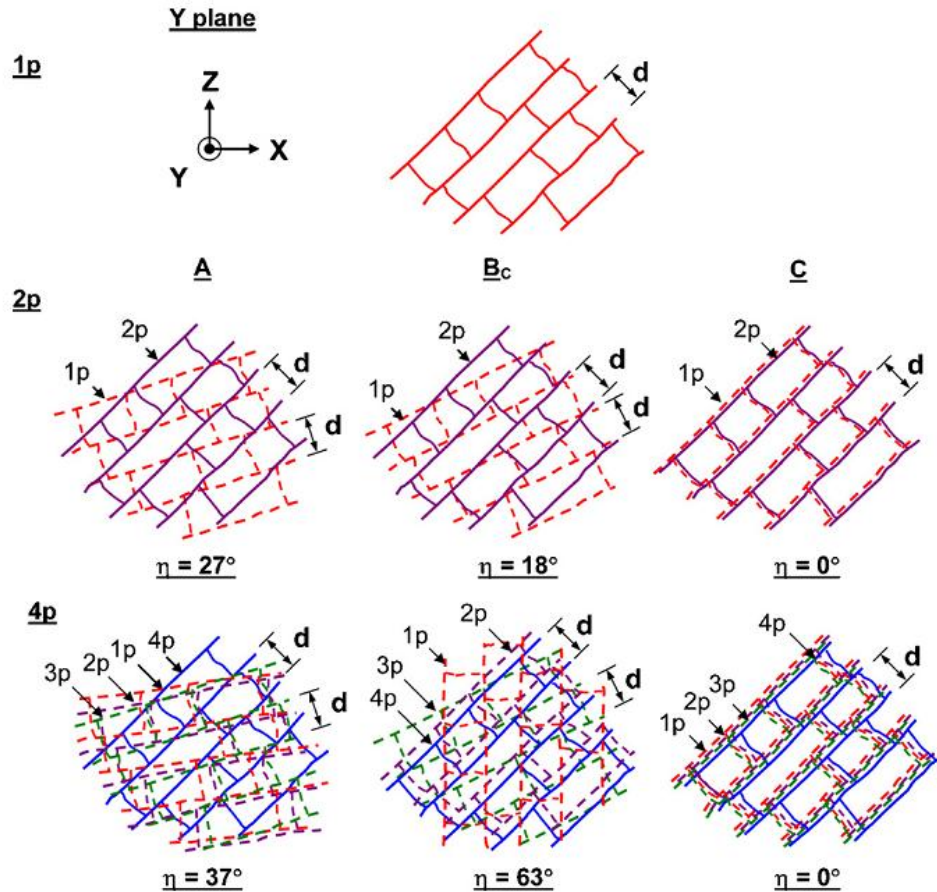
Fig. 2.11. A model for grain refinement in ECAP, results are illustrated for routes A, B$_C$ and C with the colours red, mauve, green, and blue corresponding to the first, second, third, and fourth pass, respectively. Angular ranges of slip, η, for different processing routes on Y plane are also shown. Image was taken from the work by Langdon (2007).

Route A is believed to generate very similar band structure to route B$_C$ on Y plane after two passes as angular ranges of slip, η, are 27° and 18°, respectively (Fig. 2.11). However, subsequent processing by route A does not introduce any significant changes to the band structure while η is increased to 63° when route B$_C$ is used.

Additionally, routes A and C introduce shear planes only on the Y plane while route B_C provides deformation modes on the planes X, Y, and Z. It is postulated by Langdon (2007) that fine and equiaxed grains can be obtained when angular angles of slip are wide on each plane. The angular ranges of slip for planes X, Y, and Z were calculated after four passes by route B_C as 90°, 63°, and 63°, respectively. The same parameters were equal to zero on the planes X and Z for routes A and C.

According to the model, the grain refinement process is the most efficient when route B_C is used. It is explained by the activity of more intersecting slip systems than in routes A and C. Moreover, the formation of equiaxed arrays of grains on each orthogonal direction is achievable by using route B_C because the shear planes intersect with each other on every main plane. This cannot be obtained for routes A and C since the intersection of shear patterns occurs only on the Y plane (Fig. 2.11). TEM images of nanostructured aluminium showed by Iwahashi et al. (1998) are in good agreement with the model prediction.

2.3.5. *Mechanical properties after ECAP*

A grain refinement resulting from SPD strongly influences mechanical properties of pure metals and alloys. Horita et al. (2001) investigated the effect of ECAP on mechanical properties of various aluminium alloys (Fig. 2.12). They have reported significant increase in strength after first pass, e.g. yield stress of 5083 alloy raised from ~170 MPa to ~390 MPa. Although subsequent passes resulted in successive strength improvement, it was not as efficient as after first one. The elongations dropped significantly after first pass and remain almost constant with consecutive

passes or even increased, as it was observed for 5083 alloy. The studied aluminium alloys were shown to follow Hall-Petch relation, expressed by equation (2.1). The results obtained from ECAP were compared to cold rolling with reductions corresponding to strain imposed during various numbers of ECAP passes. It was shown that despite the strength of a rolled sheet being very similar, elongation to failure is much smaller than in the ECAPed samples.
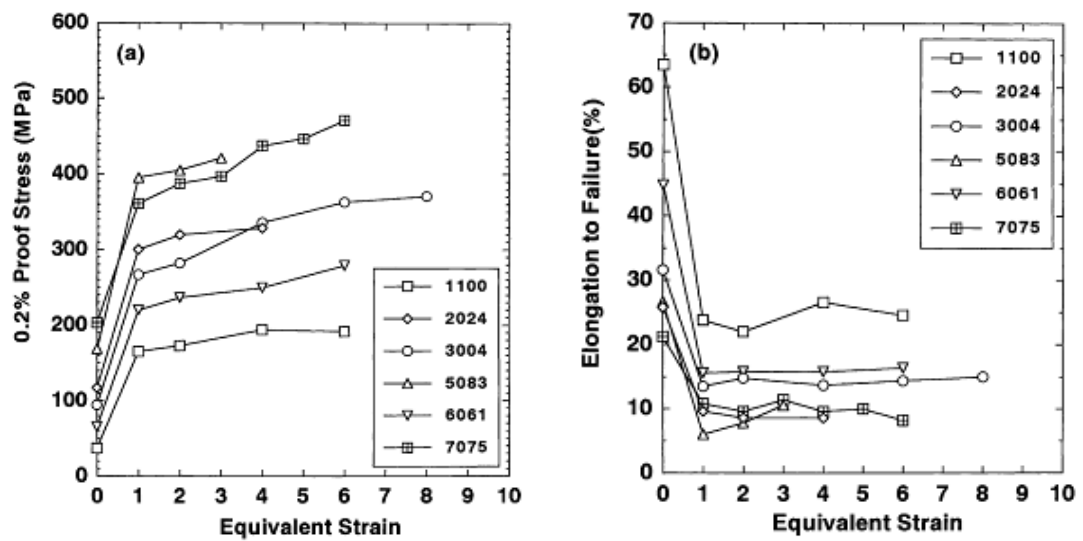
Fig. 2.12. Plots of (a) 0.2% proof stress and (b) elongation to failure versus equivalent strain for various aluminium alloys. Each ECAP pass is assumed to introduce true strain of ~1 in this study, e.g. equivalent strain of 4 corresponds to 4 passes of ECAP. Image was taken from the work by Horita et al. (2001).

Valiev et al. (2002) subjected pure copper to ECAP at room temperature. Significant yield stress increase, from ~50 MPa to ~280 MPa, was reported after two passes (Fig. 2.13). Subsequent processing up to sixteen passes led to further strengthening (~380 MPa) and ductility enhancement, comparing to sample processed by only two

passes. Therefore, it was postulated that ECAP can be successful in improving strength of metals without lowering their formability.
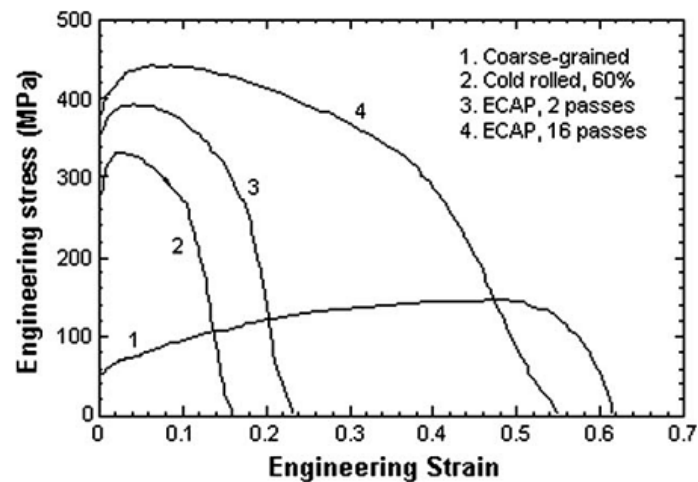
Fig. 2.13. Tensile stress-strain curves for Cu processed by ECAP and cold rolling. Image was taken from the work Valiev et al. (2002).

Nanostructured metals are considered as a separate group of materials due to their extraordinary combination of high strength and reasonably good ductility. The yield strength vs. elongation to failure diagram (Fig. 2.14) clearly shows that UFG Ti and Cu exhibit outstanding mechanical properties, comparing to CG metals (Valiev et al., 2002). Although processing of conventional metals can improve their strength, it is still much below a level that can be obtained in nanostructured metals. It was shown in the same paper that cold rolling of Al and Cu increases their strength; however, it is accompanied by a significant drop in ductility. Rolling of Cu with 61% reduction increased its strength to almost 400 MPa but decreased elongation to failure to about 4% while the nanostructured Cu exhibited the same strength with elongation of 55%.
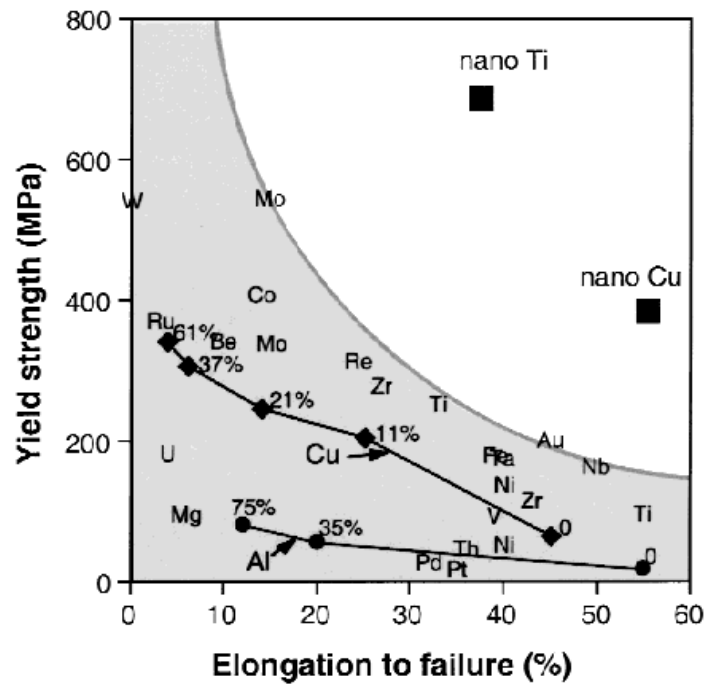
Fig. 2.14. Mechanical properties of pure metals, cold rolled Al and Cu (different reduction are shown) and nanostructured Ti and Cu. Image was taken from the work by Valiev et al. (2002).

ECAP of pure Ti followed by cold extrusion was conducted by Stolyarov et al. (2001) and an evolution of mechanical properties during subsequent processing steps was investigated. Yield stress was increased from 380 MPa to 640 MPa after eight passes of ECAP. Further processing by cold extrusion with 75% reduction raised yield stress to 970 MPa, which was greater than strength of Ti-6Al-4V alloy. Significant strength increase in UFG Ti was also reported by Estrin et al. (2013). Ultimate tensile strength of Ti Grade 2 was improved in this study by four passes of ECAP from ~525 MPa to ~850 MPa. Moreover, the reasonably high elongation to failure of 20% was reported for nanostructured Ti.

Grain size also influences mechanical properties of metals and alloys at elevated temperatures, e.g. homogenous structure with grain size smaller than ~10 μm is

required to obtain superplastic flow (Valiev and Langdon, 2006). UFG structure enables performing superplastic forming at lower temperatures and/or higher strain rates than CG metals, which could be attributed to enhanced grain boundary diffusion at elevated temperatures. Fujita et al. (2004) showed that interdiffusion coefficients of UFG structure with high fractions of HAGB were greater than the same coefficients for LAGB and CG structure. UFG metals usually exhibit higher strain rate sensitivity at elevated temperatures (Li et al., 2004; May et al., 2005; Figueiredo and Langdon, 2009a) which makes the material more resistant to necking and, as a consequence, more ductile. Superplasticity at lower temperatures and/or higher strain rates than for conventional CG metals was reported for aluminium (Xu et al., 2003; Charit and Mishra, 2005), magnesium (Lapovok et al., 2008; Figueiredo and Langdon, 2009a), and titanium alloys (Sieniawski and Motyka, 2007).

Grain size below 1 μm can be achieved in aluminium alloys by ECAP (Horita et al., 2001). Such materials can exhibit tensile elongations of 1000% at strain rate 10^{-2} s^{-1} (Horita et al., 1999) while conventional CG aluminium alloys are superplastically formed at 10^{-3} s^{-1}. Strain rate increase improves process efficiency significantly; the forming time of individual component made of conventional material is 20-30 minutes whereas the same operation can be done in ~60 seconds when UFG alloy is used (Valiev and Langdon, 2006). Moreover, using UFG materials can decrease energy cost and extend die life by reducing temperature of superplastic forming. Ota et al. (2002) achieved elongations of 420% at temperature as low as 200 °C for Al-3%Mg-0.2%Sc after eight passes of ECAP. Generally, for various alloys, the temperature of superplastic forming can be decreased by 100-200 °C through the use of ECAP (Valiev and Langdon, 2006).

2.3.6. Modifications of ECAP

Several improvements were introduced to conventional ECAP in order to improve its efficiency. Segal (2008) outlined that high normal pressure on the bottom surface of the outlet channel could be a reason for material sticking and the occurrence of scratches on a billet surface. Therefore, a new concept of a die with movable wall was presented for ECAP of flat products (Fig. 2.15a). Friction between the billet and the bottom die (1) in this configuration is 'transferred' to the interface between dies (1) and (2). As a consequence, seizing effects on billet surface can be eliminated, which has a crucial effect on product quality. Nakashima et al. (2000) proposed to realise many ECAP passes in one operation using a specially designed die (Fig. 2.15b). The multi-pass ECAP, equivalent to processing by route C, was shown to have the same effect on microstructure and mechanical properties as conventional ECAP. Rosochowski et al. (2007) designed and manufactured a die for 3D-ECAP (Fig. 2.15c), which enabled processing billets using route B_C in only one operation.

(a) (b)

(c)
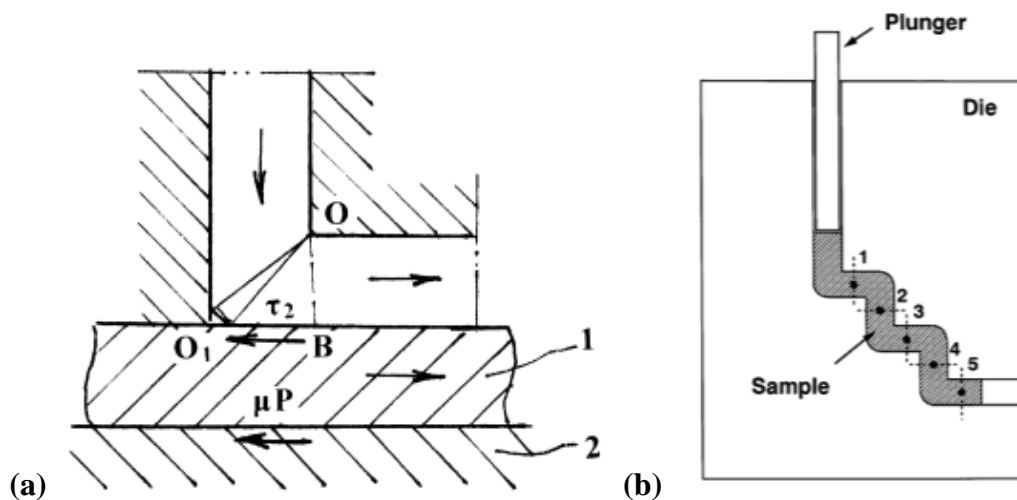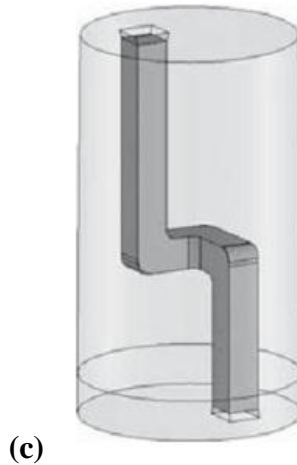
Fig. 2.15. A schematic illustration of: (a) ECAP with movable wall; (b) multi-pass ECAP; (c) 3D-ECAP. Images (a), (b), and (c) were taken from the works by Segal (2008), Nakashima et al. (2000), and Rosochowski et al. (2007), respectively.

2.3.7. *Incremental ECAP (I-ECAP)*

The modifications described above increased the potential of ECAP; however, the problem of limited billet length still remained unsolved. In most cases, the ratio of billet length to its diameter (round bars) or width (square bars) is varying from 6:1 to 8:1. Some of the continous variants of ECAP, which were described in Section 2.2.3, are addressing this problem. One of them is incremental equal channel angular pressing (I-ECAP), which was used in the experimental part of this work.

I-ECAP, which is the most recent modification of ECAP, was invented by Rosochowski and Olejnik (2007). The main goal of this improvement was to reduce feeding force during pressing by separating the stages of material feeding and plastic deformation. As a result, feeding force is very low as it must oppose only friction on a billet-container interface. The fact that material is not deformed during feeding

42

stage could be also considered as disadvantage because it increases processing time. Nevertheless, it enables processing very long billets and ensures uniform strain distribution.

Schematic illustration of I-ECAP is shown in Fig. 2.16a. The cycle starts from the material being fed by a distance less or equal to a, which is the feeding stroke (stage I). Then, the billet is fixed in this position and punch (C) deforms it plastically (stage II). The punch follows a sine wave signal while the feeding tool feeds the billet in consecutive steps. The material feeding stage is repeated when punch C is going up and a new cycle is started. Dies A and B are equivalent to the inlet channel in ECAP while die A and punch C form the outlet channel. Since the billet is not in contact with punch C in stage I, a feeding force is relatively low as it must oppose only friction between the billet and walls of the inlet channel. In order to avoid friction between the billet and the die B, a double billet variant of I-ECAP (Fig. 2.16b) was also developed by Rosochowski et al. (2008b).
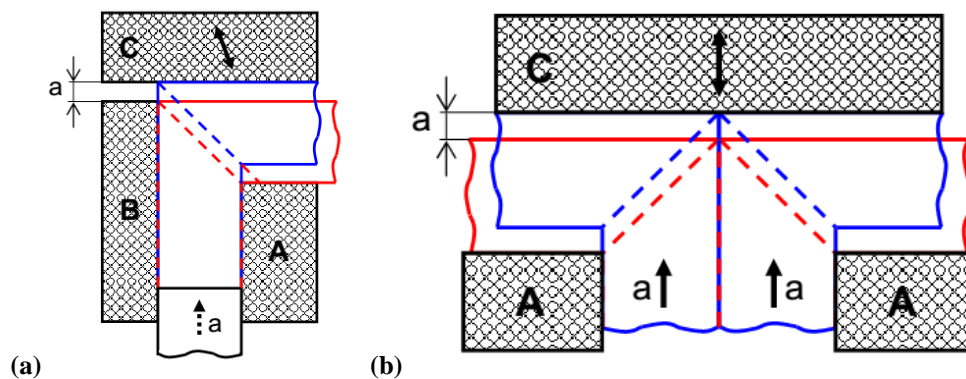
Fig. 2.16. Schematic illustration of I-ECAP (a) and double-billet variant of I-ECAP (b). Images were taken from the work by Rosochowski et al. (2008b).

Due to its incremental nature, I-ECAP is defined by different process variables than conventional ECAP. The movement of punch is described by a sine function, which is defined by its amplitude and frequency. Feeding stroke is a parameter which determines behaviour of the feeding tool. Peak-to-peak amplitude of punch C must be greater than feeding stroke to avoid plastic deformation in the stage I. Increasing frequency improves process efficiency but it also raises strain rate. Therefore, it should be reduced for materials prone to fracture at high deformation rate, e.g. magnesium alloys. For example, square bars with dimensions 10 mm $\times$ 10 mm $\times$ 200 mm made of aluminium alloy 1070 were successfully processed with frequency $f =$ 0.5 Hz, amplitude A = 2 mm (peak-to-peak) and feeding stroke d = 0.2 mm (Rosochowski et al., 2008a).

Feeding stroke has a strong influence on strain homogeneity along longitudinal axis of the billet. Rosochowski and Olejnik (2011) performed FE simulations in order to investigate this effect (Fig. 2.17). Feeding stroke was expressed in this study in terms of billet thickness percentile. It was shown that strain distribution similar to ECAP is achieved when feeding stroke is 10% of the billet thickness or less. For the 30% of the billet thickness, strain distribution became slightly non-uniform in the longitudinal direction. Finally, strongly non-uniform strain distribution in longitudinal direction was observed when feeding stroke was increased to 50%. Therefore, authors concluded that feeding stroke in I-ECAP should not exceed 10% of the billet thickness to ensure homogenous strain distribution in the longitudinal direction.
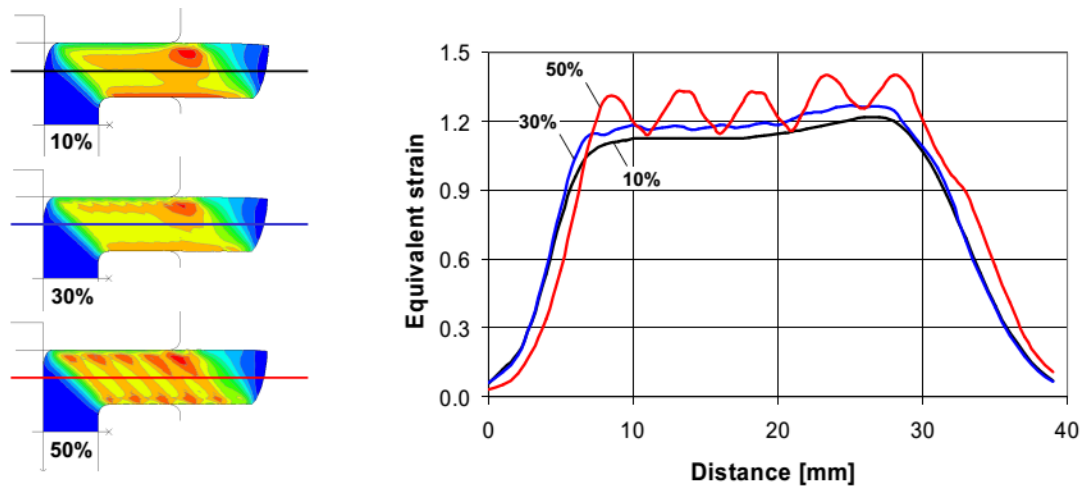
Fig. 2.17. Equivalent plastic strain for feeding stroke 10%, 30% and 50% of the billet thickness. Image was taken from the work by Rosochowski and Olejnik (2011).

I-ECAP was also successfully used for nanostructuring plates and sheets. Plates made of aluminium alloy 1070, with dimenions 4 mm × 30 mm × 100 mm, were proccessed by eight passes using route A. The obtained mean grain size was reported to be 453 nm (Rosochowski et al., 2008b). I-ECAP of sheets was conducted using a die shown in Fig. 2.18. An additional tool between two metal sheet strips was introduced to avoid using a very thin feeder. Since the separating tool was moving along with sheet strips, there was no friction between that tool and the strips. Aluminium alloy AlMgSc sheets with dimenions 2 mm × 50 mm × 190 mm were processed by six passes at 200 °C, which resulted in grain refinement to 1 μm (Rosochowski et al., 2010).
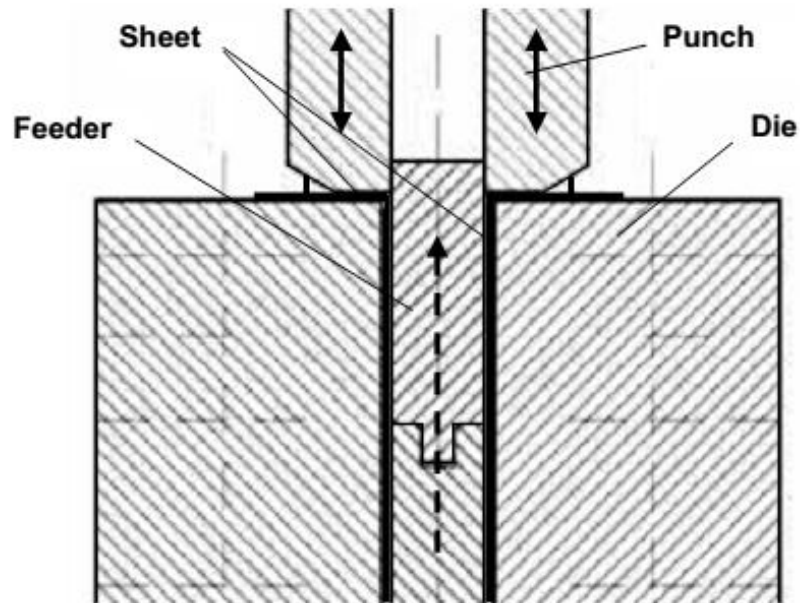
Fig. 2.18. Tool configuration used in I-ECAP of sheets. Image was taken from the work by Rosochowski et al. (2010).

2.4. Formability of magnesium alloys

2.4.1. *Deformation at room temperature*

Magnesium alloys are recognised as difficult-to-work metals due to their hexagonal closed-packed (hcp) structure. The asymmetry of hexagonal cell influences formability as only limited amount of slip systems can be activated at room temperature. It also affects tension-compression flow stress symmetry since various deformation mechanisms, e.g. twinning, could be activated in different directions of straining. Magnesium alloys are also very sensitive to variations in temperature and strain rate and temperature increase and strain rate decrease are usually required to improve formability.

The most favourable deformation mechanism operating in magnesium alloys at room temperature is slip on basal plane. Critical resolved shear stresses (CRSS) for

pyramidal and prismatic slip are much higher so their contribution to plastic deformation at room temperature is small (Yoshinaga and Horiuchi, 1963; Barnett, 2003a; Hutchinson and Barnett, 2010). Activation of basal slip is dependent on the orientation of grain. Experiments and theoretical calculations (Kleiner and Uggowitzer, 2004; Al-Samman and Gottstein, 2010) showed that Schmid factor for basal slip is increased when basal planes are inclined at ~45° to deformation direction. Since only two independent slip systems can operate on basal plane, another deformation mechanism is necessary to accommodate plastic strain and fulfil von Mises criterion (Mises, 1928), which states that five independent slip systems are required to ensure uniform deformation. Moreover, slip on basal plane is impossible if the c-axis of a hexagonal cell is aligned exactly parallel to tension/compression direction. In this case, twinning or non-basal slip needs to be activated to accommodate plastic deformation. The former operates at room temperature while the latter was reported above 200 °C (Wonsiewicz and Backofen, 1967). CRSS of non-basal slips (prismatic and pyramidal) are sensitive to temperature changes and they decrease along with temperature rise, while CRSS for twinning and basal slip are temperature independent (Barnett, 2003a). The various deformation modes in magnesium were shown in Fig. 2.19.
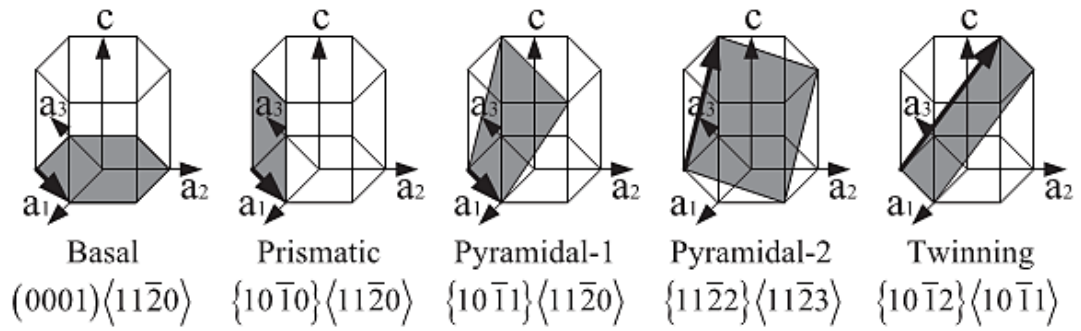
Fig. 2.19. Deformation modes in magnesium. Image was taken from the work by Mayama et al. (2011).

A comprehensive study on the grain size influence on deformation mechanisms in AZ31 magnesium alloy has been conducted by Barnett et al. (2004). Flow stress curves were obtained for hot extruded AZ31 with grain size varying from 3 µm to 22 µm at temperature ranging from ambient to 200 °C. A distinctive concave shape of flow stress curve, typical for twinning dominated deformation, was reported at room temperature even for grain size as small as 3 µm. A similar shape of a compressive curve was observed by Chino et al. (2008). Moreover, the significant differences between shapes of the flow stress curves in tension and in compression were reported in both works (Fig. 2.20a). The yield stress tension-compression asymmetry was attributed to twinning occurrence in compression. Transition from twinning to slip-dominated deformation in compression was plotted in Fig. 2.20b for various grain sizes (Barnett et al., 2004). It was concluded that twinning in compression can be avoided in fine-grained AZ31 (3-4 µm) by temperature increase up to 150 °C.
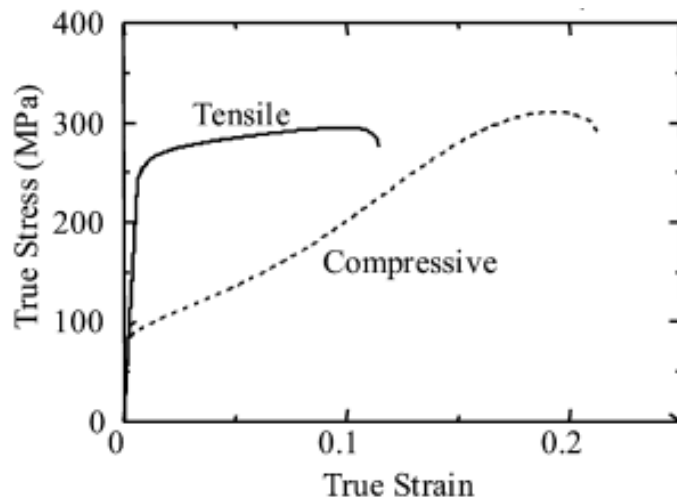
(a)
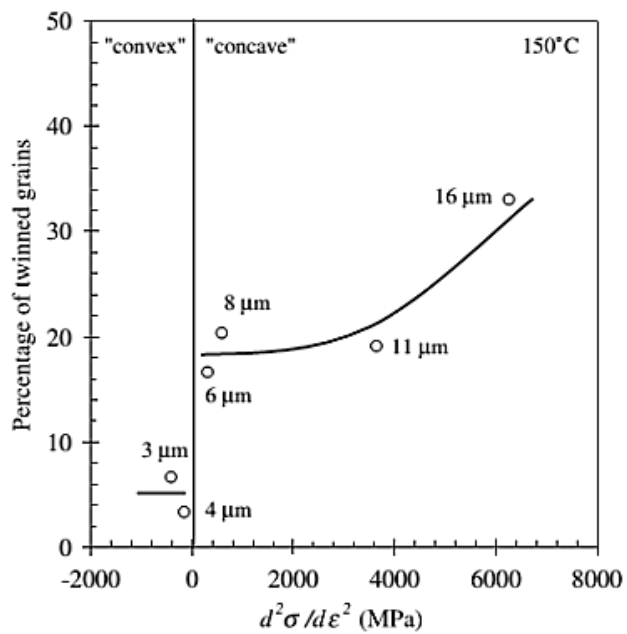
(b)

Fig. 2.20. (a) Tensile and compressive flow stress curves of extruded AZ31 magnesium alloy; (b) Diagram presenting transition from twinning to slip-dominated deformation in compression for various grain sizes. Images (a) and (b) were taken from the works by Chino et al. (2008) and Barnett et al. (2004), respectively.

2.4.2. *Twinning modes*

It was already mentioned that slip on basal plane is impossible if the c-axis of a hexagonal cell is aligned exactly parallel to tension/compression direction. In this case, twinning is activated to accommodate deformation at room temperature. Two main modes of twinning are distinguished in the literature (Yoshinaga and Horiuchi, 1963; Wonsiewicz and Backofen, 1967; Kelley and Hosford, 1968): (1) {10-12} 'tensile twinning', which enables extension along the *c*-axis, and (2) {10-11} 'contraction twinning', which enables compression along the *c*-axis. The secondary contraction twinning of the volume already deformed by a tensile twin was also revealed and it was recognised in the literature as {10-12} – {10-11} 'double twinning' (Wonsiewicz and Backofen, 1967; Kelley and Hosford, 1968). Twinning changes the orientation of basal planes; contraction and double twinning results in rotation of basal planes by 56° and 38°, respectively. Therefore, twinning reorients a grain towards a position more favourable for slip on basal plane, which can result in local softening. Double twinning was recognised by Barnett (2007b) as the main cause of reduced uniform elongation and earlier fracture due to local softening and generation of twin-sized voids. The latter observation was also confirmed by Al-Samman and Gottstein (2008a) in AZ31 samples subjected to plane strain compression. Double twinning can be suppressed by rising temperature; it was shown by Jiang et al. (2007) that volume fraction of twins decreases linearly with temperature. Tensile twins reorient basal planes by 86°, which means that grains remain in positions unfavourable for slip and further straining is continued at an increased level of stress but without lowering ductility. It was suggested that {10-12}

twins can increase strain hardening rate and uniform deformation in tension (Barnett, 2007a), which was shown in samples pulled perpendicular to the extrusion direction.

2.4.3. Deformation at elevated temperatures

The influence of deformation temperature on formability of AZ31 magnesium alloy was thoroughly studied by Agnew and Duygulu (2005). It was shown that ductility rose along with temperature and a significant increase in formability was observed at 150 °C and above. At the same time, strain rate sensitivity increased from 0.01 at room temperature to 0.15 at 200 °C, which showed that improved strain rate sensitivity is the most important macroscopic parameter responsible for formability enhancement at elevated temperatures. A significant drop in a normal strain anisotropy ratio, from r ~ 2 at room temperature to r ~ 1 at 200 °C, was also reported (Fig. 2.21). This effect was modelled using a polycrystal plasticity approach. The conclusion was drawn that thermal activation of <c+a> non-basal slip provides a satisfying explanation for the improved ductility and suppression of anisotropy.
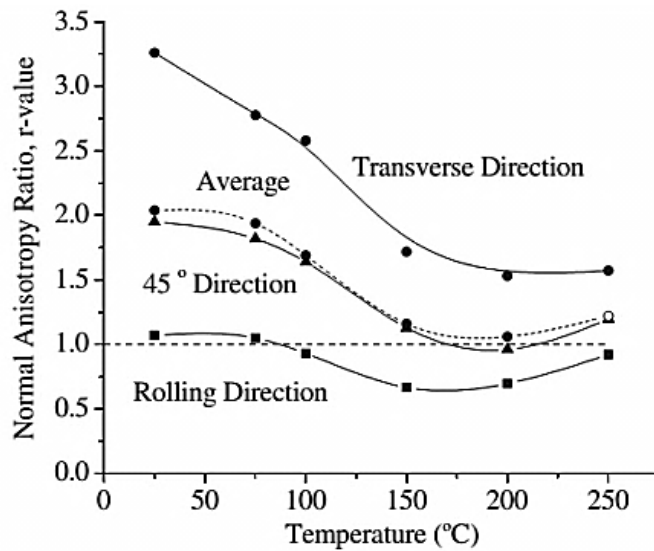
Fig. 2.21. Normal anisotropy of rolled AZ31B alloy as a function of temperature and sample orientation. Image was taken from the work by Agnew and Duygulu (2005).

Elevated temperature deformation of magnesium alloys is usually accompanied by dynamic recrystallization (DRX). The recovery processes observed during DRX are responsible for lowering strain hardening rate above 200 °C (Agnew and Duygulu, 2005). It was shown by Al-Samman and Gottstein (2008b) that new grains nucleate not only at grain boundaries but also inside twins. The recrystallized grains are randomly oriented which allows obtaining isotropic properties, which is often a challenge for wrought magnesium alloys. The size of grains created by DRX strongly depends on temperature and strain rate (Fig. 2.22), with low temperature and high strain rate favouring finer grain size (Beer and Barnett, 2007). However, if the initial grain size is much larger than the size of newly formed recrystallized grains it is more difficult to obtain homogenous microstructure at low temperatures as coarse grains cannot undergo full recrystallisation. In such case, bimodal microstructure is observed, as shown in Fig. 2.22b and c.
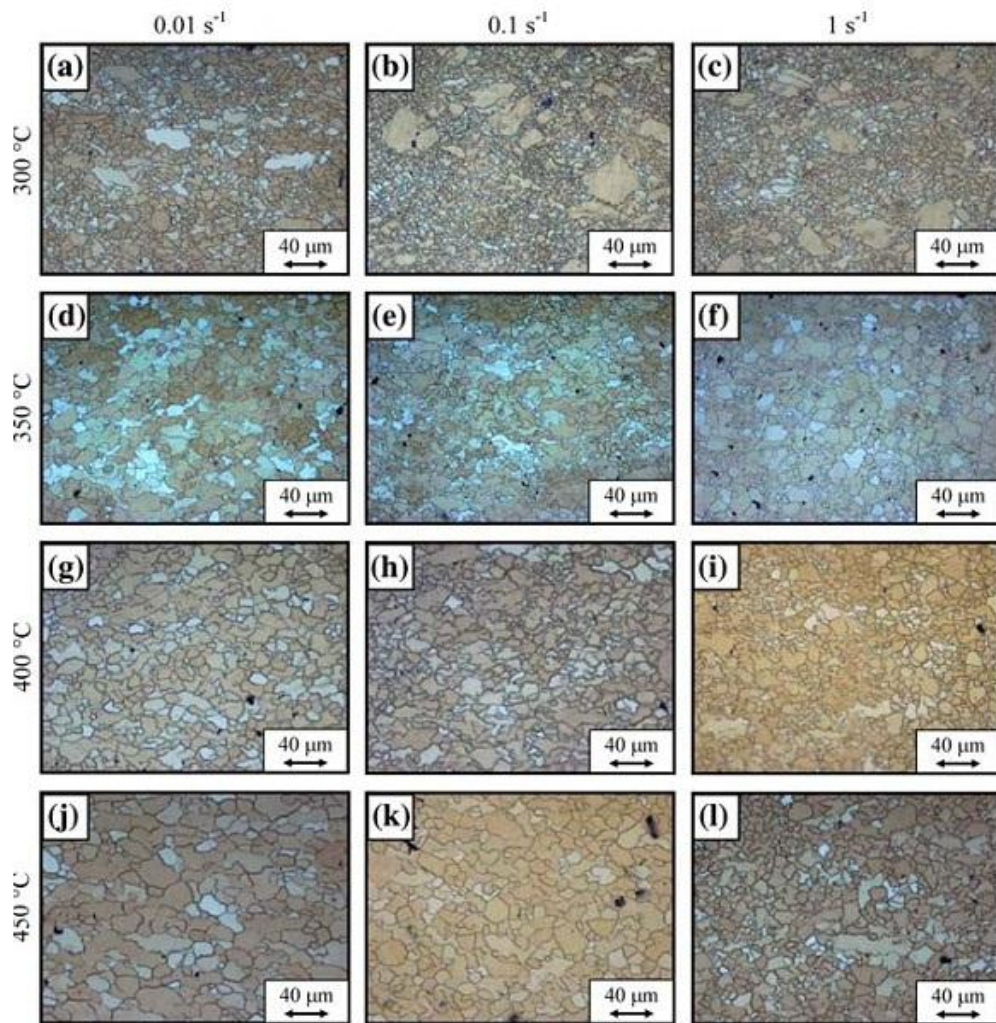
Fig. 2.22. Microstructures of AZ31 hot deformed to a compressive strain of 1.0 in various conditions. Image was taken from the work by Beer and Barnett (2007).

2.5. ECAP of magnesium alloys

2.5.1. *Grain refinement mechanism*

The mechanism of grain refinement in magnesium alloys is believed to be different from fcc metals. Su et al. (2006) proposed a model which assumes that grains are refined in ECAP due to mechanical shearing and subsequent recovery processes. The latter are present since the process is conducted at elevated temperatures to avoid

fracture. Figure 2.23 shows the three stages of development of refined and equiaxed grains. First, the originally coarse grains are deformed along a shear plane as demonstrated by shear bands within grains observed using TEM in a sample cut out from a deformation zone. Then, subgrain structures are generated due to recovery processes resulting from heating. Zones of increased dislocation density act as sites of nucleation for newly recrystallized grains. Further heating leads to grain growth and formation of fine grains with high angle grain boundaries. The newly generated grains are free from internal stresses occurring immediately after mechanical shearing.
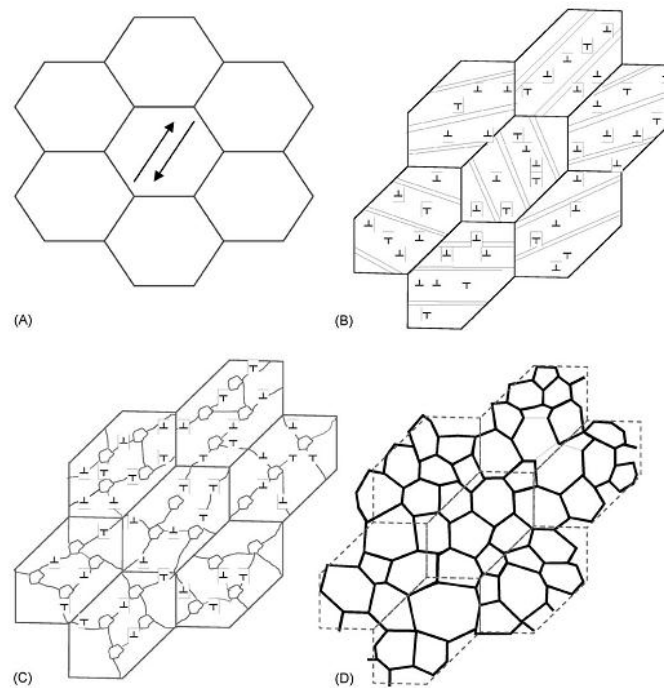
Fig. 2.23. Grain refinement model of magnesium alloys during ECAP: (a) initial microstructure; (b) mechanical shearing of grains; (c) rearrangement of dislocations and nucleation of new grains; (d) grain growth of recrystallized grains. Image was taken from the work by Su et al. (2006).

Figueiredo and Langdon (2009b) have noticed that bimodal grain size distribution, with coarse grains surrounded by large regions of very fine grains, can be observed after first pass of ECAP. Further processing by four passes using route B_C led to homogenization of the microstructure. Those experimental results could not be explained by the mechanism proposed by Su et al. (2006); therefore, they have presented a new grain refinement model. The model was based on the idea that grain refinement is controlled by dynamic recrystallisation (DRX), which was also one of the assumptions of work by Su et al. (2006). However, Figueiredo and Langdon (2009b) believed that nucleation takes place only at grain and twin boundaries. The concept of a critical grain size, d_c, was introduced to explain the occurrence of bimodal microstructure. Figure 2.24 shows the microstructure evolution during ECAP for magnesium alloys with different initial grain sizes. If the initial grain size is greater than d_c, one pass of ECAP is not enough to fully recrystallize interiors of coarse grains. Further processing is required to enable homogenization of the structure. If the mean grain size is smaller than d_c, the surface area occupied by grain boundaries is larger; therefore, more sites for nucleation of new grains exist and fully recrystallized structure can be obtained in one pass. The value of critical grain size was not established in the paper by Figueiredo and Langdon (2009b); it was only noted that this parameters is dependent on the chemical composition of an alloy and the processing temperature.
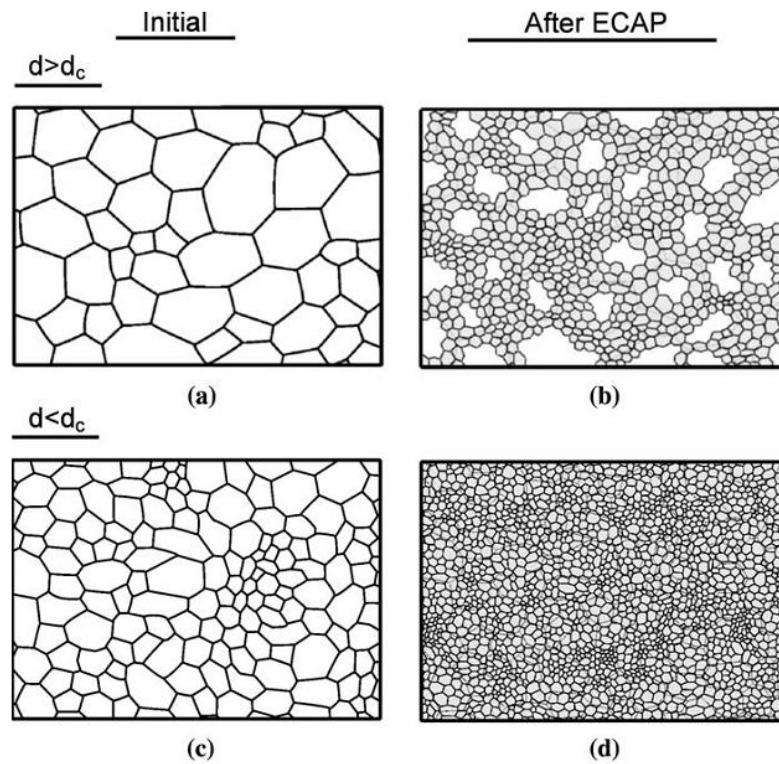
Fig. 2.24. Microstructure evolution during ECAP of magnesium alloys for different initial average grain sizes. Image was taken from the work by Figueiredo and Langdon (2009b).

Wu et al. (2010) investigated grain refinement in AZ31 magnesium alloy subjected to route A of ECAP. They have observed large elongated grains even after two passes. Moreover, EBSD characterisation revealed that those grains are fragmented by newly formed grain boundaries arising from ECAP. It was also shown that after the second pass at an elevated temperature, fine grains are observed at the newly formed grain boundaries and they gradually consume interiors of coarse grains during subsequent passes. This mechanism could not be captured by the model of Figueiredo and Langdon (2009b) as they did not predict the possibility of formation of new grain boundaries within elongated grains, which was called grain

fragmentation. However, the most important feature of the grain refinement process is still grain nucleation and growth due to DRX.

The brief review of the most important grain refinement models for magnesium alloys subjected to ECAP shows that the process is very complex. Although the three presented studies were conducted for the same alloy and for very similar processing conditions, the obtained results and drawn conclusions were not completely consistent. The model by Figueiredo and Langdon (2009b), supplemented with the observations of Wu et al. (2010), is in good agreement with the experimental results where DRX was believed to play a significant role in ECAP (Kim et al., 2002; Janecek et al., 2005; Jin et al., 2006; Ding et al., 2009). However, it does not take into account the mechanical shearing of grains, which was observed by Su et al. (2006). This shows that further research is needed to fully explain the nature of grain refinement in magnesium alloys during ECAP.

2.5.2. *Process variables*

ECAP of magnesium alloys is performed at elevated **temperatures** due to their low formability at room temperature. Most of wrought magnesium alloys are usually pressed at 200-300 °C. Temperature has an influence on grain refinement efficiency in the way that lower processing temperature leads to a finer grain size. Kim et al. (2002) pressed rod of AZ61 at 275 °C and the obtained grain size was 8 μm after eight passes. Jin et al. (2005) conducted ECAP of AZ31 at 250 °C, which resulted in grain refinement to 5 μm. They have also reported that further reduction to 2 μm can be achieved by lowering temperature to 225 °C. Further processing at 200 °C was

not successful due to crack occurrence. Seipp et al. (2012) confirmed results obtained by Jin et al. (2005) at 250 °C and the grain size they have obtained was 5.5 μm. ECAP of AZ31 was conducted at 200 °C by Mukai et al. (2001), they reported refinement to 1 μm after eight passes using route B_C. These results were not confirmed by Ding et al. (2009) as they obtained grain size of 2 μm after ECAP at 200 °C and temperature decrease to 175 °C was required to achieve 1 μm. Ding et al. (2008) have also proposed the procedure of gradual temperature decrease, which allowed reducing temperature to 115 °C in the final two out of twelve passes. The final average grain size obtained using the proposed approach was 0.37 μm.

The effect of **strain rate** on grain refinement was not investigated as extensively as temperature in the literature. The main reason was fracture observed during pressing with high speed, therefore, the emphasis was put on lowering strain rate in order to obtain billets without cracks. Ding et al. (2009) studied the effect of strain rate by pressing through a die with angle 120° with ram speeds of 10 and 0.8 cm/min, which was equivalent to strain rate of 0.1 and 0.03 s^{-1}, respectively (Kim, 2002). Microstructure characterisation showed that although the grain size was smaller when processing at higher speed, the difference between 1.6 and 2.1 μm can be considered as insignificant.

Grain size decrease with temperature reduction and strain rate increase in ECAP can be explained by the occurrence of dynamic recrystallisation (DRX). Beer and Barnett (2007) showed that finer grains are found when deformation occurs at lower temperature and/or higher strain rate. They also showed a bimodal distribution of grain size when initial coarse grains are much bigger than newly formed

recrystallized ones. Those observations, made after compression testing, can be directly related to results obtained by Figueoredo and Langdon (2009a), where coarse grains surrounded by colonies of very fine grains were reported after first pass of ECAP. The occurrence of DRX also explains why grain size cannot be reduced with increasing number of passes when temperature is kept constant (Jin et al., 2006; Ding et al, 2009). Fatemi-Varzaneh et al. (2007) showed that size of a recrystallized grain is decreasing in the initial stage of deformation but the refinement process slows down as the strain increases and, finally, it remains constant after reaching a certain value. Similarly in ECAP, even though the deformation level is increased with subsequent passes, the grain size cannot be further reduced as long as temperature is constant.

Most of researchers use **processing route** with rotation of 90° around billet's axis (route B_C) as it was shown to be the most effective route in case of aluminium and its alloys (Mukai et al., 2001). However, there is no clear evidence that the route has a similar effect on grain refinement of Mg alloys. On the contrary, Ding et al. (2009) reported that routes A, B_C, and C have almost the same effect on grain size. Equiaxed and fine grains without any signs of band formation were also obtained after processing by route C (Seipp et al., 2012). This could be explained by the fact that fine grains are formed through the DRX-related phenomena during ECAP of magnesium alloys rather than formation and intersection of subgrain bands (Iwahashi et al., 1998).

Although grain size obtained through processing by various routes is similar, significant differences were reported in developed crystallographic textures. Mukai

et al. (2001) postulated that basal planes of hcp cell of magnesium are aligned parallel to shear plane of ECAP after processing by route B_C. This observation was confirmed by Ding et al. (2008) by texture measurement after ECAP using routes A, B_C, and C. The conclusion was drawn that basal planes were inclined at nearly 45° to the material flow direction after processing by routes B_C and C. However, they remained almost parallel to this direction after processing by route A. A very similar textural effects after processing by routes B_C (Masoudpanah and Mahmudi, 2010) and C (Seipp et al., 2012) were also reported later for AZ31 magnesium alloy, which confirms that the processing route plays a significant role in texture development during ECAP of magnesium alloys.

The **die angle** determines the amount of strain imposed to material in each pass; increasing die angle from 90° to 120° results in strain decrease from 1.15 to 0.67 (Iwahashi et al., 1996). Although a high level of deformation is required to obtain fine microstructure, the grain refinement process is suppressed after reaching a certain amount of strain. Indeed, the results presented by various authors support the idea that increasing die angle does not lower the efficiency of grain refinement and enables processing metals with limited ductility. Figueiredo and Langdon (2009a) reported that the grain size of ZK60 magnesium alloy was the same after six passes of ECAP using either die with 90° or 110°. Ding et al. (2009) showed that processing using 90° die led to faster refinement of microstructure during the first pass but a final grain size after four passes was the same as after using 120° die. Therefore, die angle does not have a strong influence on average grain size obtained after ECAP.

2.5.3. *Formability of magnesium alloys during ECAP*

Process variables have a strong influence on formability of magnesium alloys during ECAP. Unstable flow, which can lead to fracture, is observed when temperature is too low or pressing speed too high. Kang et al. (2008) have investigated effects of temperature and ram speed on fracture behaviour of AZ31 subjected to one pass of ECAP using a die with angle 90° between channels. They showed that material underwent fracture by segmentation at 150 °C (Fig. 2.25a) even with pressing speed as low as 10 mm/min., which corresponded to strain rate 0.01 s^{-1}. However, Bryla et al. (2009) reported that AZ31 was pressed at 150 °C with the very similar speed of 0.1 mm/s without fracture. According to Kang et al. (2008), processing at 200 °C can be successful only when strain rate in deformation zone is smaller than 0.03 s^{-1} (Fig. 2.25b). Pressing speed can be increased to 300 mm/min. (strain rate 0.25 s^{-1}) at 250 °C (Fig. 2.25c).

It was also noticed by Kang et al. (2008) that fracture was preceded by flow localisation, which occurrence can be attributed to flow softening observed for AZ31 at elevated temperatures. Shear bands arising from strain localisation were also observed by Lapovok et al. (2009) after ECAP at 250 °C and it was reported that spacing between bands decreased with the increasing strain rate. In other words, more shear bands were revealed within the same area when the pressing speed rose.
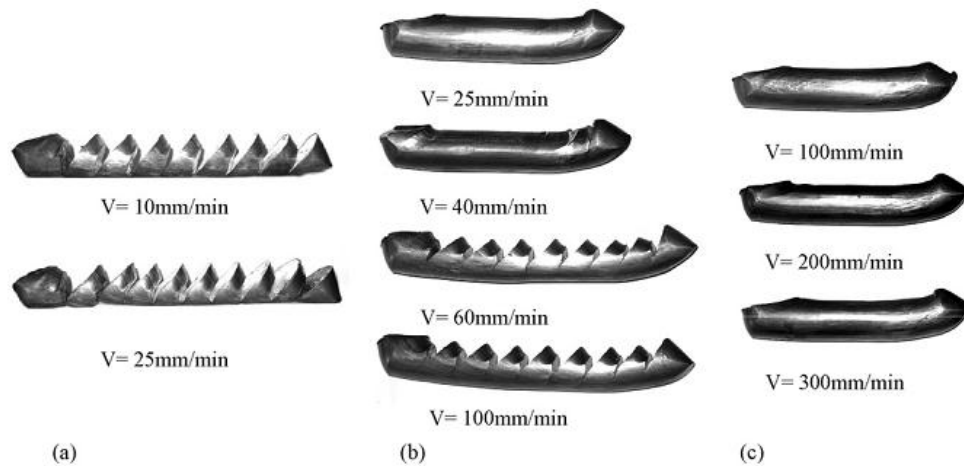
Fig. 2.25. Samples of AZ31 after one pass of ECAP at 150 °C (a), 200 °C (b) and 250 °C (c) pressed with various velocities. Image was taken from the work by Kang et al. (2008).

Several improvements may be introduced to the process in order to increase formability of difficult-to-work alloys. Increasing the die angle was shown to be one of the most effective methods of lowering processing temperature, e.g. ZK60 was successfully pressed at 200 °C using a die angle of 110° while pressing with a die angle of 90° resulted in fracture (Figueiredo et al., 2007). Another approach is to modify mechanical properties of a material before subjecting it to ECAP. FE simulations performed by Figueiredo et al. (2007) showed that increasing strain rate sensitivity leads to formability enhancement at elevated temperatures. This kind of modification can be introduced by direct extrusion prior to ECAP. It was confirmed experimentally for ZK60 that increased strain rate sensitivity improved formability during ECAP at 200 °C.

Lowering temperature of ECAP can be also achieved by applying back-pressure in the outlet channel of a die. It can help with reducing a gap between a billet and the

curved outer contour of the die. Moreover, more uniform strain distribution and smaller grain size can be obtained by this technique (Lapovok, 2005). Formability of AZ31 was shown to be significantly improved by applying a very high back-pressure (three times larger than yield stress of the alloy), which enabled conducting ECAP at room temperature (Gu et al., 2013). Nevertheless, back-pressure does not solve the problem of strain localisation which was shown by FE simulation (Figueiredo et al., 2010a).

Gradual temperature decrease with subsequent passes was shown to be successful in lowering temperature during the final step of processing. Ding et al. (2008) proposed the following procedure for ECAP of AZ31 using a die angle of 120°: four passes at 200 °C, then, another four passes at 150 °C, two passes at 125 °C, and two passes at 115 °C. Lowering temperature below 150 °C without earlier preprocessing was not possible as the fracture occurred. Biswas et al. (2010) used similar approach to conduct ECAP of pure magnesium at room temperature. Their procedure was as follows: four passes at 250 °C, then, temperature was decreased with each step to: 200 °C, 150 °C and 100 °C, and the final, eight pass, was conducted at room temperature. As it was shown, a remarkable temperature decrease can be obtained by using this procedure; on the other hand, it requires large number of passes, which decreases process efficiency.

2.5.4. *Mechanical properties of ECAPed magnesium alloys*

Grain size strengthening was reported for AZ31 after repetitive oblique shear strain using caliber rolling (Mukai et al., 2010). Yield stress after 18 passes at room

temperature exceeded 400 MPa which was attributed to a development of fine subgrains, smaller than 1 μm, and a weakening of texture. Grain refinement by multi-directional forging can also lead to strength increase as relation hardness vs. grain size after processing by this technique followed Hall-Petch equation within grain size range 20-0.2 μm (Xing et al. 2005). ECAP can also result in strength increase to ~400 MPa of yield strength when grain size is reduced to 0.37 μm by processing at 115 °C (Ding et al., 2008). Xia et al. (2005) have also reported increase in hardness with grain size decreasing from 20 μm to 0.5 μm, which was in line with a Hall-Petch relation.

On the other hand, most of ECAP studies on magnesium alloys indicate decrease in yield stress rather than the expected grain size strengthening. Yield stress dropped from 200 MPa for extruded AZ31 to 135 and 93 MPa after four passes using route C and B_C, respectively (Seipp et al., 2012). Moreover, it was shown that strength was decreasing with the number of passes via route C; yield stress of 166, 135, and 73 MPa was reported after two, four, and eight passes, respectively. Material softening with grain size decrease from 25 μm to 8 μm was also shown for AZ61 (Kim et al., 2002). According to Agnew et al. (2004) and Seipp et al. (2012), this effect could be explained by a development of very strong texture. Basal planes are inclined at 45° to tensile direction after ECAP, which favours basal slip. It can improve room temperature formability (Mukai et al., 2001; Agnew et al., 2004; Masoudpanah and Mahmudi, 2010) but material strength is decreased at the same time.

Mukai et al. (2001) have shown that ECAP followed by annealing can remarkably improve room temperature ductility of AZ31 magnesium alloy (Fig. 2.26). The

obtained mean grain size was about 1 μm after ECAP and 15 μm after subsequent annealing. Agnew et al. (2004) confirmed the results obtained by Mukai et al. (2001) and, additionally, they reported that annealing had not changed the texture developed during ECAP. Therefore, ductility enhancement was explained by recovery effects and grain growth during heat treatment.
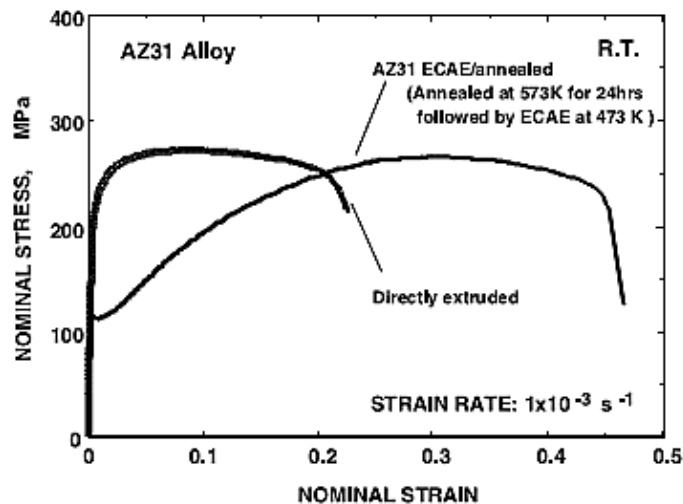
Fig. 2.26. Flow stress of directly extruded AZ31 and the same material after ECAP and annealing. Image was taken from the work by Mukai et al. (2001).

In summary, strongly textured fine-grained magnesium alloys produced by ECAP with grain size within range 1-15 μm exhibit strength decrease and significantly enhanced ductility, which can be additionally improved by subsequent annealing. It can be concluded that above 1 μm texture plays more important role than grain size related effects during plastic deformation. However, when the grain size is smaller than 1 μm, strengthening resulting from dislocation pile-up on grain boundaries becomes dominant.

Grain size also affects formability at elevated temperatures, especially superplastic properties of magnesium alloys. Fine microstructure with grain size below 10 μm is usually required to achieve elongations bigger than 100%, however, elongations as high as 1000% can also be observed. Superplasticity was reported for AZ31 with grain size 5 µm at temperatures 325-450 °C and strain rates 10^{-4}-10^{-5} s^{-1} (Watanabe et al., 1999; Watanabe et al., 2000; Lin and Huang, 2002).

Grain refinement below 1 μm can shift temperature of superplastic forming towards lower values and enables increasing strain rate, which improves process efficiency. Elongation of 460% was achieved in AZ31 alloy at 150 °C with strain rate 1×10^{-4} s^{-1} (Lin et al., 2005). Samples in this study were processed by direct extrusion followed by eight passes of ECAP, which resulted in grain refinement to 0.7 μm. More spectacular results were obtained by Figueriedo and Langdon (2009a) for ZK61 magnesium alloy processed by direct extrusion and ECAP; elongation at 200 °C and strain rate 1×10^{-4} s^{-1} exceeded 3000% (Fig. 2.27) after only two passes. A similar processing route, including extrusion and ECAP, was applied to magnesium alloys Mg-9%Al (Matsubara et al., 2003) and Mg-8%Li (Furui et al., 2006) which enabled obtaining elongations above 500% at 200 °C.
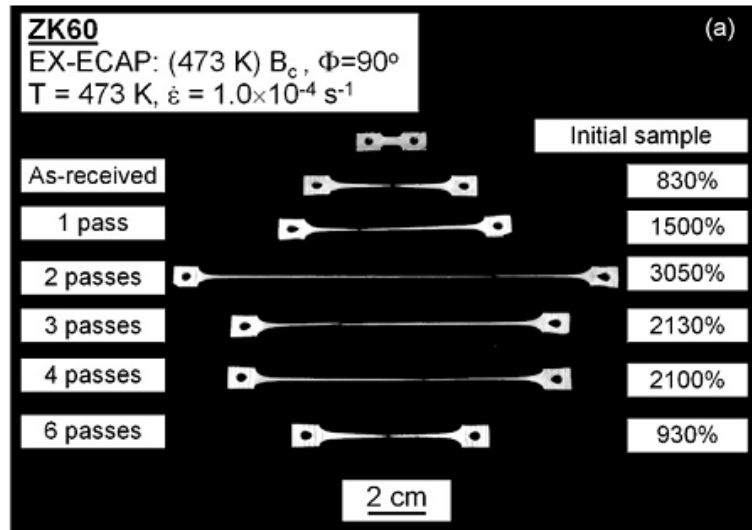
Fig. 2.27. Appearance of fine-grained ZK60 specimens after testing to failure at 200 °C with initial strain rate 1×10^{-4} s^{-1}. Image was taken from the work by Figueriedo and Langdon (2009a).

2.5.5. *Corrosion resistance*

Magnesium is known for its low standard electrode potential (-2.37 VNHE), which makes it one of the poorest corrosion resistant metals among all conventional metallic structural materials (Jiang and Ma, 2011). Nevertheless, recent studies have shown that grain refinement through ECAP increased corrosion resistance of ZE41A (Jiang et al., 2009) and ZK60 alloys (Orlov et al., 2011). It was shown in the latter work that the combination of grain refinement and solute redistribution is required to produce a material with improved mechanical and corrosion properties. High corrosion rate of magnesium alloys is a problem for automotive industry as well as for potential medical applications. Biodegradable magnesium alloys are very promising materials for orthopaedic (Steiger et al., 2006) and cardiovascular implants (Zartner et al., 2006). Such implants can be completely dissolved within human body due to the corrosion process. However, this process requires better

control and too fast dissolution rate is still a challenge for researchers. Grain refinement is believed to be one of the possible solutions to this problem.

2.6. Summary

Nanostructured metals and alloys are very promising materials for various markets, i.e. automotive, aerospace and medical. Improved strength enables reducing weight of structural elements in many applications (Ding et al., 2008). At the same time, small grain size enhances formability at elevated temperatures (Figueriedo and Langdon, 2009a), which reduces the cost of shaping final parts. SPD methods are the most popular techniques of refining grain structure due to their similarity to conventional metal forming processes. Especially ECAP is a well-established method of nanostructuring metals and alloys. Nevertheless, it does not allow processing continuous billets, which is the main reason why the method is not used in industrial practice.

According to the recent literature reports, I-ECAP could be a promising technique of producing fine- and ultrafine-grained metals (Rosochowski and Olejnik, 2011); however, it was used only for aluminium alloys up to now. Due to the incremental nature of the process, selection of the proper processing parameters is required to avoid fracture reported in many papers dedicated to ECAP of magnesium alloys (Kang et al., 2008; Figueiredo et al., 2007). Grain refinement of magnesium alloys subjected to I-ECAP is suspected to have similar effects on microstructure and mechanical properties to conventional ECAP, as it was already reported for

aluminium alloys. However, the clear evidence of that has been never been shown for magnesium alloys.

Textural modifications induced by ECAP are believed to improve elongation to failure of magnesium alloys due to facilitation of slip on basal plane and suppression of twinning (Mukai et al., 2001; Agnew et al., 2004). Twins are usually revealed *ex situ* mainly in large grains and they are suspected to act as sites of fracture initiation in coarse-grained alloys (Barnett, 2007b; Al-Samman and Gottstein, 2008a). However, a prove of twin transformation into a microcrack has never been shown explicitly since it cannot be revealed using conventional characterisation methods. Differences in fracture mechanisms occurring in fine- and coarse-grained magnesium alloys require *in situ* examination to provide better understanding of a grain size effect on formability.

The above considerations indicate the existing knowledge gaps in the field of grain refinement of magnesium alloys, which are addressed in the present work. The most popular wrought magnesium alloy AZ31B is subjected to I-ECAP for the first time to confirm the potential of the method for an industrial production of innovative materials. Effects of processes variables on microstructure and mechanical properties of obtained materials are studied. Additionally, *ex situ* and *in situ* microstructural characterization is incorporated to show a relation between grain size and deformation mechanisms occurring in magnesium alloys.

Chapter 3
Details of experiments

The experimental part in this study included: (1) conducting I-ECAP experiments, (2) investigating mechanical properties, and (3) microstructural characterization of obtained materials. Equipment used to conduct the listed actions and its general principles of operation are described in this chapter. The microstructural and mechanical characterisations of materials used in this work are shown in Section *3.4 Materials*.

3.1. I-ECAP experimental rig

The equipment for running I-ECAP experiments has been developed by Dr Andrzej Rosochowski's research group for several years at the University of Strathlyde. It was designed to be used on a 1000 kN servo-controlled hydraulic press (Fig. 3.1).

A schematic illustration of the control and data acquisition systems for I-ECAP is shown in Fig. 3.2. There is a punch (P) attached to the piston of the press, which follows a command signal sent from the Cubus software developed by Zwick Testing Machines Ltd. The software receives a feedback signal from a displacement transducer (LVDT1) and compares it with the command signal to ensure that the real response of the press is as close to the command signal as possible. A load cell (LC1), placed between a punch holder and the piston, sends data to the software to monitor the current load and to ensure that the press capacity is not exceeded.

Fig. 3.1. Hydraulic press used in this work for I-ECAP experiments.

HA	Hydraulic Actuator
SV	Servo Valve
LVDT	Displacement Transducer
NI	National Instruments Modules
MC	Motor Controller
M	Electric Motor
SJ	Screw Jack
LC	Load Cell
P	Punch
TC	Temperature Controller
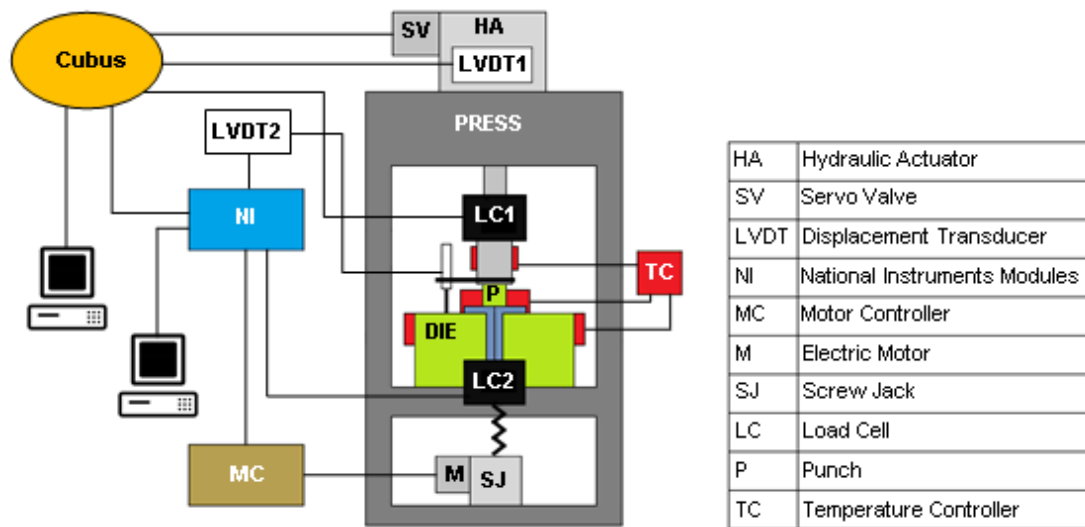
Fig. 3.2. Control and data acquisition system for I-ECAP. Image courtesy of Mr Karl Schmidt, undergraduate student at DMEM, University of Strathclyde.

A National Instruments LabView application (NI) was developed to control the movement of a motor-driven screw jack (SJ) which realises feeding of billets (Fig. 3.3). The application receives data from the load cell (LC2), placed on top of the screw jack, and stops the process when the screw jack load capacity of 200 kN is exceeded. Material feeding is synchronised with the punch movement. Therefore, additional displacement transducer (LVDT2) was located near the deformation zone in order to obtain more accurate punch position than that from the LVDT1. Data gathered by LVDT2 is sent to the NI application.

Fig. 3.3. Screenshot from NI application used to control feeding of billets.

A double-billet variant of I-ECAP, with 90° angle between channels, was realised in this work using the described equipment. Billets with square cross-sections 10 mm × 10 mm were fed using the motor-driven screw jack (SJ) whose action was synchronized with the reciprocating movement of the punch (P). The punch followed an externally generated sine waveform signal with frequency 0.5 Hz and peak-to-

peak amplitude of 2 mm. The feeding stroke of 0.2 mm was initiated when the punch was going up. The frequency and the amplitude of the punch movement as well as the feeding stroke were kept the same in all experiments conducted in this work. Strain rate corresponding to the selected process parameters and billet dimensions was 0.8 s^{-1}; it was obtained from FE simulation performed in ABAQUS (ver. 6.10). Strain introduced to billets during each pass of I-ECAP with the 90° die was ~1.15 (Iwahashi et al., 1996).

I-ECAP experiments in this work were conducted at elevated temperatures varying from 125 °C to 250 °C. Three sources of heating were used in the tool assembly to keep a stable temperature during processing (Fig. 3.4). The heating system for I-ECAP includes heating band (1) with diameter 280 mm and power 3000 W attached to a steel die pre-stressing ring. Additionally, two aluminium blocks (2), each with three inserted Watlow Firerod cartridges of 250 W, are resting on the pre-stressing ring to stabilise temperature near the deformation zone. Readings from a thermocouple located 15 mm from the die channel are sent to a PID temperature controller. A separate 600 W band heater with its own thermocouple is attached to the punch holder (3) to keep a constant temperature of the punch. A hollow cooling adaptor (4) incorporating a channel for water circulation is put between the punch holder and the load cell to avoid overheating the latter one. The total power of the heating system for the I-ECAP rig is 5100 W.
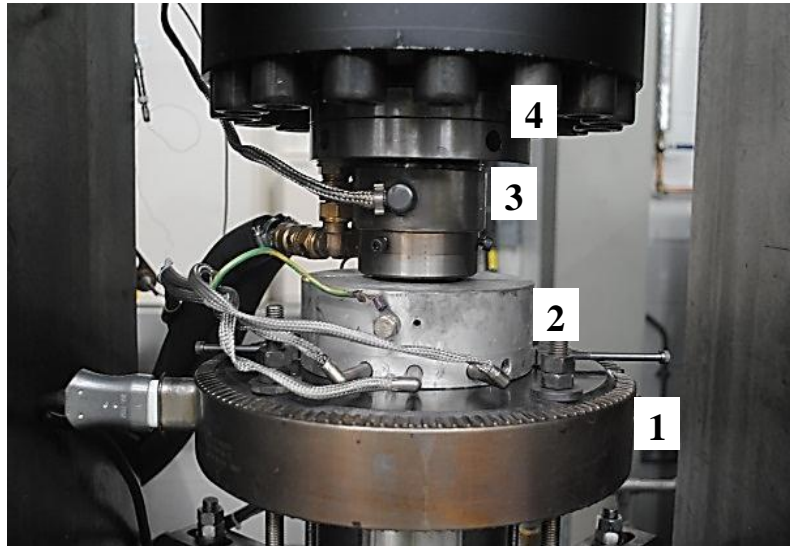
Fig. 3.4. Elements of I-ECAP heating system

3.2. Mechanical testing

Mechanical properties were investigated in this study on an Instron 5969 universal testing machine with the maximum load capacity 50 kN (Fig. 3.5). The machine is owned by the Advanced Materials Research Laboratory at the University of Strathclyde. Tension and compression tests were carried out at room temperature with the initial strain rate 1×10^{-3} s^{-1}. Flat tensile specimens, with thickness 2 mm and the gauge section dimensions 2.5 mm $\times$ 12 mm, were machined using wire electrical discharge machining. The height and diameter of the compression specimens was 8 mm and 7 mm, respectively. The ratio of height to diameter is smaller than in case of standard compression sample. Anisotropic flow and buckling in severely deformed samples is very likely to occur; therefore, sample height was shortened in order to obtain more reliable stress-strain relations. True stress-strain curves were obtained directly from tensile tests as strain was measured using a video-

extensometer. True strain in compression was evaluated from readings of the cross-head displacement.
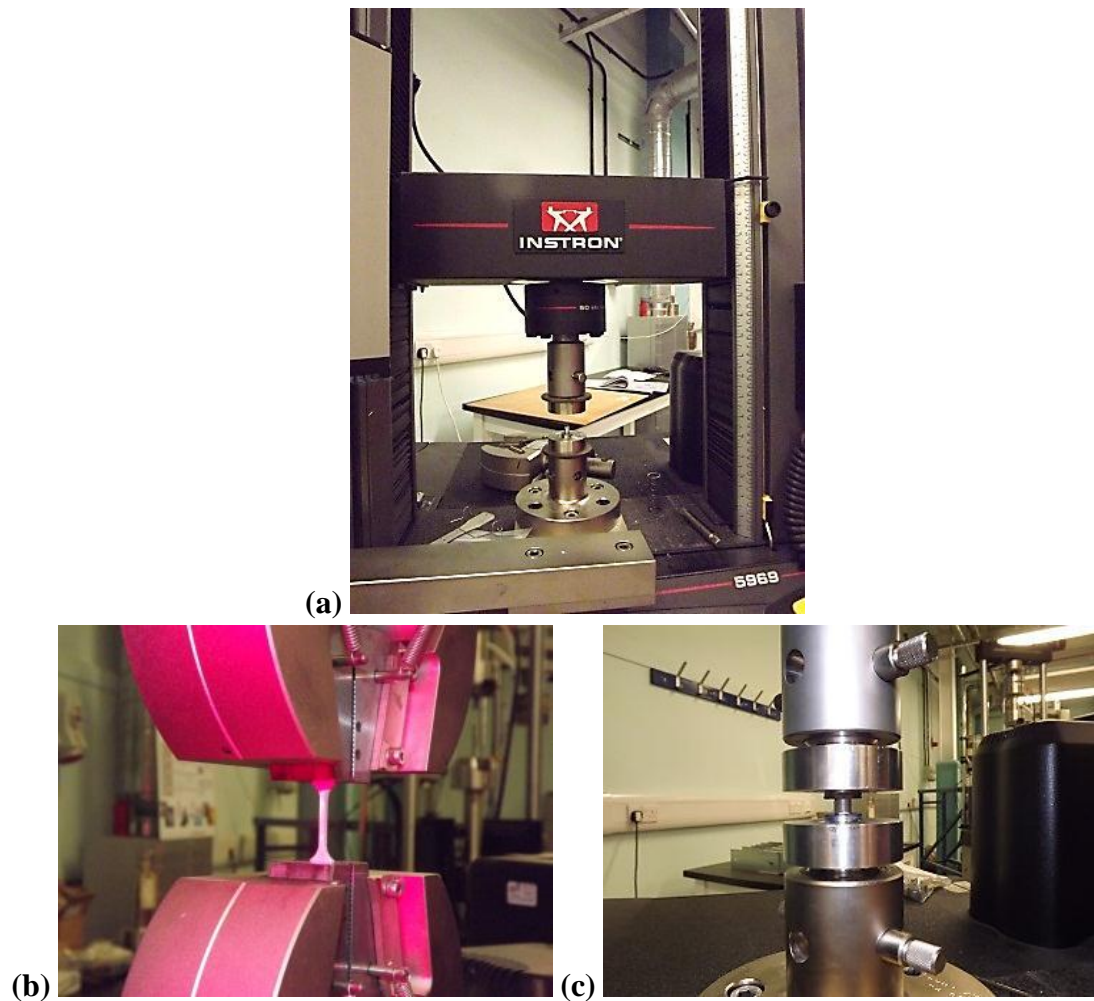
Fig. 3.5. Instron 5969 universal testing machine (a), tensile testing with video-extensometer (b), and compression testing (c).

3.3. Microstructural characterisation

Olympus GX51 optical microscope (Fig. 3.6b) and Quanta FEG 250 scanning electron microscope (Fig. 3.6c), available at the Advanced Forming Research Centre at the University of Strathclyde, were used to perform microstructural characterization. The sample preparation procedure included grinding, polishing and

etching. Samples were ground using SiC paper P600 and P1200. Then, they were mechanically polished on Buehler EcoMet 300 Pro Grinder-Polisher (Fig. 3.6a) using polycrystalline suspensions with particles sizes: 9, 3, and 1 μm. Colloidal silica was used for final polishing. After polishing, specimens were etched using acetic picral in order to reveal twins and grain boundaries. The mean grain size was measured by a linear intercept method using Olympus analySIS software. Representative images were chosen for grain size measurements; at least 500 grains were measured for each specimen.

The EBSD images were obtained using a Jeol 7001FLV scanning electron microscope equipped with a Nordlys II EBSD detector from Oxford Instruments. This work was performed in LEM3 Laboratory at ENSAM-Arts et Métiers ParisTech, Metz, France. After grinding and polishing steps, samples were additionally chemically etched using Nital 10% and polished with alumina 0.02 μm for EBSD characterisation. The analysed zones were about 400 μm × 270 μm with a 0.2 μm step size to be representative for the whole material; the indexation fraction was over 90%.

Fig. 3.6. Equipment used for sample preparation and microstructural characterisation of specimens: (a) Buehler EcoMet 300 Pro Grinder-Polisher; (b) Olympus GX51 optical microscope; (c) Quanta FEG 250 scanning electron microscope.

3.4. Materials

A commercially available AZ31B (Mg – 3%Al – 1%Zn – 0.5%Mn) magnesium alloy purchased from Magnesium Elektron (Manchester, UK) was used in the studies presented in Chapters 4, 5, and 6 of this work. The company has not provided the

processing history details (temperature, deformation level) as they keep it confidential. The material was supplied either in the form of hot-extruded round rods with the diameter of 16.8 mm or a hot-rolled 20 mm thick plate. The rods were delivered as-fabricated while the plate was annealed after rolling. The initial microstructure of the rod was heterogeneous with coarse grains (~83 µm) surrounded by colonies of small grains (~12 µm), as shown in Fig. 3.7. The microstructural image was taken on the plane along extrusion direction (ED). Small grains were arranged in long strings aligned along ED, which were separated by coarse-grained regions. Occurrence of small grain colonies was attributed to dynamic recrystallization during hot extrusion.
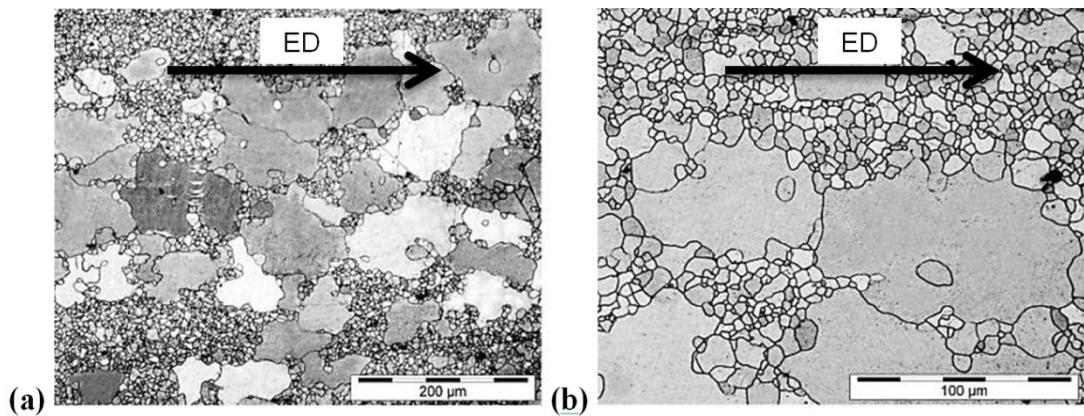
Fig. 3.7. Microstructure of as-supplied AZ31B extruded rod along ED direction (a) and zoomed region showing coarse grains (~83 µm) surrounded by colonies of small grains (~12 µm) (b).

A deep relief on the surface of the hot-rolled sample was revealed on the plane parallel to the rolling direction (RD) after polishing but before etching (Fig. 3.8a). It was attributed to a high level of deformation introduced during rolling as such pattern was not observed on the plane perpendicular to RD. The relief significantly impeded preparation of the sample for microscopic observations. The microstructure

of the sample, with the average grain size of ~8 µm, was relatively homogeneous on the plane perpendicular to RD (Fig. 3.8b) while bands of small grains (~3 µm) were revealed along RD (Fig. 3.8c). Twins were not observed in the as-supplied materials. Black dots observed in the Fig. 3.8a were recognised, using wavelength dispersive spectroscopy (WDS), as hard intermetallic AlMn particles; they were also observed in the extruded rod.
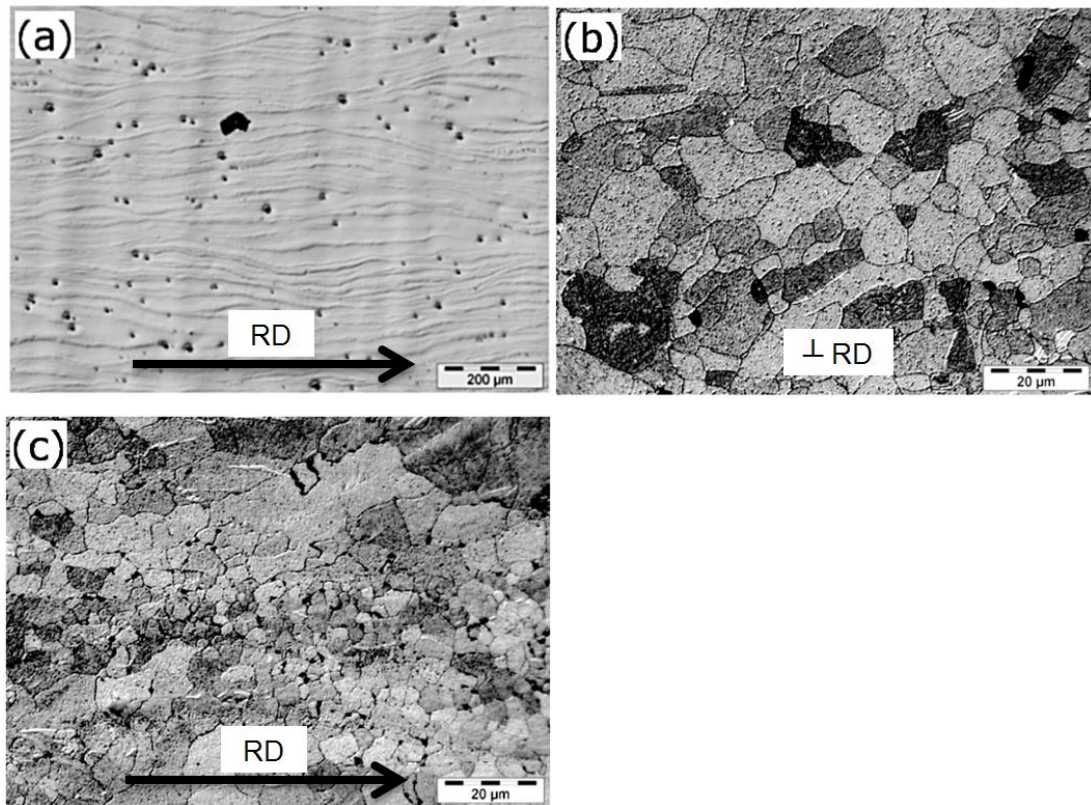
Fig. 3.8. Optical microscope image of the surface on the plane parallel to RD before etching (a), microstructures perpendicular to RD (b) and along RD (c).

Tensile tests carried out along ED and RD showed that the room temperature ductility of the plate was two times larger than that of the rod. However, strength of the rod was 55 MPa higher than the plate. It suggested that the plate could be easier

to process than the rod in terms of temperature and load capacity requirements. The stress-strain curves are displayed in Fig. 3.9.
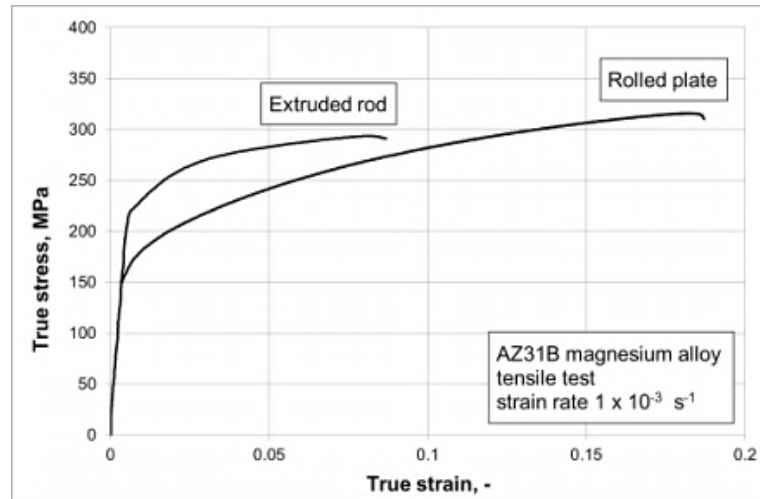
Fig. 3.9. Room temperature tensile stress-strain curves of as-supplied rod and plate

Chapter 4

Formability of AZ31B magnesium alloy bars during I-ECAP

4.1. Introduction

Temperature is a crucial parameter in ECAP of magnesium alloys. Billet failure by segmentation is observed when temperature is too low (Kang et al., 2008). On the other hand, remarkable grain refinement can be achieved only when a heat induced grain growth is suppressed. Recent studies have shown that ECAP temperature can be lowered by:

1) applying back-pressure (Lapovok, 2005),

2) increasing strain rate sensitivity of a material by direct extrusion (Figueiredo et al., 2007),

3) increasing die angle (Figueiredo et al., 2007),

4) decreasing temperature with subsequent passes (Jin et al., 2006; Ding et al., 2008; Biswas et al., 2010),

5) decreasing strain rate (Kang et al., 2008; Bryla et al., 2009),

The first approach was not tried for I-ECAP due to the continuous nature of the process and technical limitations arising from this fact. Die angle and strain rate were kept constant for all conducted experiments. Any change of the die angle would require redesigning of the whole tool assembly and it is one of the recommendations for the future work. Strain rate decrease would extend a processing time and, consequently, process efficiency would be significantly lowered.

The research presented in this chapter was focused on effects of the initial grain size and the processing route on formability of AZ31B magnesium alloy during I-ECAP. The former was indirectly studied in the literature through the application of a gradual temperature decrease procedure (Jin et al., 2006; Ding et al., 2008; Biswas et al., 2010) as the subsequent passes reduced the grain size which enabled further lowering of temperature. The latter was not thoroughly studied in the works dedicated to ECAP of magnesium alloys. A diagram showing the relation between minimum allowable processing temperature and grain size is plotted in this chapter using results of conducted I-ECAP experiments and the selected literature data for ECAP. The effect of processing route on the billet shape and fracture mechanism is studied through experimental work and numerical analysis.

4.2. Experimental procedure

Mechanical testing and microstructural characterisation of the as-supplied materials were conducted prior to processing according to the procedures described in Sections 3.2 and 3.3, respectively. A double-billet variant of I-ECAP, with 90° angle between channels, was realised using the equipment described in detail in Section 3.1. The equivalent strain imposed in each pass was ~1.15; all experiments were run with the same strain rate of ~0.8 s^{-1}. Heating of billets was realised by holding them for 15 minutes prior to processing in the preheated die. The die temperature during processing was kept constant within ±2 °C, based on the readings obtained from a thermocouple located near the deformation zone.

Preliminary experiments showed that lubrication with conventional molybdenum disulfide (MoS_2) grease resulted in material sticking to the die walls. Therefore, composite coating was applied on the billet surface prior to lubrication with MoS_2. The process is classified as a non-chromate conversion coating with precipitation of ceramic phase by sol-gel mechanism (Ostrovsky, 2006). Billet preparation procedure included: 1) surface cleaning, 2) pickling, 3) application of composite coating, 4) lubrication with MoS_2 grease. The process was realised at the Warsaw University of Technology, Poland.

The composite coating layer improved the grease adhesion significantly. However, another solution to friction problem was sought as the application of composite coating was relatively time consuming. Therefore, the graphite-based dry film lubricant Formkote T-50 was sprayed on a billet surface (Fig. 4.1). Before application, the surface was sandblasted to improve adhesion of the lubricant. The surface quality of I-ECAPed billets was very good after both types of lubrication: (1) composite coating + MoS_2 and (2) sandblasting + Formkote T-50.
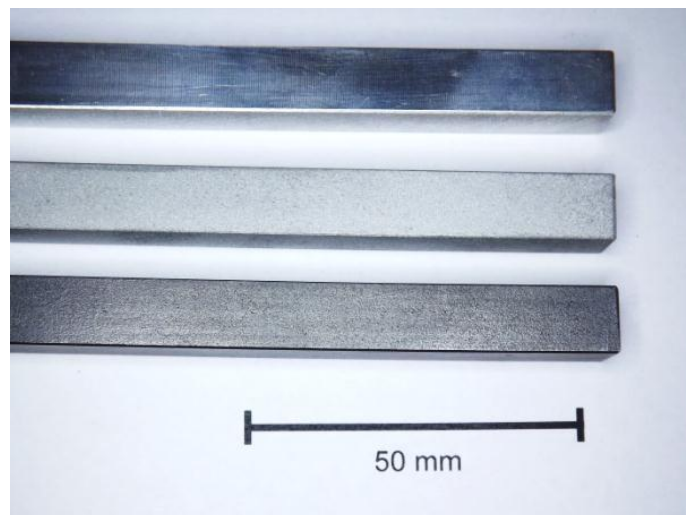
Fig. 4.1. Billets after machining (upper), sandblasting (middle), and sandblasting followed by spraying with Formkote T-50 (lower).

83

I-ECAP experiments were carried out in order to find the lowest possible processing temperature and investigate an influence of the initial grain size and the processing route on formability of AZ31B magnesium alloy. Billets were processed by routes A, B_C, and C at temperatures varying from 125 °C to 250 °C. Four to six passes were planned for each experimental variant. However, fracture occurred before reaching the intended number of passes in some cases.

Table 4.1 shows the experimental plan and the results of the conducted experiments. The effect of temperature on fracture occurrence in the extruded rod was investigated through experiments with samples 1-2, and 7-11 (Table 4.1). Route effects on the billet shape and formability were shown in samples 3-6 and 9-11. The lowest possible temperature of the fine-grained plate was revealed by processing samples 12-15.

Table 4.1. Details of I-ECAP experiments

Sample no.	Material	No. passes	Temperature	Route	Result	Comments
1	Extruded rod	1	200 °C	n/a	✘	Damaged
2	Extruded rod (annealed*)	1	200 °C	n/a	✘	Damaged *Annealed 8 hours at 300 °C
3	Extruded rod	4	4 × 250 °C	A	✔	
4	Extruded rod	4	4 × 250 °C	B_C	✔	
5	Extruded rod	4	4 × 250 °C	C	✔	
6	Extruded rod	5	5 × 250 °C	4 × B_C + A	✔	
7	Extruded rod	3	2 × 250 °C + 1 × 200 °C	B_C	✘	Damaged
8	Extruded rod	3	2 × 250 °C + annealing* + 1 × 200 °C	B_C	✔/✘	Minor cracks *Annealed 8 hours at 300 °C
9	Extruded rod	6	4 × 250 °C + 2 × 200 °C	A	✔	
10	Extruded rod	6	4 × 250 °C + 2 × 200 °C	B_C	✔/✘	Minor cracks
11	Extruded rod	6	4 × 250 °C + 2 × 200 °C	C	✘	Damaged
12	Rolled plate	1	175 °C	n/a	✘	Damaged in 1st pass, fracture lines along rolling direction
13	Rolled plate	4	4 × 200 °C	C	✔	
14	Rolled plate	4	200 °C + 175 °C + 150 °C + 150 °C	A	✔	
15	Rolled plate	4	200 °C + 175 °C + 150 °C + 125 °C	A	✘	Damaged

4.3. Results of I-ECAP experiments

4.3.1. I-ECAP of bars machined from the extruded rod

Square bars machined from the hot-extruded rod of AZ31B were subjected to I-ECAP at 200 °C but the obtained billets were completely damaged (sample 1 in Table 4.1). Therefore, annealing for 8 hours at 300 °C was introduced prior to

processing of sample 2 in order to homogenise the microstructure (~60 μm). However, the applied heat treatment did not improve formability so the final result was the same as for the billets without the annealing step (Fig. 4.2). The processing temperature was increased to 250 °C in the next set of experiments and four passes of I-ECAP were successfully completed using routes A, B_C, and C, which are referred to in Table 4.1 as samples 3, 4, and 5, respectively.
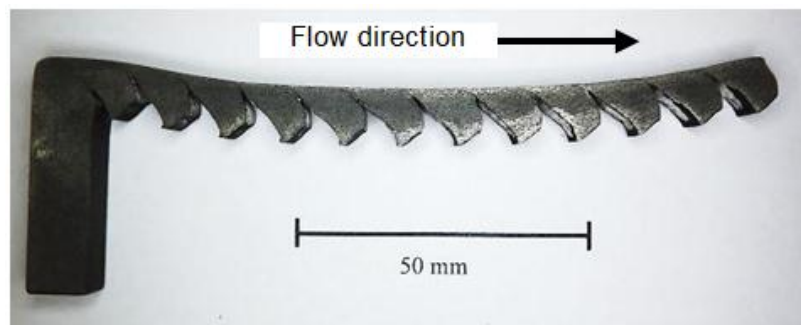
Fig. 4.2. Sample no. 2 after annealing and I-ECAP at 200 °C.

Since a finer microstructure can be produced in magnesium alloys subjected to SPD at lower temperatures, further attempts were made to avoid fracture at 200 °C. The idea was based on the gradual temperature decrease with subsequent passes of I-ECAP. Sample 7 was processed by two passes at 250 °C and third pass was conducted at 200 °C (following route B_C), but large cracks were observed, as displayed in Fig. 4.3. Therefore, an additional annealing step, 8 hours at 300 °C, was introduced for sample 8 after two passes of I-ECAP at 250 °C, which should have resulted in a reduction of internal stresses with a concurrent microstructure homogenisation. Although the grain size was probably finer than in the case of sample 2, small cracks were still observed on the billet surface; therefore, this processing route was classified as unsuccessful as well.
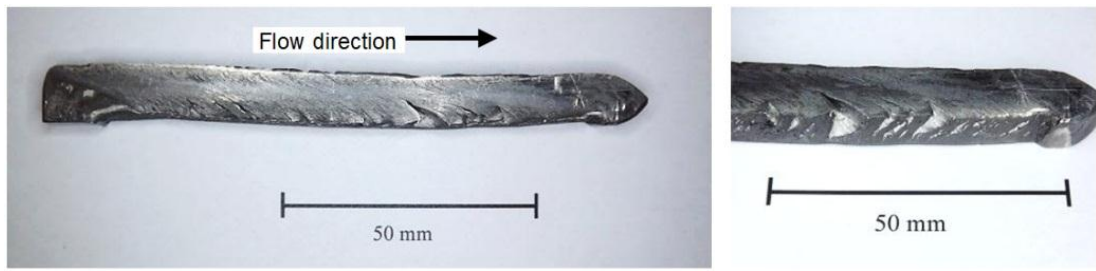
Fig. 4.3. Billet processed by two passes at 250 °C and one pass at 200 °C by route B$_C$ (sample 7).

Samples 9-11 followed 4 passes of I-ECAP at 250 °C to reduce the average grain size to ~6 µm. Then, samples were subjected to another two passes at 200 °C. The obtained results were surprising as billets processed by route A were not fractured while those processed using route B$_C$ exhibited minor cracking in the corner where the material did not fill the exit channel completely. Moreover, some billets subjected to route B$_C$ were completely free from surface cracks even though the same parameters were used. Sample 11, which was pressed by route C, was massively damaged after I-ECAP, as shown in Fig. 4.4.
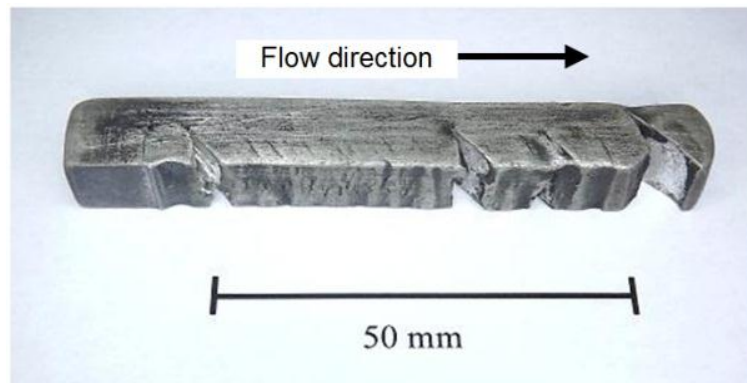
Fig. 4.4. Massively damaged sample 11 after 4 passes at 250 °C and two passes at 200 by route C.

4.3.2. I-ECAP of bars machined from the hot-rolled plate

It was shown for the extruded rods that a finer initial microstructure enabled lowering temperature of I-ECAP. Therefore, another set of experiments was conducted using square bars machined from the hot-rolled plate, which exhibited finer grain structure and greater ductility, compared to the hot-extruded rods. First pass of I-ECAP was conducted at 175 °C on sample 12, but long fracture lines, were revealed nearly parallel to the billet axis, as shown in Fig. 4.5. They could be arising from the bands of small grains observed in the initial sample along RD (Fig. 3.8c). Sample 13 was subjected to four passes of I-ECAP at 200 °C. Route C was chosen for this variant as it has been already shown to be the most prone to fracture. In contrast to the results obtained for sample 11, the processed bars had good surface quality, which proved that a finer grain structure enables reducing temperature of I-ECAP.
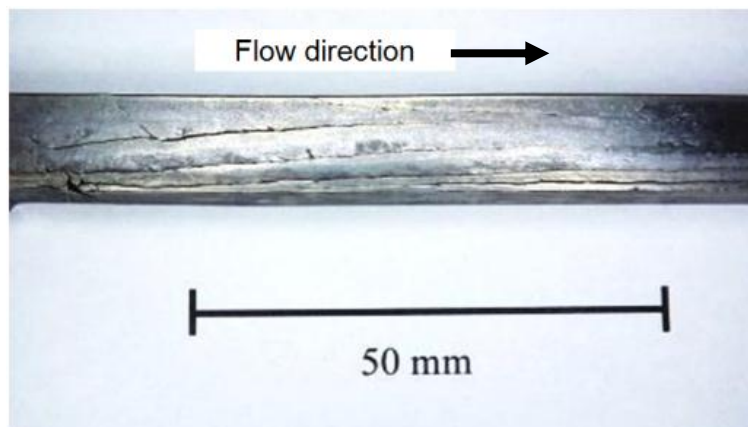
Fig. 4.5. Fracture mechanism in rolled sample subjected to I-ECAP at 175 °C.

The gradual temperature decrease approach was used for samples 14 and 15. In the case of sample 14, temperature was reduced by 25 °C in two steps from initial 200

°C to 150 °C; the fourth pass was conducted again at 150 °C to homogenise the microstructure. Route A was chosen as it has been already shown for sample 9 to be the least prone to fracture. As this approach turned out to be successful, further temperature reduction in the last pass was attempted for sample 15 but massive damage was observed at 125 °C. The billets after fourth pass of I-ECAP at 150 °C and 125 °C are shown in Fig. 4.6.
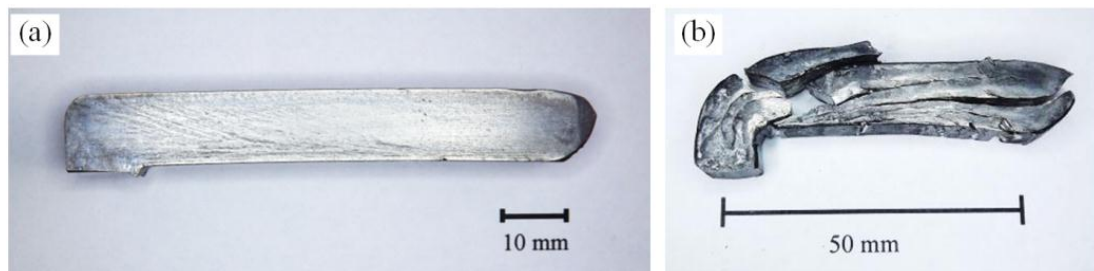
Fig. 4.6. Successful sample 14 after fourth pass of I-ECAP at 150 °C (a) and severely damaged sample 15 after reducing temperature to 125 °C (b).

In some cases, fracture was observed only at the beginning or at the end of a billet, when a gradual temperature reduction was applied (Fig. 4.7a). It could be attributed to a low deformation level occurring in those zones during I-ECAP. The FE simulation results, displayed in Figure 4.7b, showed that equivalent plastic strain in the non-deformed regions was less than 0.15. Therefore, the grain size could not be refined significantly in those regions and they acted often as fracture initiation sites. Such end-effects were not revealed when temperature was kept constant for all passes.
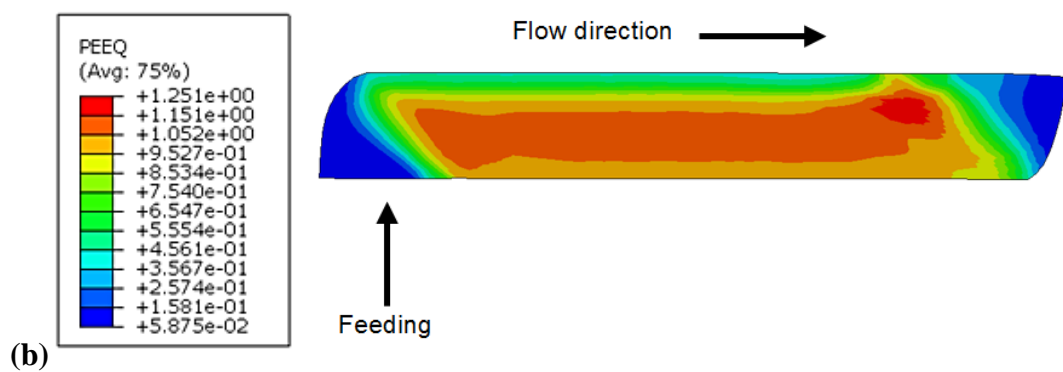
Fig. 4.7. Shear fracture localised at the end of the sample (a) and contours of equivalent plastic strain from FE simulation indicating non-deformed zones after I-ECAP (b).

4.3.3. Summary of the experimental results

The conducted experiments showed that the hot-extruded rod of AZ31B can be processed by I-ECAP at 250 °C without fracture. Temperature reduction to 200 °C was possible only after four passes at 250 °C. Moreover, it was revealed that processing route has the influence on formability during I-ECAP since billets processed by route A showed to be less prone to fracture than those processed by routes B_C and C. The effects of processing route on the billet shape and the occurrence of fracture are described in Section 4.5.

The fine-grained plate was more ductile during I-ECAP at low temperatures than the extruded rod. Thus, it was possible to reduce billet temperature to 150 °C without fracture in third and fourth pass while processing of the rod required four passes at 250 °C to successfully go down to 200 °C in pass five and six. The disadvantage of the gradual temperature decrease procedure is the occurrence of shear failure at the end of a sample arising from an inefficient grain refinement in this region. The problem could have been solved by cutting off the ends of the sample before reducing temperature of I-ECAP.

4.4. Processing window for I-ECAP of AZ31B magnesium alloy

The diagram of allowable processing temperature (Fig. 4.8) was determined on the basis of the obtained experimental results. Fracture is predicted in samples with various grain sizes subjected to I-ECAP with route A since it was shown to be less prone to failure than the others. It is concluded that the initial grain size should be less than 10 µm to conduct I-ECAP at 200 °C, and temperature should be increased to 250 °C for coarse-grained (60-80 µm) samples. The lowest temperature of successful I-ECAP in the current study was 150 °C and it was achieved by earlier processing at 200 °C and at 175 °C. It was shown in the literature that ECAP at 175 °C results in grain refinement to ~1.5 µm (Ding et al., 2009).

The diagram was used to find a relation between the initial average grain size and the lowest allowable processing temperature. It was noticed that the best fitting between grain size and temperature can be obtained by using a logarithmic equation given by:

$$T \geq A \ln(d) + B, \tag{4.1}$$

where: T – allowable temperature in I-ECAP, d –initial average grain size, expressed in μm, A, B – empirical coefficients obtained from experiments, which are: A=27.03 and B=140.72.
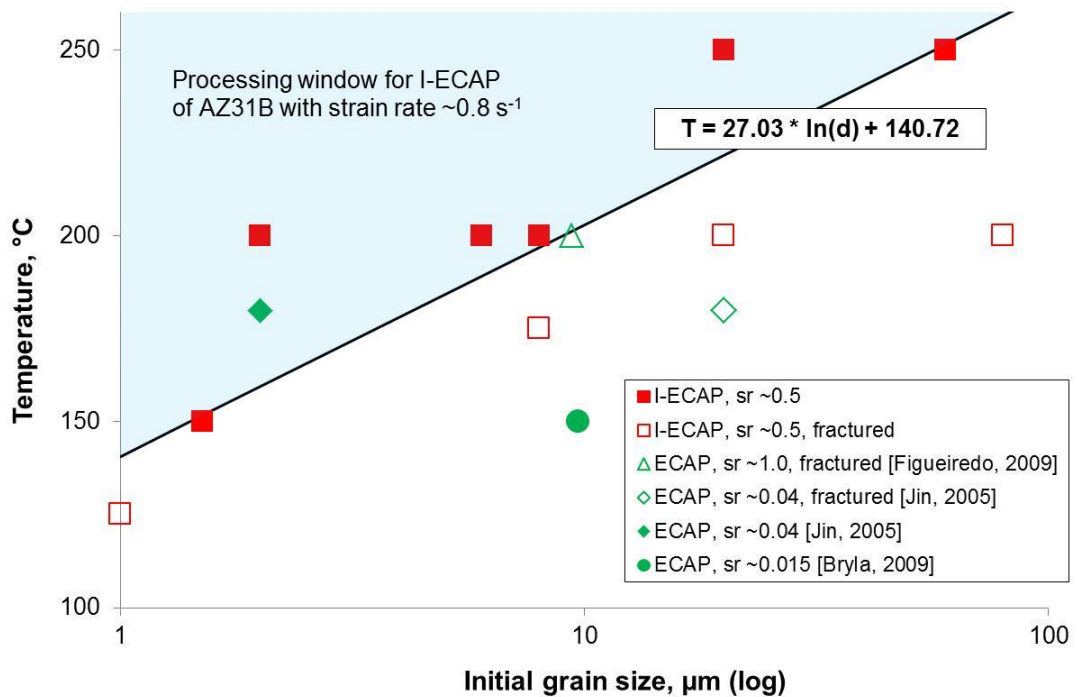
Fig. 4.8. Diagram of allowable processing temperature obtained from I-ECAP (route A) experiments of AZ31B with strain rate ~0.8 s⁻¹. Experimental results of ECAP derived from literature are plotted for comparison. Filled marks represent successful pressing, while hollow marks indicate fracture. In the chart legend, 'sr' is strain rate expressed in s⁻¹, 'T' is temperature and 'd' is the average grain size.

The curve defined by equation (4.1) determines the window of allowable processing parameters for I-ECAP with strain rate ~0.8 s⁻¹. The experimental results were compared with data obtained for conventional ECAP (Jin et al., 2005; Bryla et al., 2009; Figueiredo and Langdon, 2009a). Most of the results are consistent with the

findings of the current research. However, ECAP with the very low strain rate ($\sim$0.015 s^{-1}) was carried out without the occurrence of fracture at temperature as low as 150 °C using a sample with the initial grain size 9.7 µm (Bryla et al., 2009). On the other hand, fracture of a billet with the initial grain size 9.4 µm subjected to ECAP at 200 °C and strain rate $\sim$1.0 s^{-1} failed by segmentation (Figueiredo and Langdon, 2009a). It shows that the curve defined by equation (4.1) could be moved down on the diagram for the strain rates lower than 0.8 s^{-1} but strain rate increase would shift it towards higher values.

4.5. Route effects on billet shape and fracture

4.5.1. *Shapes of billets*

Significant differences in the shapes of billets machined from the extruded bars and subjected to various routes of I-ECAP were observed (Fig. 4.9). The material completely filled the exit channel when billets were processed by route A while rotation by 180° and 90° resulted in an incomplete filling of the exit channel and, as a consequence, asymmetrical shapes of the billets. The height of the billet subjected to route C was 9 mm (Fig. 4.9c), compared with 10 mm obtained using route A (Fig. 4.9a). An asymmetrical billet shape was also observed for sample 4 (in Table 4.1), which was rotated by 90° around its axis after each pass. The sample height was non-uniform along cross-section and was varying from 7.5 to 9 mm (Fig. 4.9b).
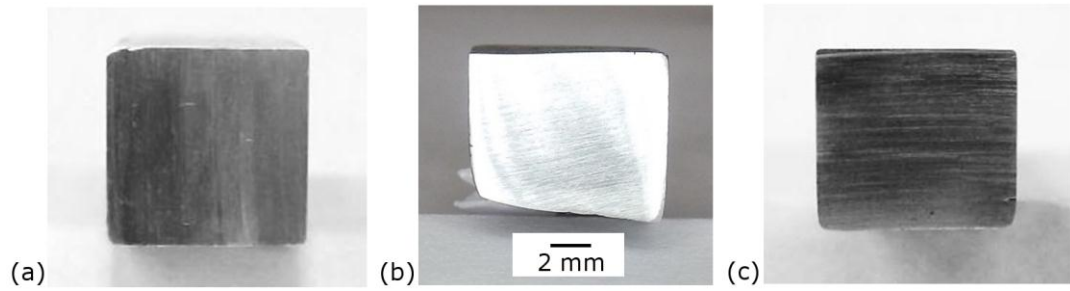
Fig. 4.9. Cross-sections of the billets processed by routes A (a), B_C (b), and C (c) of I-ECAP. Billet width is 10 mm in each case. The scale bar was drawn for all images.

Distinctive flow pattern (curved lines) was observed on a billet surface after four passes by route B_C (Fig. 4.10). It indicates that the material flow velocity is non-uniform along longitudinal direction of the billet. The fact that such lines were not revealed after processing by routes A and C confirms that their occurrence is related to the applied rotation of the billet. The differences in lengths of the billets showed in Fig. 4.10 are caused by their different cross-sectional dimensions. The billet which did not fill the exit channel completely is the longest, accordingly to the law of volume conservation. Described distortions of billets' shapes were not reported before in the literature after conventional ECAP. An explanation of this phenomenon is proposed in this work and it can be found in Section 4.5.2.
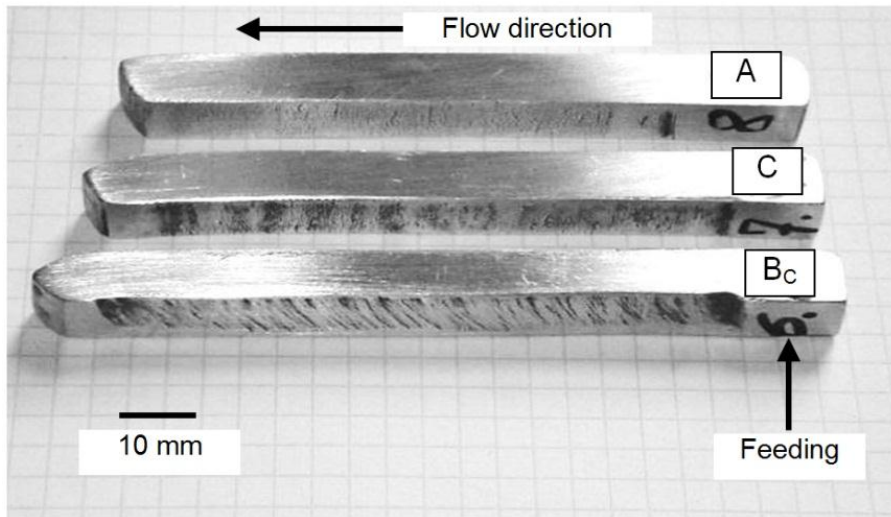
Fig. 4.10. Billets processed by various routes of I-ECAP at 250 °C.

In order to reduce the asymmetry of the billet processed by route B_C, a combination of routes B_C and A was applied (sample 6 in Table 4.1). The billet was subjected to four passes at 250 °C using route B_C. Tensile tests showed that true strain at fracture was increased from ~0.09 to ~0.23. Additional pressing, without any rotation after fourth pass, was conducted at the same temperature. The gap observed in sample 4 was reduced from 2.5 to 0.2 (Fig. 4.11), which showed that distortion of the billet shape observed after processing by route B_C can be almost completely suppressed by only one pass of I-ECAP via route A. However, true strain at fracture was decreased for sample 6 from ~0.23 to ~0.11. It is apparent from Fig. 4.11b, that mechanical properties of the sample processed by four passes using route B_C with additional pass without any rotation were very similar to the sample after four passes with route A. It clearly shows that the last rotation has the strongest influence on the mechanical properties of AZ31B magnesium alloy subjected to I-ECAP.
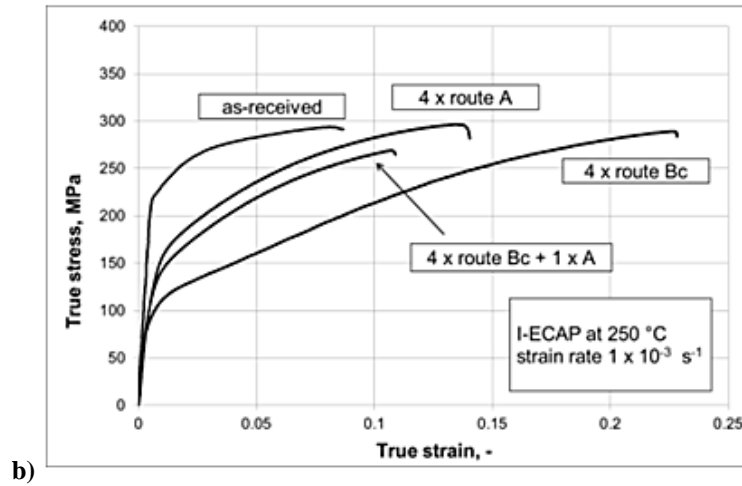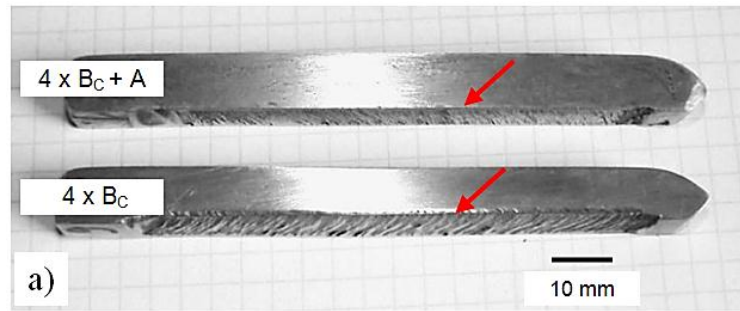
Fig. 4.11. (a) Billet processed by four passes using route B$_C$ (lower) and with one additional pass without any rotation (upper); arrows indicate the gap between the lower surface of the billets and the die. Tensile strain-stress curves of billets subjected to different sequences of rotations are shown in (b).

4.5.2. Numerical prediction of billet shape

Plane strain FE simulations performed by Figueiredo et al. (2007) have already shown that strain rate sensitivity of magnesium alloys can be responsible for the incomplete material filling of the exit channel during ECAP. In order to investigate the effect of strain rate sensitivity on a billet shape during I-ECAP, FE simulations with a strain rate dependant yield stress model were run. The Johnson-Cook model (Johnson and Cook, 1983) was used to describe material behaviour during plastic

96

deformation. The general idea of the model is that equivalent plastic strain rate is related to the ratio of the yield stress at nonzero strain rate to the static yield stress. The yield stress is given by the following equation:

$$\sigma = \sigma^0 \left[1 + C \ln \left(\frac{\dot{\varepsilon}^{pl}}{\dot{\varepsilon}_0} \right) \right], \qquad\qquad (4.2)$$

where, $\dot{\varepsilon}^{pl}$ is equivalent plastic strain rate given by the Johnson-Cook model, $\dot{\varepsilon}_0$, equal to 0.01, is a constant equivalent plastic strain rate corresponding to the static deformation conditions, σ^0 is a static yield stress, σ is yield stress at nonzero strain rate and C is a material constant.

The effect of heat generation within a billet due to plastic deformation was investigated in order to estimate its effect on billet temperature. Readings from a thermocouple located 15 mm from the deformation zone (side wall of the die) have not shown any temperature fluctuations greater than ±1 °C. If the temperature increase within the billet was significant, it should have been captured by the thermocouple. It should be also emphasised that the processes is relatively slow as each cycle takes 2 seconds (frequency of punch movement 0.5 Hz) and the time of plastic deformation is even less than 0.5 second while the rest of time is consumed by material feeding and punch movement; therefore, there is enough time to stabilise temperature within the billet. Additionally, it was already reported for aluminium and steel that temperature increase within the billet is negligible if pressing velocity is low (Quan et al., 2009). It is concluded that a large volume of the die and the surrounding pre-stressing ring (diameter 280 mm and height 60 mm) is capable of absorbing heat generated within the billet and temperature is stable.

FE simulations of I-ECAP were performed in order to estimate temperature increase due to adiabatic heating and stabilisation of temperature attributed to heat exchange between the billet and the die. Two-dimensional coupled stress-thermal analysis was performed in Abaqus/Explicit ver. 6.10. Simulations were run with an isotropic von Mises material model sensitive to strain rate and temperature changes (Fig. 4.12a); flow stress curves were derived from the literature (El Mehtedi et al., 2007). Thermal properties of AZ31B alloy were as follows: conductivity 156 W/mK and specific heat capacity 1017 J/kgK. Heat exchange coefficient on a billet–die interface was assumed to be 11 kW/m^{2}K, the same as in the FE simulation of extrusion performed by Cyganek and Tkocz (2012). Fraction of energy generated by inelastic deformation transformed to heat was 0.9. Initial temperature of the billet and the dies was 250 °C. Temperature increase within the dies due to contact with the billet was not taken into account since they were modelled as analytical rigid objects. It is a reasonable assumption since temperature increase was not recorded by the thermocouple located close to the die wall. Friction effects were assumed to be negligible in this process.

The results of FE simulations carried out for adiabatic conditions showed that temperature could increase from 250 °C to 323 °C when no heat exchange is assumed. Temperature field obtained from the simulation (Fig. 4.12b) coincides with distribution of plastic strain (Fig. 4.12c) as temperature increase is proportional to plastic work, which is related to equivalent stress and equivalent plastic strain. The temperature decrease in adiabatic conditions is significant; however, when a heat transfer between the billet and the dies is taken into account, temperature within the billet is much lower. When the upper die plastically deforms the billet, temperature increase is observed in the deformation zone (Fig. 4.12d).Then, heat is transferred to

the dies during material feeding; therefore, temperature is slightly higher in the regions which are not in contact with the dies (Fig. 4.12e). The most important conclusion from those simulations is that temperature increase during both stages, deformation and feeding, is less than 2 °C. Additionally, a heat exchange on interface between the billet and side walls of the die was not modelled as 2D simulations were run, which even overestimates temperature increase. The effect of adiabatic heating was shown to be negligible by experimental observations and numerical analysis; therefore, isothermal conditions were assumed in simulations investigating an effect of strain rate on material flow behaviour.

(a)

(b)

(c)

(d)

(e)
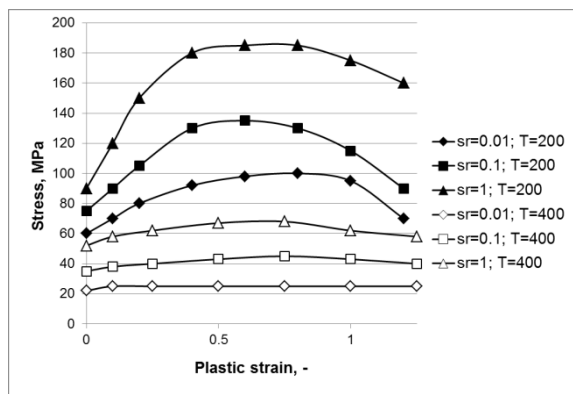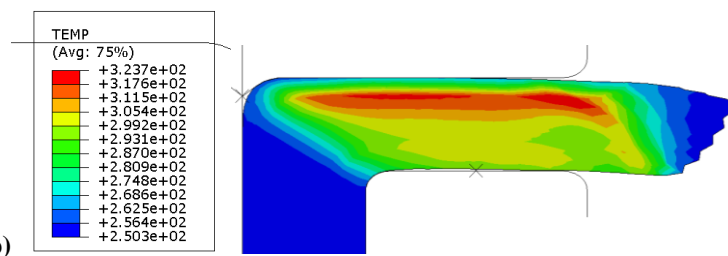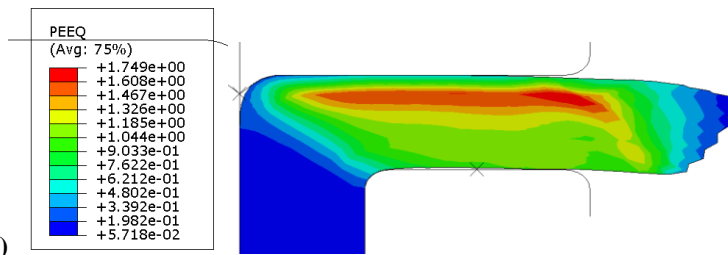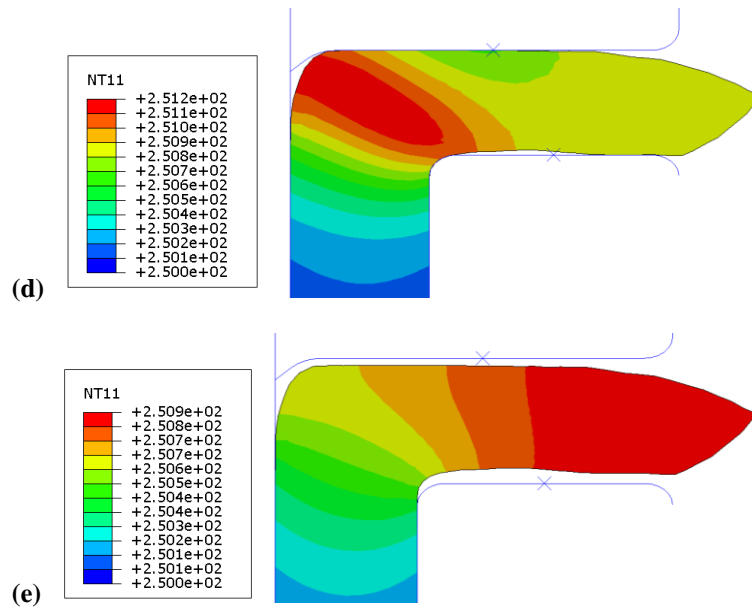
Fig. 4.12. (a) Flow stress-strain curves used in the coupled stress-thermal FE analysis, based on the experimental data from the work by El Mehtedi et al. (2007). FE simulation results for adiabatic conditions: (b) temperature and (c) equivalent plastic strain. Temperature field from the coupled thermal-stress analysis with incorporated boundary condition of heat exchange during (d) deformation and (e) feeding.

In order to investigate an effect of strain rate on material behaviour, plane strain simulations with various *C* parameters were performed in ABAQUS/Explicit commercial FE software (ver. 6.10). Contact between billet and dies was defined by the Coulomb model with friction coefficient 0.1. Flow behaviour in the static condition was described by an isotropic strain hardening model. The yield stress curve, obtained in uniaxial compression test at 250 °C and strain rate 0.01 s^{-1}, was derived from the work by Fatemi-Varzaneh et al. (2007), the data were introduced into FE model in tabular form (discrete points). A decrease in yield stress starting at strain ~0.15 (Fig. 4.13) is attributed to dynamic recrystallisation occurring in

magnesium alloys above 200 °C. Isothermal conditions were assumed in the performed simulations.
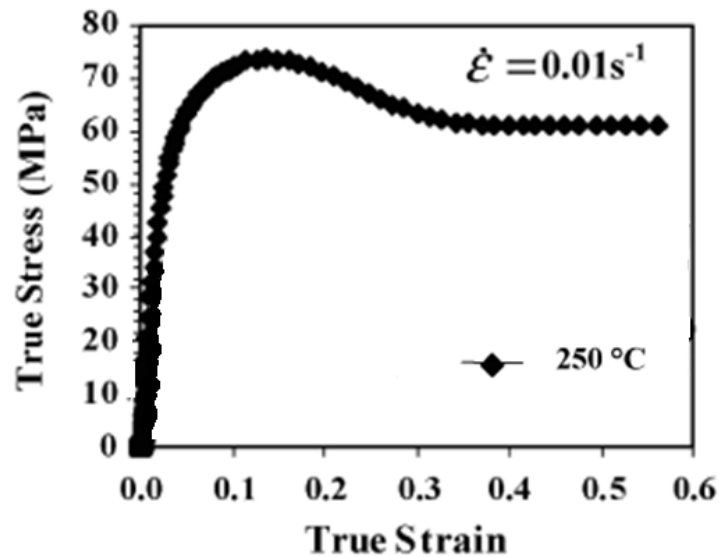
Fig. 4.13. Flow stress curve obtained at 250 °C used in FE simulations. Image was taken from the work by Fatemi-Varzaneh et al. (2007).

Modelling results for C equal to 0, 0.5, and 1.0 were compared with the billet shape after first pass of I-ECAP (Fig. 4.14). It was assumed that strain rate sensitivity can be estimated by measuring a distance between the upper flat surface and billet nose (Figueiredo et al., 2007); the distance increases with the C value rising. It is apparent from Fig. 4.14 that the billet shape prediction made by FE simulation is the most accurate for $C = 0.5$.
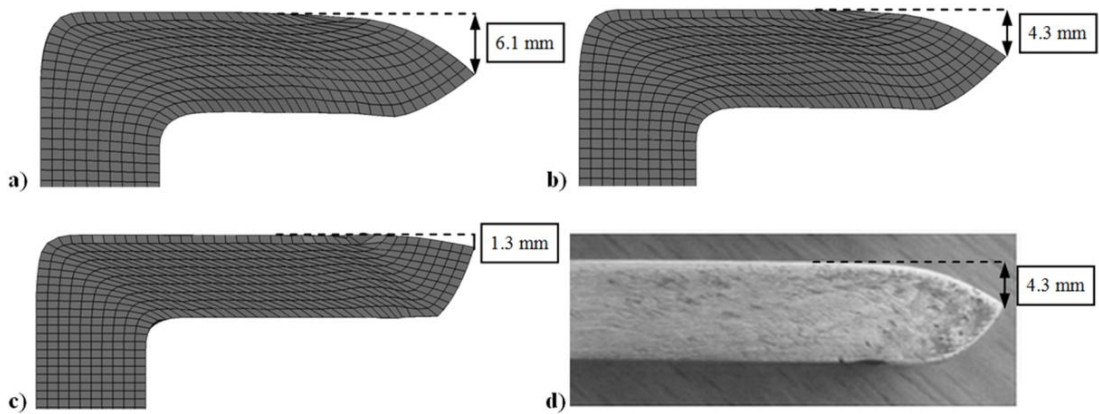
Fig. 4.14. Strain rate sensitivity effect on sample shape; FE modelling results for different C values: 1.0 (a), 0.5 (b), 0 (c) and specimen after first pass of I-ECAP (d).

Distributions of equivalent plastic strain for the strain rate sensitivity $C = 0.5$ and $C = 0$ are shown in Fig. 4.15a. Strain profile along a transverse path is plotted in Fig. 4.15b. Strain localization is observed for the strain rate sensitive material while more uniform strain distribution is characteristic for a strain rate independent flow. Starting from 2 mm below the upper surface, strain value for $C = 0$ is 1.2 ± 0.05. The strain distribution is less uniform when C is increased to 0.5. The maximum value 1.4 occurs 2-3 mm below the upper surface and falls down to 1.1 at the bottom surface.

b)
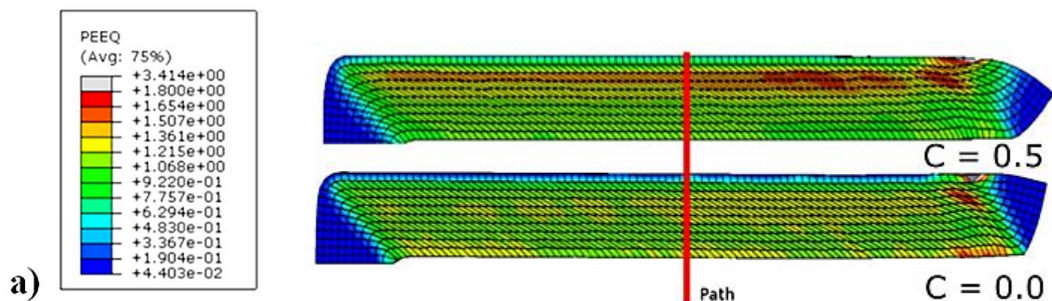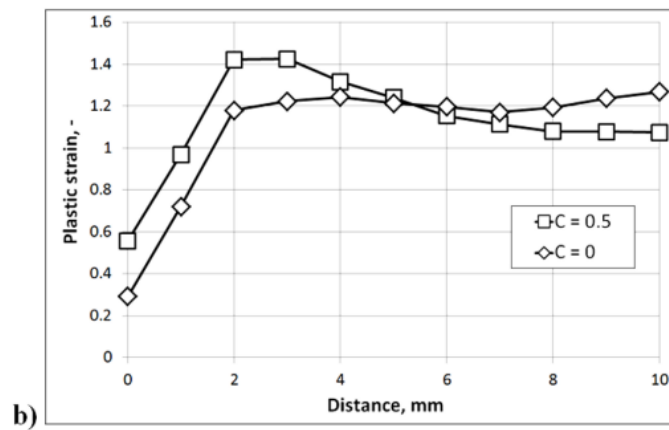
Fig. 4.15. Equivalent plastic strain distribution for C = 0.5 and C = 0 (a) and strain profile along a transverse path (b).

The billet distortion after processing by route B_C presented in Fig. 4.9b and 4.10 indicates that flow behaviour cannot be described using a 2D analysis. Therefore, a three-dimensional FE model of I-ECAP was developed in order to find an explanation for the observed cross-sectional asymmetry (Fig. 4.9b) and flow lines on the bottom surface (Fig. 4.10). It was assumed that non-uniform strain distribution in the billet (Fig. 4.15) led to non-uniform mechanical properties. After the first pass of I-ECAP, the maximum strain was localised 2 mm from the upper surface. Thus, it was concluded that an upper part of the billet exhibited different mechanical properties from the lower part. Higher strain introduced in the centre of the upper part could result in a smaller grain size, which favours formation of high angle grain boundaries that facilitate diffusion processes (Fujita et al., 2004) and lower the force needed to deform material at elevated temperature. This effect can be observed when comparing the load readings from first and fourth pass of I-ECAP; it is clear that the force is reduced with subsequent passes (Fig. 4.16).

103
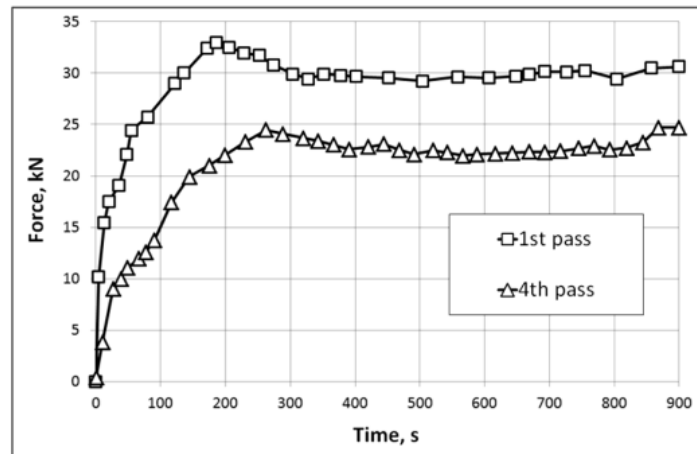
Fig. 4.16. Force readings during first and fourth pass of I-ECAP by route B$_C$.

Therefore, after the first pass the upper part of the billet could be 'softer' than the lower one, assuming deformation at an elevated temperature. Rotation by 90° changes the softer/harder orientation from upper/lower to right/left. In other words, properties near the left side wall of the die are different from properties near the right side. It explains why distortion is observed only when rotation 90° is applied and is not seen for routes A and C.

FE simulations were run using an isotropic material definition to verify the proposed interpretation. The billet was divided into two parts of the same volume by a plane parallel to the extrusion direction (Fig. 4.17). Different material models were ascribed to each part. After rotation by 90°, the right part had the yield stress 30% lower than the left part due to strain inhomogeneity arising from the previous pass. The FE results showed that the proposed approach explains the occurrence of flow

lines on the bottom surface of the billet (Fig. 4.10) but it is not able to predict a gap in the billet corner (Fig. 4.9b).
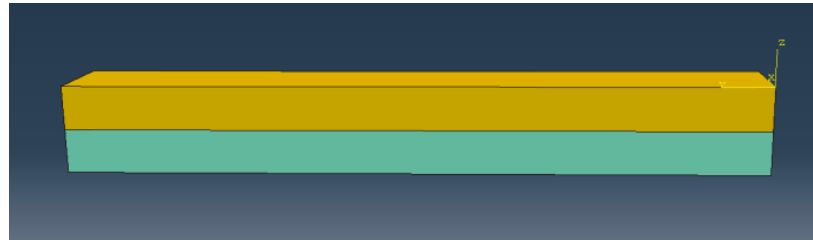
Fig. 4.17. Billet divided in ABAQUS/CAE into two sections with different material properties.

The obtained results confirmed that a more advanced material model is required to fully explain the observed phenomena. Therefore, it was considered that non-uniform grain size distribution arising from the inhomogeneous strain field in the previous I-ECAP pass could lead to different strain rate sensitivity in the upper and the lower part of the billet.

Despite a possible non-uniform grain size distribution in the billet cross-section giving a reasonable explanation for the inhomogeneous mechanical properties, it was not confirmed experimentally. The optical microscope images taken in the lower and the upper part of the billet cross-section showed that the difference in grain size was within 1 μm. Therefore, it is very unlikely that it could significantly influence mechanical properties since a difference of at least few microns is required to notice changes in strain rate sensitivity at elevated temperature (Panicker and Chokshi, 2011).

Another explanation for the occurrence of inhomogeneous mechanical properties in the billet cross-section was based on the textural changes introduced by ECAP (Ding

et al., 2008). Strong texture produced during ECAP indicates that crystallographic orientations of grains are significantly changed after processing. The effects of strain level and loading direction on a grain rotation are also one of the assumptions of crystal plasticity modelling (Mayama et al., 2011). Thus, it is postulated in this work that non-uniform deformation caused different grain reorientations in the upper and the lower parts of the billet which led to different strain rate sensitivities. A counterargument could be stated that strain non-uniformity arising from the first pass is suppressed by subsequent passes. However, it was already shown that the last rotation has the strongest effect on mechanical properties and a billet shape (Fig. 4.11). Hence, it is concluded that non-uniform properties were generated each time billet was rotated by 90°.

To implement the above considerations in FE simulation, the two parts of the billet were assumed to exhibit a different yield stress dependence on strain rate; equation (4.2) was used to describe this relation. It was assumed that the left part had higher strain rate sensitivity ($C = 2$) than the right one ($C = 0.1$). The proposed model was capable of predicting a gap in the billet corner (detail A' in Fig. 4.18c) as well as flow lines on the billet surface (Fig. 4.18d). It should be noted here that the effect of texture on strain rate sensitivity was not confirmed in this work experimentally due to difficulties with sample preparation for EBSD, which was attributed to a high level of deformation introduced during I-ECAP. However, the obtained numerical results showed that the model gives a reasonable explanation of the observed phenomenon.
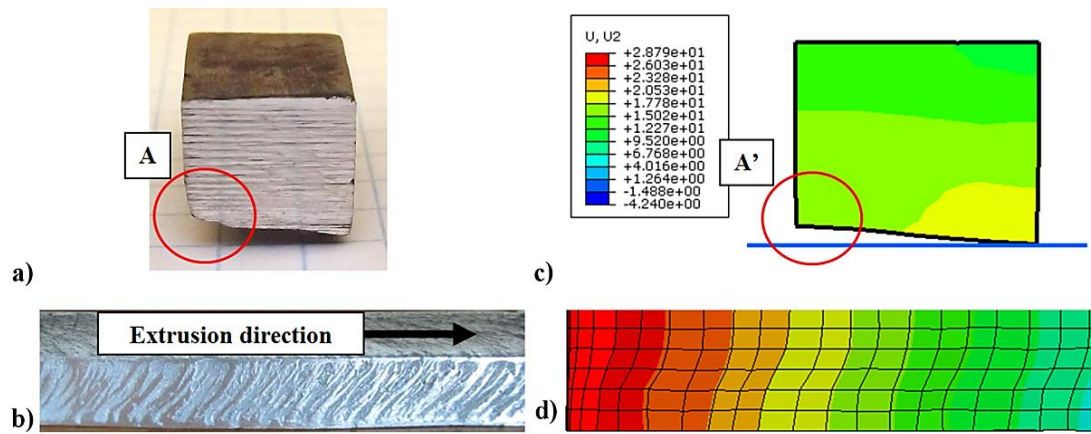
Fig. 4.18. Billet processed by route B$_C$ of I-ECAP: cross-section view (a) and a bottom surface with flow lines (b); corresponding FE simulation results of displacement in the transverse cross section (c) and along the extrusion direction (d).

4.5.3. Fracture

It was already shown in Section 4.3.1 that billets processed by route B$_C$ were more prone to failure comparing to route A. Moreover, the locations of the fracture initiation points were different for both routes. In the case of routes A and C, previously extruded billets underwent damage by segmentation during I-ECAP, which is the same mode as reported by Kang et al. (2008). However, it is apparent from Fig. 4.19a that fracture was initiated in a billet's corner where the material did not fill the exit channel completely in the case of billet processed by route B$_C$. Then, it propagated towards the billet centre along shear planes arising from I-ECAP.

The described mechanism of damage was not reported before for conventional ECAP; therefore, an FE simulation was used in this work to explain the observed phenomenon using the developed model, which takes into account inhomogeneity of mechanical properties arising from the previous I-ECAP passes. It is well established that the occurrence of fracture during metal forming is related to a stress field within

a billet. The most common fracture criteria predict material damage in zones dominated by a tensile stress. Therefore, distribution of pressure was studied in the cross-section of a billet processed by I-ECAP using FE simulation (Fig. 4.19b). Pressure is varying on the cross-section from -55 MPa to 60 MPa, where negative pressure indicates tensile stress. It is apparent that the highest negative stress is observed on the billet surface which is not in contact with the die. In contrast, a positive value of stress is seen in the corner, where the material fills the exit channel.

It is concluded from the performed FE simulations that the highest likelihood of fracture occurs in the corner where the material did not fill the exit channel completely. Thus, a direct relation between the distortion of billet shape and fracture mechanism is revealed. The observation that incomplete channel filling during processing by route B_C causes fracture can be also related to route C since it was proved experimentally in this work that the gap between the die and the lower surface of a billet was about 1 mm (Fig. 4.9c). Therefore, it can be concluded that incomplete filling of the exit channel leads to earlier fracture in the case of routes B_C and C.

a)

S, Pressure
(Avg: 75%)
+3.328e+02
+7.000e+01
+5.864e+01
+4.727e+01
+3.591e+01
+2.455e+01
+1.318e+01
+1.818e+00
-9.545e+00
-2.091e+01
-3.227e+01
-4.364e+01
-5.500e+01
-7.508e+01

b)
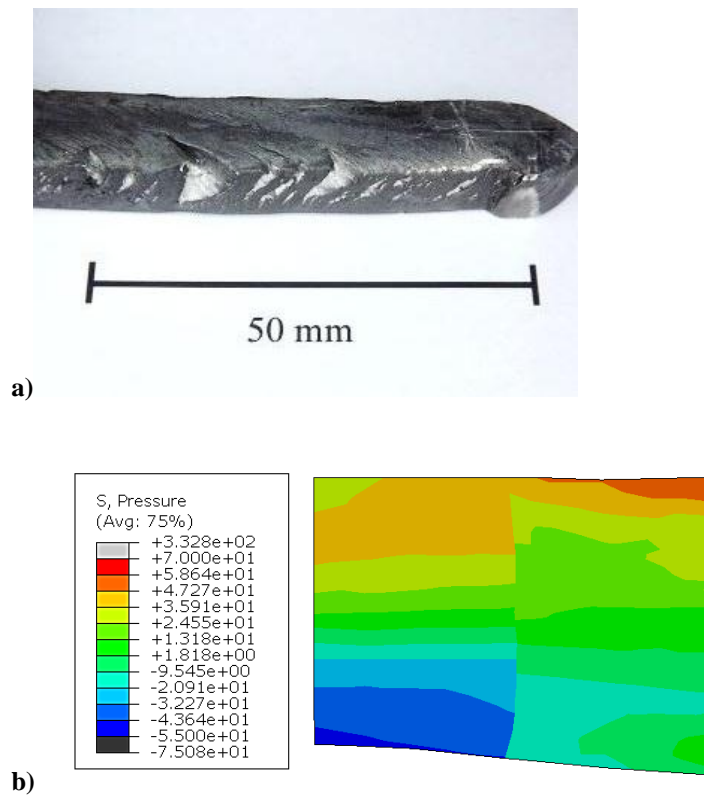
Fig. 4.19. Sample damaged after processing by four passes of I-ECAP using route B_C (a) and pressure field (mean stress) in the billet cross-section obtained from FE simulation.

4.6. Summary

Formability of AZ31B magnesium alloy during I-ECAP was investigated in this chapter. The effects of temperature, initial grain size, and processing route were studied experimentally. I-ECAP trials were conducted using materials with different initial grain sizes at temperatures within the range 125-250 °C. The processing routes known in the literature as A, B_C, and C were applied to investigate their effect on formability.

The results of experiments were used to plot a diagram of the process temperature vs. grain size for I-ECAP of AZ31B magnesium alloy (using route A). A mathematical relation between the initial grain size and the minimum allowable processing temperature was found. It was also revealed that temperature of I-ECAP can be reduced to 200 °C and 150 °C when the average initial grain size is as small as ~10 µm and ~1.5 µm, respectively. The results plotted on the diagram showed a good agreement with the literature data for conventional ECAP with similar strain rates.

Processing by I-ECAP with different routes showed that routes B_C and C are more prone to fracture than route A. The asymmetrical shape of a billet processed by route B_C, not reported before after ECAP, was also displayed in this chapter. The observed distortion was explained by an inhomogeneous strain rate sensitivity arising from a non-uniform strain distribution. The proposed interpretation was supported by FE simulation using a strain rate sensitive material model. The developed numerical model also predicted the location of the fracture initiation zone in a billet.

Chapter 5

Mechanical properties and microstructures of magnesium alloy bars processed by I-ECAP

5.1. Introduction

Due to a low formability of magnesium alloys, ECAP is usually realised at elevated temperatures. A typical processing temperature varies from 175 °C to 250 °C; the lower the temperature the smaller the grain size obtained. The average grain size reported for different conditions was: 1 μm at 150 °C (Bryla et al., 2009), 2 μm at 200 °C (Jin et al., 2006) and 6 μm at 250 °C (Seipp et al., 2012). In order to enable further grain refinement, the processing temperature must be decreased along with a simultaneous decrease of strain rate to avoid fracture. Different experimental plans were proposed in order to conduct ECAP at temperatures lower than 200 °C without crack occurrence. They are based on the concept of gradual temperature decrease with subsequent passes (Jin et al., 2006; Ding et al., 2008; Biswas et al., 2010). The smallest reported grain size obtained using this method was equal to 0.37 μm at the final temperature 115 °C (Ding et al., 2008).

In contrast to fcc metals, yield stress of magnesium alloys is usually decreased by ECAP processing. The inverse Hall-Patch effect, a negative slope of yield stress versus inverse mean grain size, was reported for ECAPed AZ61 (Kim et al., 2002). The yield strength decrease with subsequent passes of ECAP was also shown by Masoudpanah and Mahmudi (2010) and Seipp et al. (2012). A significant strength improvement of AZ31 magnesium alloy (0.2% proof strength equal to 372 MPa) was

reported only for grain size smaller than 1 μm (Ding et al., 2008). Mukai et al. (2010) reported similar properties (yield stress ~400 MPa) for the mean grain size 1.5 μm after multi-directional rolling. Ductility of magnesium alloys is usually enhanced by ECAP. Additionally, maximum elongation can exceed 40% after ECAP followed by annealing (Mukai et al., 2001).

In this chapter, the effects of temperature and processing route of I-ECAP on mechanical properties, grain size, and texture of AZ31B magnesium alloy are investigated. Microstructural characterisation of tensioned and compressed coarse- and fine-grained samples was performed in order to determine a dominating deformation mechanism. The tension-compression yield stress asymmetry of coarse- and fine-grained material was also studied. Additionally, the influence of texture on the twinning activity in fine-grained samples obtained by various routes of I-ECAP and subjected to side compression was shown. The effect of heat treatment after I-ECAP on grain size and mechanical properties was also investigated. Finally, a numerical model was developed to verify if microstructure evolution during subsequent passes of ECAP/I-ECAP can be predicted using equations usually used to simulate dynamic recrystallisation.

5.2. Experimental procedure

Initially, mechanical properties and microstructures of as-received materials were examined; the results are shown in Section 3.4. Then, bars machined along extrusion direction (ED) from hot-extruded AZ31B were subjected to I-ECAP at 250 °C using different routes. Billets processed by routes A, B_C, and C are referred to in Table 4.1

as samples 3, 4, and 5, respectively. Microstructural and textural characterisations of fine-grained specimens were performed after four passes of I-ECAP.

Samples 9-11 were subjected to four passes of I-ECAP at 250 °C with various routes (as shown in Table 4.1) and two additional passes at 200 °C to investigate the effect of temperature decrease on mechanical properties and microstructure. The same processing route was kept for all six passes. Results are presented only for samples processed via routes A and B_C since sample 11 was severely damaged. In order to study the effect of temperature decrease during processing by route C, a billet machined from the rolled plate was subjected to four passes of I-ECAP at 200 °C. Temperature decrease to 150 °C without fracture was also possible only for the rolled plate. Mechanical properties and microstructure were examined after the following procedure: one pass at 200 °C, one pass at 175 °C, and two passes at 150 °C.

Microstructures of the coarse-grained extruded sample and the fine-grained samples 9-11 were characterised *ex situ* after tension and compression tests to study the effect of grain size on the deformation mechanism. Mechanical tests were carried out along ED. Images were taken in the region of uniform deformation in samples tested to fracture in tension. Compression tests were stopped after reaching true strain of 0.1±0.01. Specimens for microstructural characterization were cut out from the middle of the deformed compression samples. The tensile and compression samples were characterised on the planes parallel to the direction of tension and compression, respectively.

The effect of heat treatment on microstructure and mechanical properties was studied using samples 5, 13, and 14 (Table 4.1), which were processed at 250 °C, 200 °C,

and 150 °C, respectively. The different processing temperatures resulted in different average grain sizes varying from ~1 μm to ~6 μm. The specimens were kept in the furnace for 6 hours at 300 °C. Additionally, billet processed by four passes of I-ECAP via route A was subjected to the same heat treatment to investigate the effect of annealing on flow behaviour in compression.

5.3. Mechanical properties

5.3.1. Mechanical properties after various routes of I-ECAP

The influence of the I-ECAP processing route on mechanical behaviour of magnesium alloy AZ31 B is shown in Fig. 5.1. Samples 3-5 (Table 4.1), processed by routes A, B_C, and C are referred to in this section as A, B, and C, respectively. The as-received extruded sample is referred to as AR. True tensile strain-stress curves are plotted in Fig. 5.1a. The failure strain was increased from the initial value of 0.09 reported for the extruded rod, irrespectively of the route used. However, ductility enhancement for sample A was less effective than for sample B and C. Tensile strain at failure increased by 55%, 156%, and 155% for routes A, B_C, and C, respectively. Thus, processing by routes B_C and C had the same effect on the ductility enhancement at room temperature. Using different processing routes had only a limited effect on tensile strength of the material. True tensile strength was 290±5 MPa for sample AR as well as for A and B samples. However, tensile strength decreased to 262 MPa for sample C. Yield stress decreased from initial 220 MPa to 135 MPa for sample A. Increase in tensile ductility reported for samples B and C came along with yield stress decrease to 80 MPa and 60 MPa, respectively.

Results of compression tests carried out at room temperature are shown in Fig. 5.1b. It is apparent from the presented plot that the shape of the flow stress curve strongly depends on the processing route. A concave shape of the flow stress curve is observed for the extruded rod as well as billet processed by route A. Similarly to tensile tests results, yield stress was decreased after I-ECAP by approximately 50 MPa compared to AR sample. A remarkable ductility enhancement was reported for routes B_C and C, compressive true strain at failure was increased from 0.13 to 0.2±0.02. Moreover, a convex shape of the flow stress curves and decreased strain hardening rate were observed for samples B and C, compared to samples AR and A.

(a)

(b)
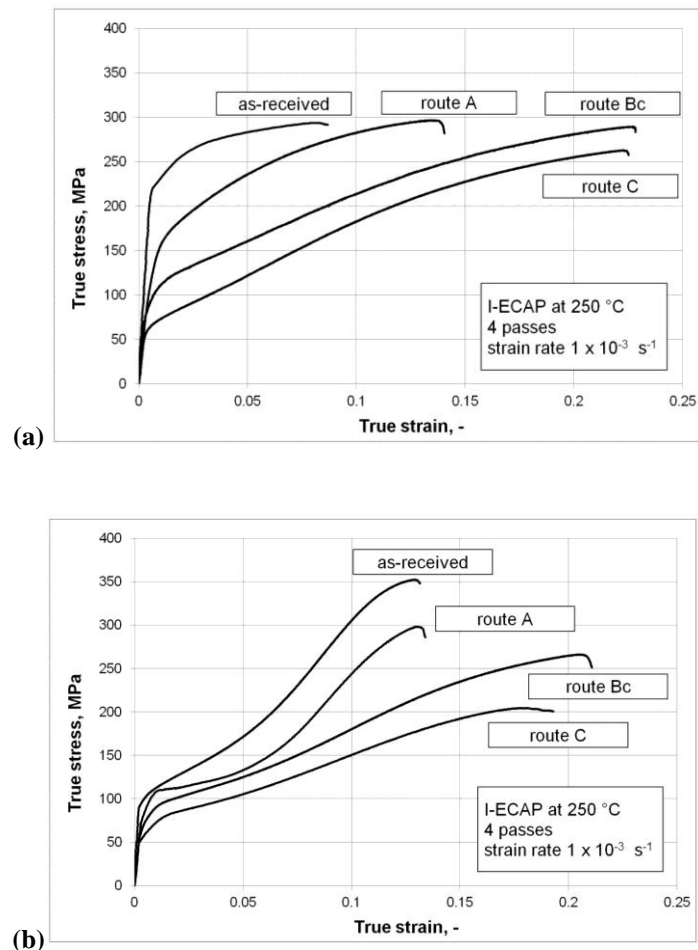
Fig. 5.1. Tensile (a) and compressive (b) true stress-strain curves for as-received and I-ECAPed samples.

Tension and compression flow stress curves for each processing route were plotted in Fig. 5.2 in order to better display a tension-compression asymmetry. Yield stress asymmetry, A_{YS}, defined as a ratio of tensile yield stress to compressive yield stress was calculated for each sample. The largest asymmetry is visible for the extruded sample, $A_{YS} = 2.25$. Yield stress asymmetry was decreased by I-ECAP to 1.5 and 1.25 for samples A and B, respectively. Processing by route C led to suppression of tension-compression yield stress asymmetry ($A_{YS} = 1.01$). It is apparent from Fig. 5.2 that flow behaviour in tension is significantly different from that in compression for samples AR and A. Higher strain hardening rates observed in compression tests of those samples could be attributed to the occurrence of {10-12} tensile twins (Kelley and Hosford, 1968). Strain hardening rate in compression decreased in samples B and C, which makes their compressive flow behaviour similar to tensile one.

(a)

(b)

(c)

(d)
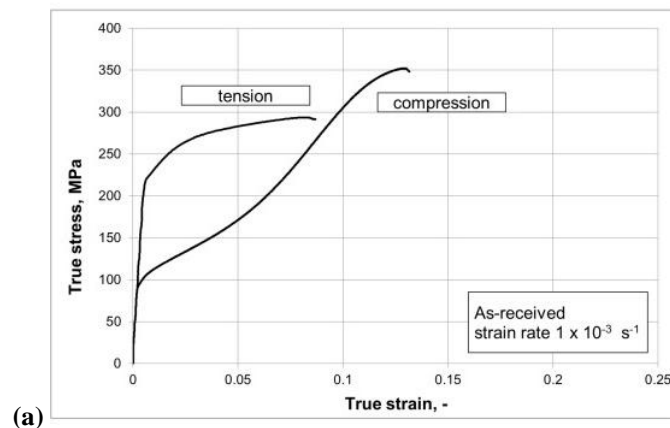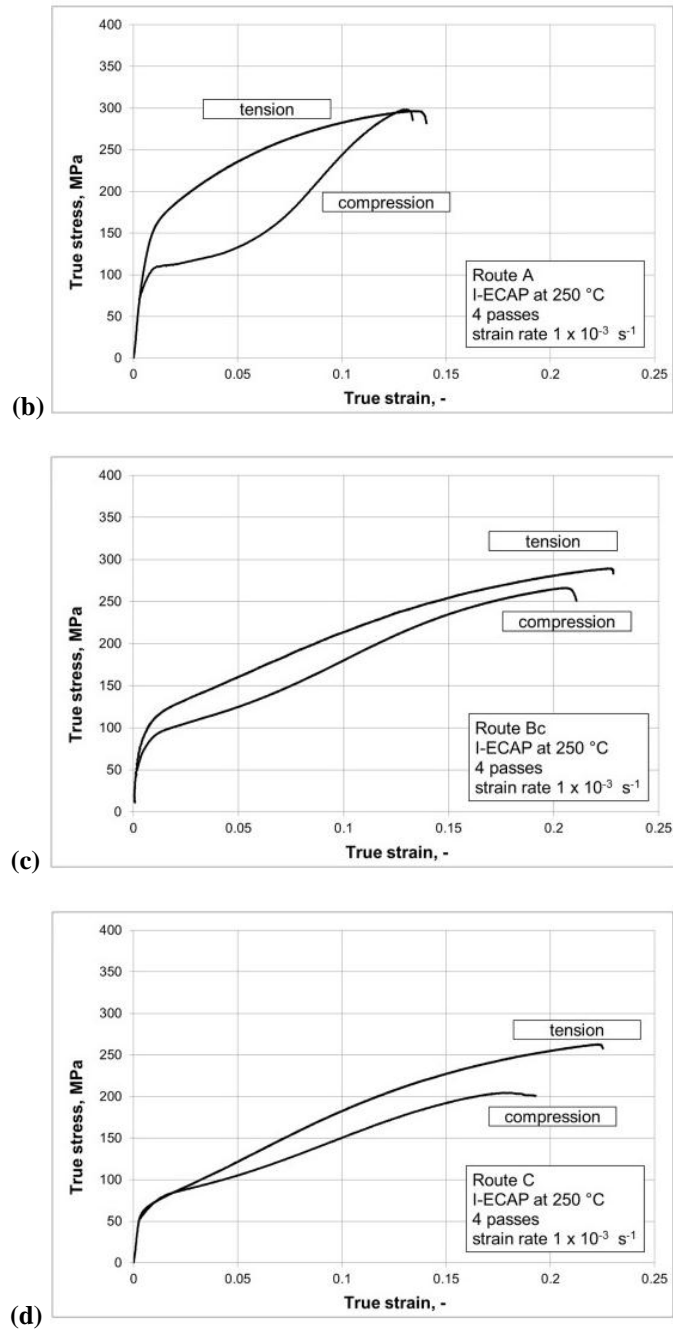
Fig. 5.2. True stress-strain curves showing tension-compression yield stress asymmetry of as-received sample (a) and samples processed by different routes of I-ECAP: A (b), B_C (c) and C (d).

117

Tensile and compression samples after testing are shown in Fig. 5.3. Samples obtained from the as-received material and from the billet processed by route C of I-ECAP (samples from billets processed by other routes behaved in the same way) are displayed to compare different phenomena observed during deformation of coarse- and fine-grained magnesium alloy. It is clear from Fig. 5.3a and 5.3b that fracture mechanisms of specimens AR and C are different. Failure of AR sample can be described as an abrupt, very moderate ductile fracture (almost brittle) across a very short neck. I-ECAPed samples exhibited uniform deformation without evident signs of necking. Moreover, each fine-grained sample fractured along a shear plane coinciding with the orientation of the I-ECAP shear plane. AR and C specimens compressed to strain 0.1 are shown in Fig. 5.3c. The compression flow behaviour of both samples is quite different. Anisotropic flow observed for sample C is not present in sample AR. Material flow prevails in the direction perpendicular to ED (marked as R in Fig. 5.3c); however, it is not clear if it is transverse or normal direction. Ratio of the biggest to the smallest radius, $A_R=R/r$, was introduced as a measure of anisotropy. Anisotropic flow was not observed for AR sample but A_R parameter was equal to 1.08, 1.1, and 1.13 for samples A, B, and C, respectively.
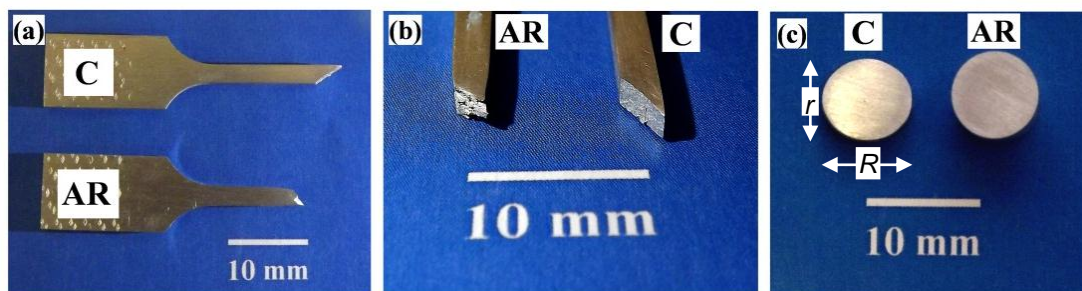
Fig. 5.3. I-ECAPed (sample C) and as-received (sample AR) tensile (a) and (b) and compressive (c) samples after testing. Shear failure is observed for I-ECAPed tensile sample and flow anisotropy in I-ECAPed compressive sample.

5.3.2. Mechanical properties after I-ECAP at low temperatures

An effect of I-ECAP temperature decrease was studied by conducting four passes at 250 °C, to refine grain size and improve formability, and two additional passes at 200 °C. Tensile flow stress curve of sample processed by six passes using route B_C (referred to in Table 4.1 as sample 10) is very similar to sample processed by four passes using the same route (sample 4), as shown in Fig. 5.4a. Therefore, temperature decrease and increased level of strain have not influenced mechanical properties. In contrast, processing by six passes using route A (sample 9) resulted in both strength and ductility improvement, comparing to sample 3, processed by four passes at 250 °C. Yield strength was raised by additional two passes at 200 °C from ~135 MPa to ~200 MPa after processing by route A. It is also worth noting that ultimate tensile strength exceeded 350 MPa while it was lower than 300 MPa for extruded sample. It shows that ductility can be significantly enhanced by I-ECAP, from 0.09 to 0.19, without lowering strength.

Compressive behaviour of I-ECAPed samples was not changed significantly by additional two passes at 200 °C since the concave shape of the flow stress curve was still observed for sample processed by route A (sample 9) and suppressed for route B_C (sample 10), as shown in Fig. 5.4b. Compressive strength was improved in both cases, comparing to properties after four passes at 250 °C. Yield stress of sample processed by route B_C was comparable to the extruded rod (~120 MPa) while strength of sample A exceeded 150 MPa after six passes of I-ECAP.

(a)

(b)
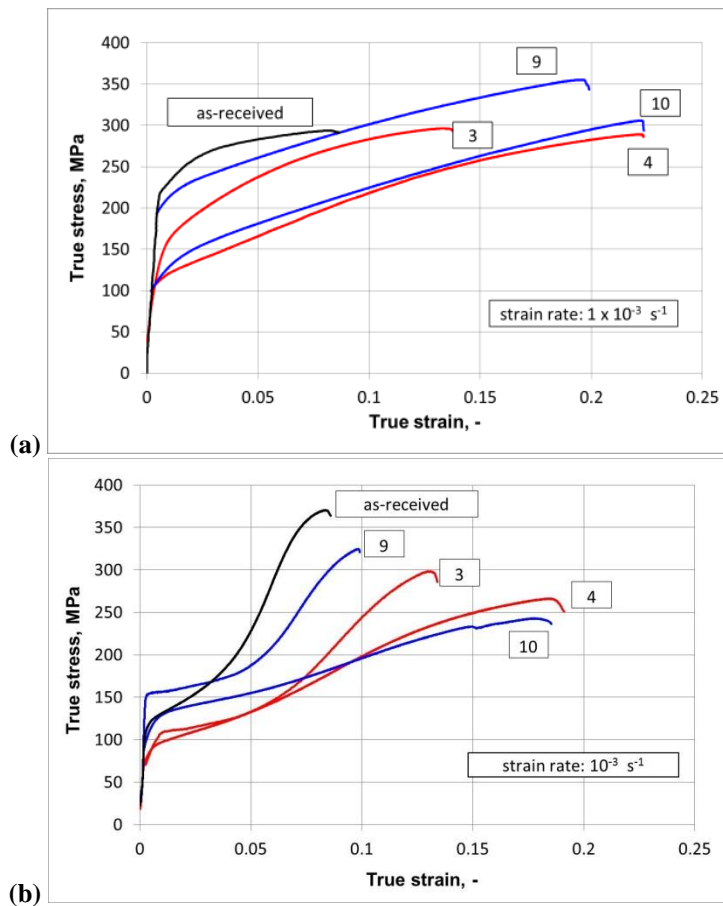
Fig. 5.4. Tensile (a) and compressive (b) flow stress curves for samples processed by six passes of I-ECAP, four at 250 °C and two at 200 °C, by route A (sample 9) and route B$_C$ (sample 10); samples 3 and 4 represent four passes of I-ECAP at 250 °C using route A and B$_C$, respectively.

The rolled sample exhibited room temperature yield strength of 165 MPa and true strain to fracture 0.18 (Fig. 5.5), which means that initial formability was two times bigger than in the case of the extruded rod. Processing by four passes at 200 °C using route C of I-ECAP resulted in the significant reduction of yield stress (64 MPa) and mild reduction of ductility (tensile strain at break ~0.12). A significant improvement of mechanical properties was achieved for sample 14, which was processed by route A with temperature reduction to 150 °C during two final passes. Yield stress reached 290 MPa without significant loss of ductility (tensile strain at break ~0.16). Tensile

strength after processing at 150 °C was 361 MPa, which was the highest value obtained in this work.
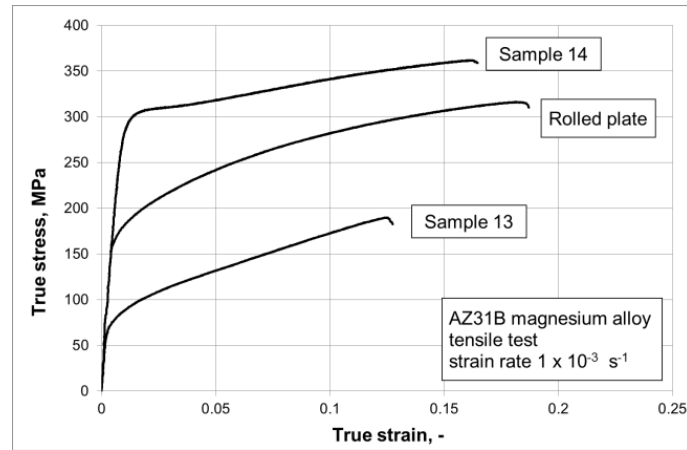
Fig. 5.5. Tensile flow stress curves of: (1) as-received rolled plate; (2) sample 13 – processed by four passes of I-ECAP at 200 °C using route C; (3) sample 14 – processed using four passes of route A: first pass at 200 °C, second at 175 °C, and two final passes at 150 °C.

5.3.3. *Mechanical properties after I-ECAP followed by heat treatment*

Specimen processed by four passes at 250 °C using route C (sample 5) was kept 6 hours in a furnace preheated to 300 °C. After heat treatment, the sample displayed significant ductility enhancement accompanied by simultaneous strength improvement (Fig. 5.6a). Yield stress was raised from ~60 MPa to ~80 MPa, which is still much below 220 MPa measured for extruded sample. Nevertheless, fracture strain was increased from 0.22 to 0.37, which is more than four times bigger than in the case of as-received sample. Moreover, tensile strength was even higher for the annealed sample (338 MPa) than for the as-supplied one (293 MPa).

(a)

(b)

(c)
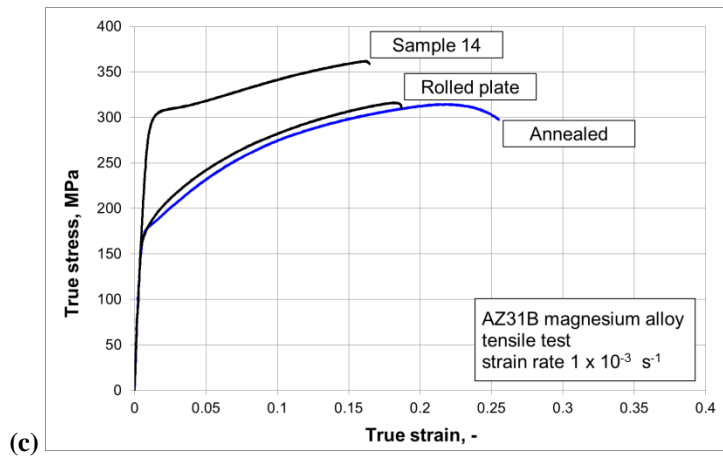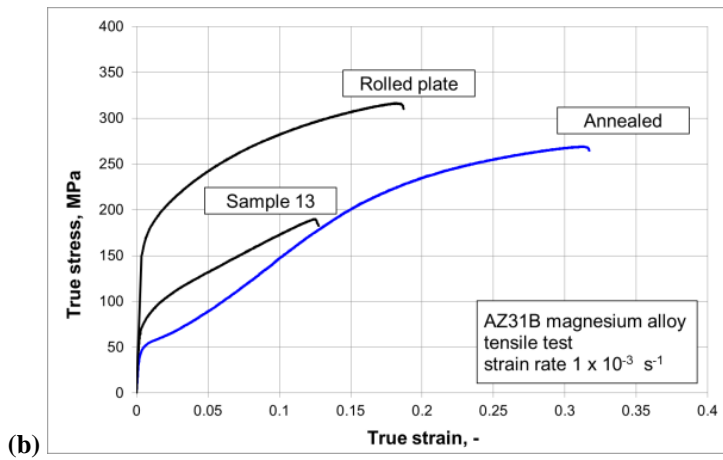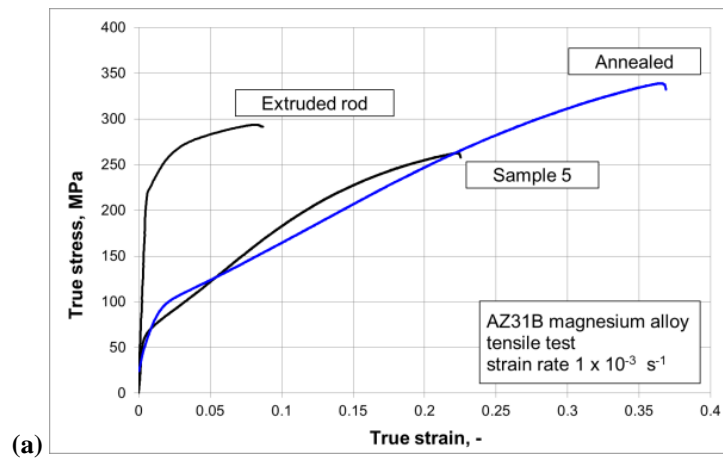
Fig. 5.6. Tensile flow stress curves of samples processed by four passes of I-ECAP and four passes of I-ECAP followed by annealing for 6 hours at 300 °C: (a) I-ECAP at 250 °C using route C (sample 5); (b) I-ECAP at 200 °C using route C (sample 13), and (c) I-ECAP at 150 °C using route A (sample 14).

122

Room temperature true strain at break of the sample processed by route C at 200 °C was more than doubled, from 0.12 to 0.31, by annealing at 300 °C (Fig. 5.6b). Nevertheless, yield stress, which was already reduced by I-ECAP processing to 64 MPa, dropped further to 43 MPa. The tensile flow stress curve of sample processed at 150 °C followed by annealing is shown in Fig. 5.6c. The high strength of as-processed sample was decreased from 290 to 165 MPa, which was the same value as measured for the initial state (rolled plate). Combination of I-ECAP at 150 °C and annealing at 300 °C resulted in ductility increase since true strain at fracture of the annealed specimen was 0.26, compared to 0.18 for the initial plate.

Sample 3 processed by four passes at 250 °C by route A was annealed for 6 hours at 300 °C to investigate the effect of heat treatment on the strain hardening rate in compression. It is apparent from Fig. 5.7 that the distinctive shape of the compressive flow stress curves obtained for the as-received rod and for the sample processed by route A did not change due to annealing. Ductility after heat treatment was increased to 0.15 but this change can be considered as negligible, comparing to the results obtained in tension after the same heat treatment for sample processed by route B_C (Fig. 5.6a).
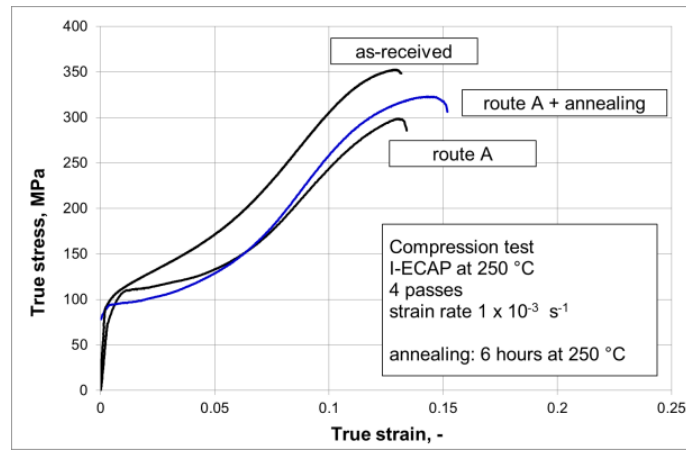
Fig. 5.7. Compressive flow stress curves of samples processed by four passes of I-ECAP at 250 °C using route A (sample 3) followed by annealing for 6 hours at 300 °C.

5.4. Microstructures

5.4.1. Microstructures after I-ECAP

A remarkable homogenization and grain refinement was achieved after four passes of I-ECAP at 250 °C, irrespectively of the route used. The measured mean grain sizes were very similar for each processing route and they were 5.53, 5.42 and 5.37 μm for routes A, B_C, and C, respectively. The effect of the billet rotation between subsequent I-ECAP passes on the microstructure homogenization and grain shape was not observed. The representative microstructure image of sample processed by route A (sample 3), with the corresponding grain size distribution chart, is shown in Fig. 5.8. More than 50% of grains are within range 3-6 μm; they are equiaxed grains, most likely arising from dynamic recrystallization (DRX) taking place at 250 °C. Nevertheless, serrated coarse grains, as large as ~20-30 μm, account for 4% of all grains. They could be interpreted as unrecrystallized grains observed in the initially extruded sample (Fig. 3.7). Similar grain size and microstructure homogeneity after ECAP processing at 250 °C were reported by Seipp et al. (2012). Experimental

124

results confirming occurrence of DRX in ECAP of magnesium alloys were also presented by Ding et al. (2009) and Janecek et al. (2007).
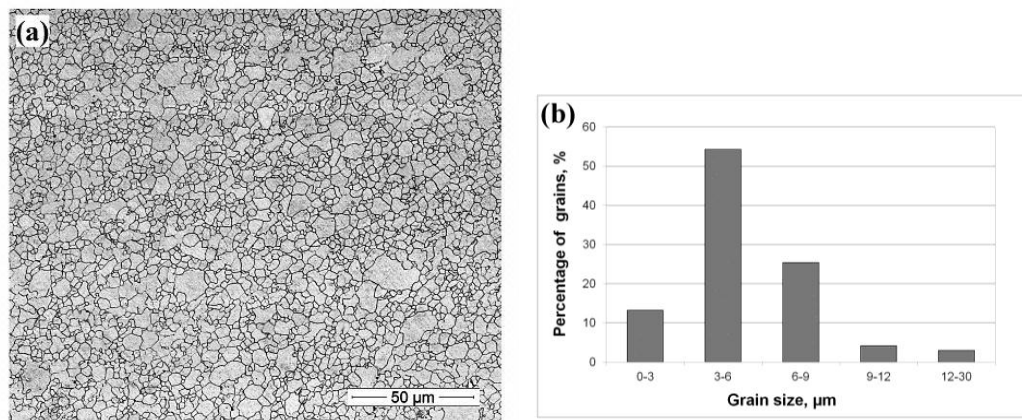
Fig. 5.8. Microstructure image (SEM) of sample processed by route A (mean grain size _d_ = 5.53 μm, standard deviation _SD_ = 1.53 μm), representative for all samples processed by I-ECAP at 250 °C in the present study (a) and corresponding grain size distribution chart (b). The mean grain size was measured using linear intercept method.

Grain size was also measured in samples processed by four passes at 250 °C followed by two passes at 200 °C using various routes. Since sample processed by route C was severely damaged, only results for samples processed by route A (sample 9) and route B_C (sample 10) are shown in Fig. 5.9. The observation that the processing route does not affect a grain size, reported for samples processed by various routes at 250 °C, was also confirmed after two additional passes at 200 °C. The temperature decrease resulted in further grain refinement and the grain sizes after processing by routes A and B_C were 2.4 and 2.6, respectively. The coarse, serrated grains observed for sample 3, were not revealed after processing at 200 °C. The grain refinement arising from the temperature decrease can be attributed to the

occurrence of DRX as the size of recrystallized grains is increasing with deformation temperature (Fatemi-Varzaneh et al., 2007).
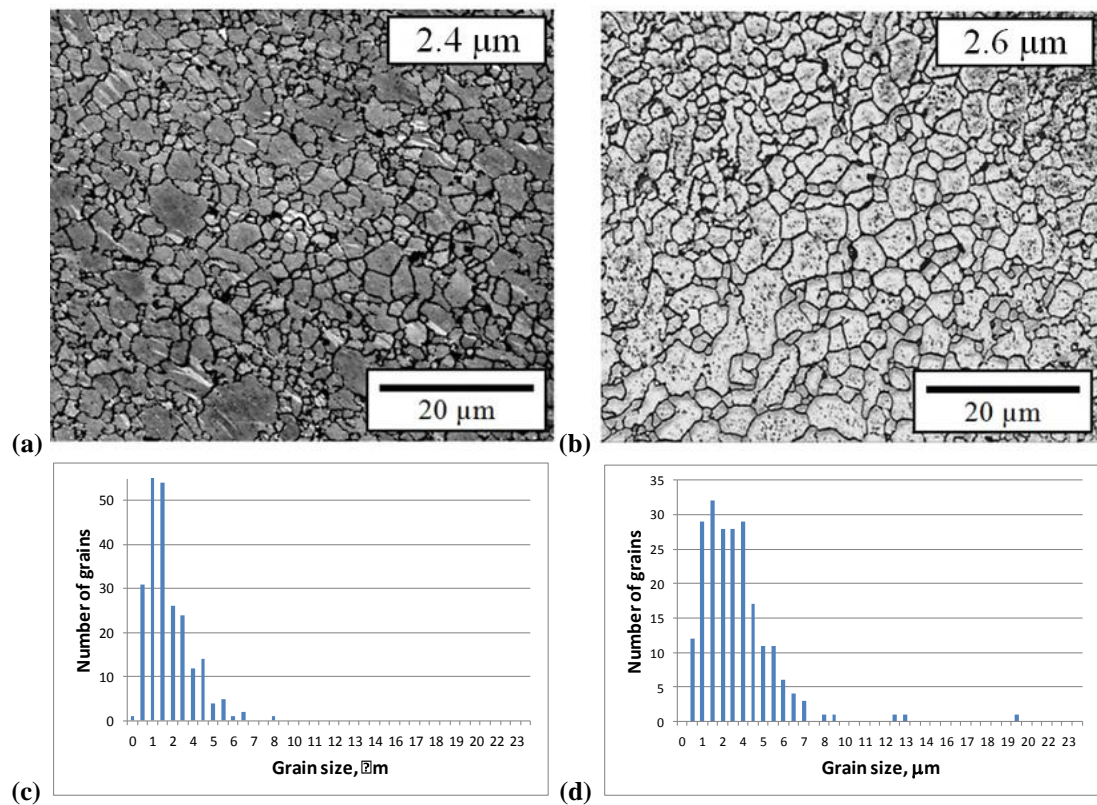
Fig. 5.9. Microstructure images (SEM) of samples processed by six passes of I-ECAP, four at 250 °C and two at 200 °C, by routes A (a) and B$_C$ (b) and corresponding grain size distribution charts in (c) and (d), respectively.

Bars machined from the rolled plate with the average grain size ~8 μm were subjected to I-ECAP at 200 °C and 150 °C; they are referred to in Table 4.1 as samples 13 and 14, respectively. Grain refinement in the case of a billet processed at 200 °C was less efficient than in the extruded sample processed by six passes of I-ECAP (Fig. 5.9) and a measured average grain size was ~3.5 μm (Fig. 5.10a). The microstructure is dominated by ~3-4 μm grains but large grains ~8 μm, observed also in the initial state (Fig. 3.8), are still present.

The smallest grain size was achieved in this study by lowering temperature during two final I-ECAP passes to 150 °C. The mean grain size after four passes was ~1 μm with the most of grains lying within 0.5–1 μm and occasionally observed ~1.5 μm grains (Fig. 5.10b). The result obtained at 150 °C confirmed that microstructure refinement is strongly related to processing temperature.
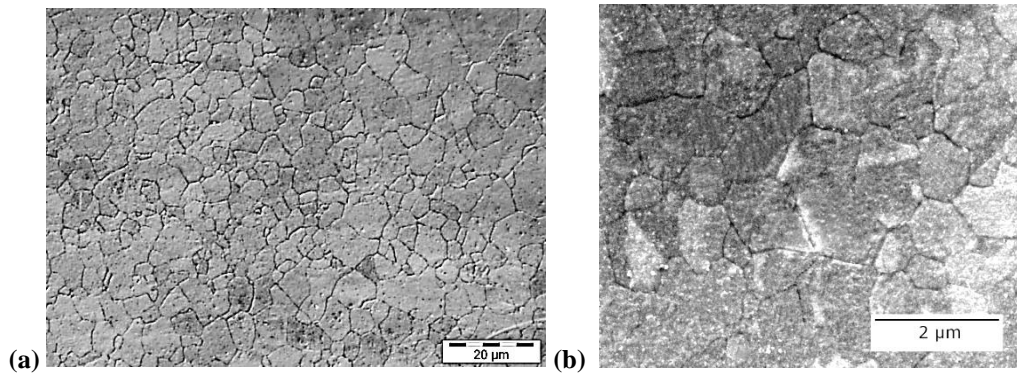
Fig. 5.10. Microstructures of rolled samples processed by four passes of I-ECAP: (a) at 200 °C using route C (OM image); (b) using gradual temperature decrease: first pass at 200 °C, second at 175 °C, and two final passes at 150 °C (SEM image).

The summary of grain size measurements performed for various parameters of I-ECAP was shown in Table 5.1. The mean grain size decreases along with temperature decrease, reaching ~1 μm at 150 °C. It is also shown that processing route does not have any significant effect on the obtained grains size.

Table 5.1. Summary of grain size measurements

Sample no.	No. passes	Temperature during final pass, °C	Route	Mean grain size, μm	Standard deviation, μm
3	4	250	A	5.53	2.2
4	4	250	B_C	5.42	1.9
5	4	250	C	5.37	2.3
9	6	200	A	2.4	1.3
10	6	200	B_C	2.6	1.4
13	4	200	C	3.5	1.7
14	4	150	A	0.91	0.32

5.4.2. Microstructures of deformed coarse-grained samples

Microstructure images of the extruded sample subjected to tension and compression are shown in Fig. 5.11. As seen in Fig. 5.11a and Fig. 5.11b, almost every coarse grain (bigger than ~50 μm) subjected to tension underwent massive twinning. It is also apparent from those images that some grains are deformed by twins operating on only one plane whereas there is a relatively large group of grains, in which activity of two and more twinning systems is observed. EBSD technique was used by Al-Samman and Gottstein (2008a) to show that different {10-12} twin variants can operate within the same grain. It is apparent from Fig. 5.11b that twins as well as slip traces are hardly observed for grains smaller than ~20 μm. Similar results were obtained for samples compressed to strain 0.1 (Fig. 5.11c and 5.11d), where massive twinning in coarse grains, sometimes operating on more than one slip plane, is not

accompanied by deformation in smaller grains. Voids or shear bands were not revealed in the tested samples.
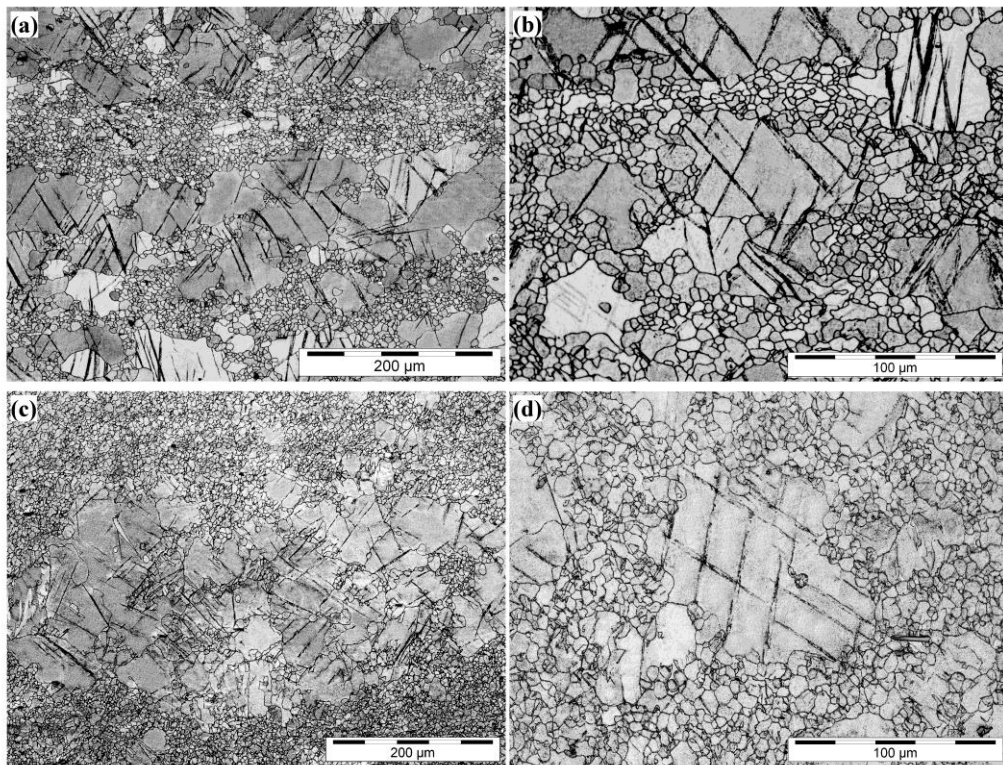
Fig. 5.11. Microstructure images (OM) of as-received extruded sample subjected to tension (a) and (b) and compression (c) and (d). Zoomed regions (b) and (d) are shown to reveal fine grains free from twinning. Tensile direction in (a) and (b) is horizontal.

5.4.3. Microstructures of deformed fine-grained samples

Samples 3-5 (Table 4.1), processed by routes A, B_C, and C are referred to in this section as A, B, and C, respectively. As shown in Fig. 5.12, microstructure images of fine-grained samples subjected to tension revealed occurrence of deformation bands in each sample. In sample A, some bands of extremely deformed grains are parallel to tensile direction (TD) and some inclined at ~45° to TD, while in samples B and C only the latter are observed. For samples B and C, a large number of twins as well as
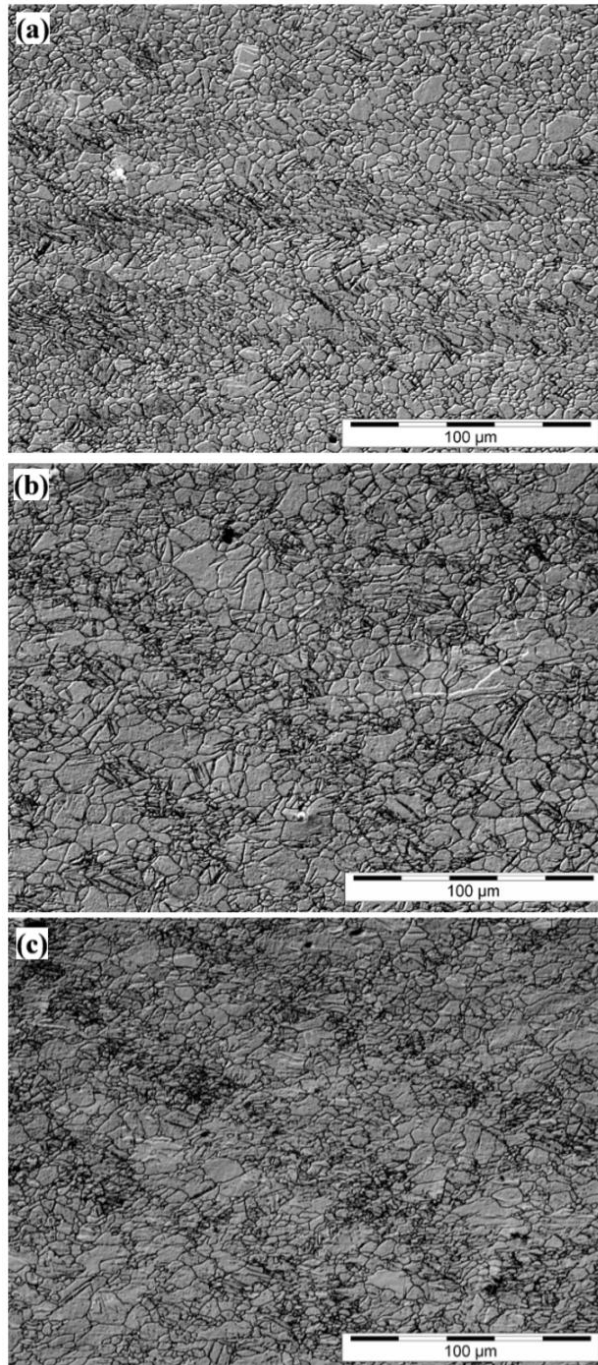
Fig. 5.12. Microstructure images (OM) of fine-grained tensile samples processed by routes: A (a), B$_C$ (b) and C (c) deformed to fracture. Shear bands are revealed in each sample. Tensile direction is horizontal.

slip traces are observed within a band. However, dark regions, arising from a larger amount of localised deformation than in sample A, make detailed observation more difficult. A small relief on the surface visible in grains outside bands is attributed to a slip dominated flow. This region is also almost free from twins. The number of shear bands observed in different samples is not the same. Samples B and C exhibits more extensive shear banding than sample A.

Microstructures of samples subjected to compression are shown in Fig. 5.13. Twins are observed in each sample, irrespective of the route used. However, twinning is more intensive in sample A, comparing to B and C. No relation between grain size and twinning activity was found in the examined samples. As seen in Fig. 5.13b and Fig, 5.13c, twins are observed in small (~5 μm) and large grains (~15 μm). However, large grains without signs of twinning are also revealed. It is shown that twinned grains form small colonies or bands. In sample A, colonies of twinned grains are bigger that in samples B and C but grains free from twins are also observed. It was not revealed if any 'mesoscopic' effects, e.g. shear bands, are arisen from those small colonies/bands. In contrast to the coarse-grained sample, occurrence of only one twin variant in the most of twinned grains is observed.
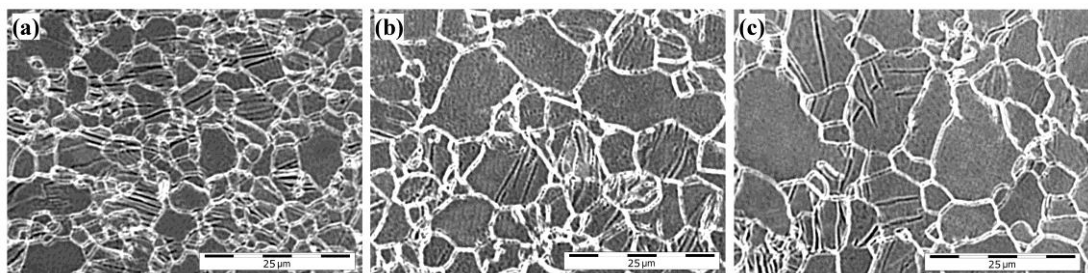
Fig. 5.13. Microstructure images (OM) of fine-grained samples: A (a), B (b) and C (c) compressed to true strain 0.1. Dark lines are twins revealed in fine grains.

5.4.4. Microstructures after heat treatment

The grain size of sample 14 processed at 150 °C was increased from ~1 μm to ~3.7 μm during annealing for 6 hours at 300 °C (Fig. 5.14a and d). The same heat treatment resulted in grain growth from ~3.5 μm to ~4.5 μm in the case of sample 13, which was I-ECAPed at 200 °C (Fig. 5.14b and e). It shows that the initial grain size has an effect on the size of recrystallized grains, which is also supported by the grain size increase from ~5.5 μm to ~6.2 μm in sample 5, processed at 250 °C (Fig. 5.14c and f). Nevertheless, it could not be unequivocally established if the microstructures of samples I-ECAPed at 200 °C and 250 °C underwent full static recrystallisation or only a local grain growth since the measured grain sizes before and after annealing were very similar. The same cannot be concluded for ~1 μm structure after processing at 150 °C as it is clearly visible in Fig. 5.14a and Fig. 5.14d that static recrystallisation took place in the entire sample. Barnett and Beer (2009) claimed that microstructure restoration during post-deformation annealing can be attributed not only to static recrystallization, but also to continued growth of nuclei formed by dynamic recrystallization during processing. Despite annealing temperature in their study was higher (400 °C), it could also the case of the samples tested in this work.
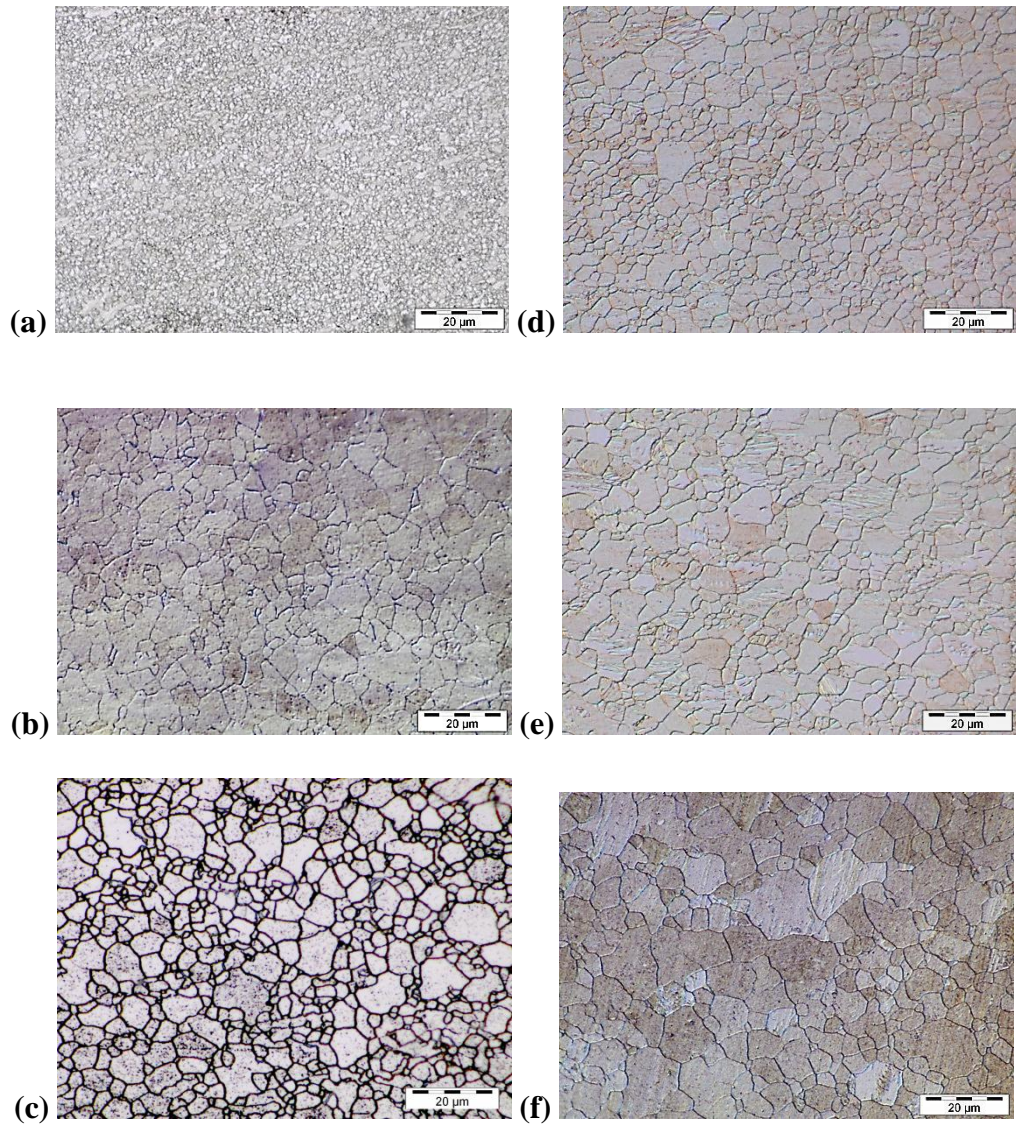
Fig. 5.14. Microstructures images (OM) after I-ECAP at 150 °C (a), 200 °C (b), and 250 °C (c) and corresponding images after annealing for 6 hours at 300 °C (d-f). The mean grain sizes (*d*) and standard deviations (*SD*) of annealed samples are as follows: (d) *d* = 3.7, *SD* = 1.7; (e) *d* = 4.5, *SD* = 2.2; (f) *d* = 6.2, *SD* = 3.4.

5.5. Textures

Micro-textures of samples 3-5 processed at 250 °C were calculated from EBSD images (Fig. 5.15a-c). The supplied rods were obtained by direct extrusion and it was reported in the past that strong ring fibre texture is produced in this kind of forming

operation (Kleiner and Uggowitzer, 2004). Basal planes are aligned almost parallel to ED; the angle between basal plane and extrusion plane is ~5°. Strong basal textures, with intensities in the range 12-16, were obtained after I-ECAP. Sample processed by route A exhibits a basal plane inclination of 20° with texture intensity equal to 12 and a basal plane inclination of 13° with texture intensity 6. Grains are orientated more favourably for basal slip in the two other I-ECAPed samples. The inclination angles of basal planes in samples processed by route B_C and C are 46° and 35°, respectively. Moreover, the basal planes are inclined at approximately 45° to transverse direction in sample B_C, which is not observed in sample C. It would lead to similar mechanical properties along ED but different flow behaviour when testing along transverse direction (through-thickness).

EBSD maps obtained for samples processed by routes B_C and C were shown in Fig. 5.15g and h, respectively. Microstructures are dominated by fine grains; however, single coarse grains are still observed even after fourth pass of I-ECAP. Despite more coarse grains are visible in sample B_C than in C, OM and SEM observations, performed in various areas of the samples, proved that mean gain size is almost the same (please refer to *Section 5.4.1*). There is no evident texture appearance in Fig. 5.15g, some fine grains are oriented parallel to planes (001) and (120); however, there is no clear relation between grain size and its orientation. In contrast to sample B_C, texture is observed in sample C, characterised on the same plane. The EBSD map is dominated by green and blue colours, which correspond to (010) and (120) planes, respectively. The difference observed for both samples can be easily explained by analysing unit cells, which artificially represent orientation of a crystal in the peak of maximum texture intensity in a pole figure; they were drawn for routes A, B_C and C

in Fig. 5.15d, e and f, respectively. It is apparent that basal planes are aligned perpendicular to the plane of observation in case of route C; therefore, grains with basal orientation are hardly observed in this map. Unit cells after processing by route B_C is tilted with respect to all three main axes. As a consequence, strong texture is not observed in this case on any of the main planes.

It should be noted here that inverse pole figures capture very well fibre textures in rolled or extruded magnesium alloys; however, some information can be lost when main crystallographic planes are not aligned parallel to the plain of observation. It is the case of a billet processed by various routes of ECAP or I-ECAP, when c-axes are tilted by 20°-50° with respect to ED. Most of reports dedicated to ECAP of magnesium alloys show full of half pole figures to provide better representation of texture (Agnew et al., 2005; Ding et al., 2008; Biswas et al., 2010; Seipp et al., 2012), as it was also shown in Fig. 5.15a-c.

(a)   (b)   (c)

(d)   (e)   (f)

(g)

(h)
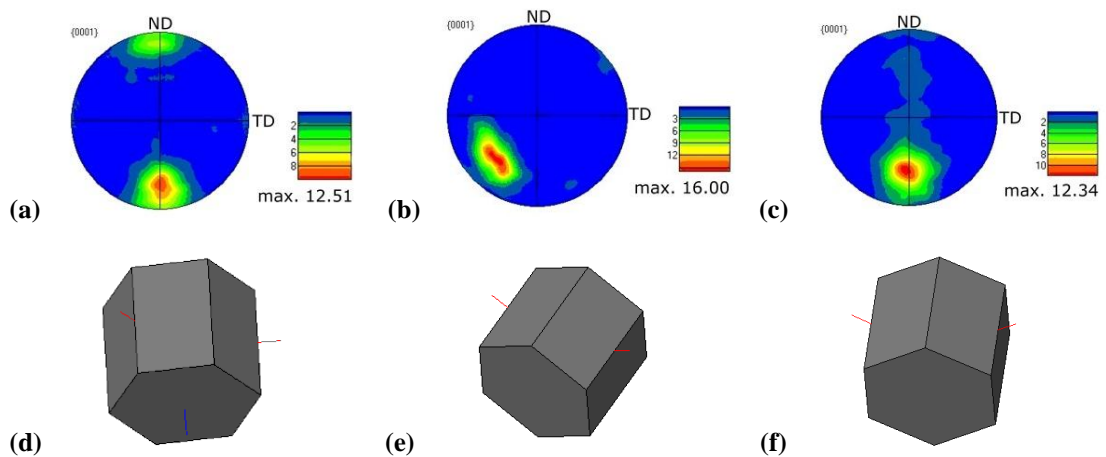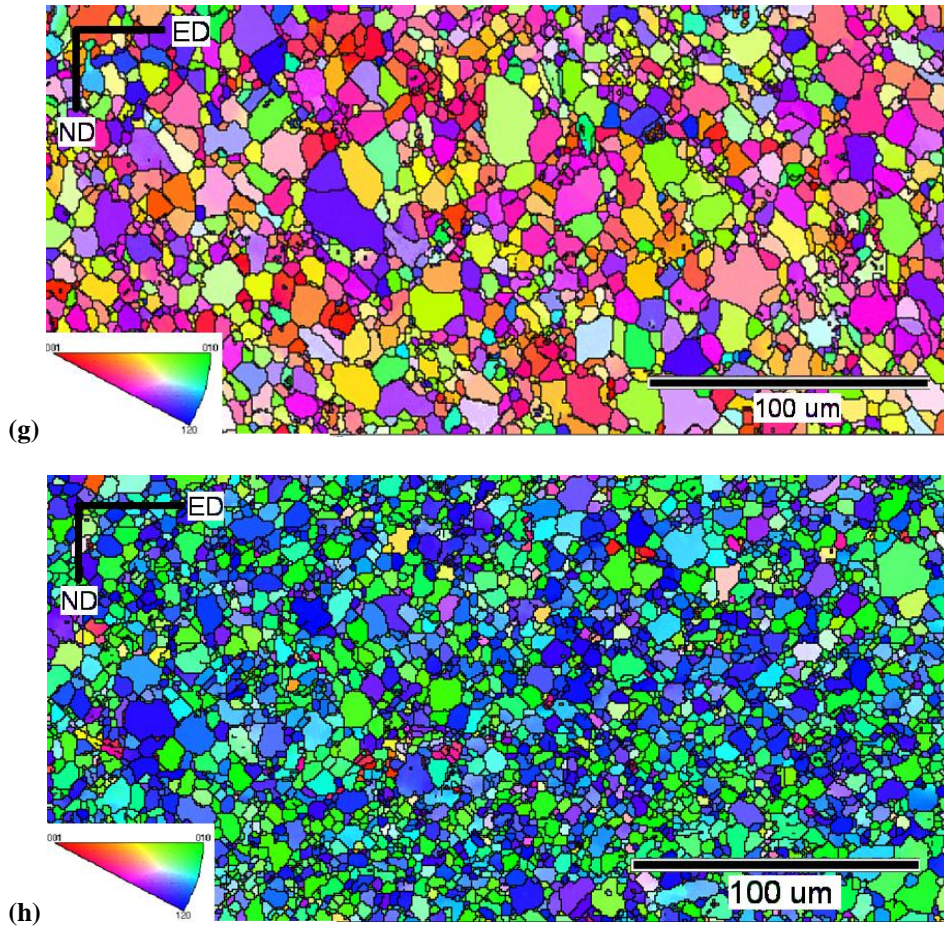
Fig. 5.15. (0001) pole figures showing textures after four passes of I-ECAP at 250 °C by routes: A (a), B$_C$ (b), and C (c) and corresponding hexagonal unit cells (d-f) representing orientation of a crystal in the peak of maximum texture intensity. Coordinate system in figures (d-f) corresponds to pole figures (a-c). EBSD maps obtained for samples processed by routes B$_C$ and C are shown in (g) and (h), respectively.

5.6. Discussion of experimental results

5.6.1. *Effects of grain size and texture on mechanical properties*

Mechanical properties of the extruded AZ31B magnesium rod were significantly changed by I-ECAP. The initial high strength and low ductility of the extruded sample can be explained by the presence of coarse grains and texture produced during extrusion. The alignment of basal planes, almost parallel to ED, resulted in

the increased yield strength and reduced ductility. Twinning in extruded coarse-grained samples subjected to tension and compression observed in the current work was also reported by Chino et al. (2008). It was shown in the same paper that twinned coarse-grained (70 µm) samples fractured earlier in tension as well as compression than fine-grained (8 µm) samples, which did not undergo twinning. Grain refinement resulting in ductility enhancement is also confirmed in the current work.

The mean grain size obtained after processing by I-ECAP at 250 °C (~5.5 µm) and 200 °C (~3 µm) is comparable to the results obtained after conventional ECAP (Seipp et al., 2012, Xia et al., 2005). Grain refinement led to formability enhancement accompanied by a yield stress decrease, which is usually observed for AZ31 magnesium alloy subjected to ECAP (Kim et al., 2002; Masoudpanah and Mahmudi, 2010). However, results obtained for sample processed by route A (sample 3) indicate that grain size cannot be the only explanation for the change of mechanical properties after I-ECAP. Different texture development, associated with different processing routes, also contributes to modification of mechanical properties. Results of texture measurement show that slip on basal plane is a favourable mode of deformation in samples processed by routes B_C (sample 4) and C (sample 5). It explains lower yield stress and enhanced ductility of those samples. In sample 3, basal planes are inclined by 13-20° to ED which makes slip on basal plane much more difficult. Activation of 'harder' deformation mechanisms gives rise to strength improvement, compared to samples 4 and 5.

The effect of temperature decrease to 200 °C during 5th and 6th passes on mechanical properties of sample processed by route B_C (sample 10) is ambiguous. Although grain size was reduced from ~5.5 μm, after four passes at 250 °C, to ~2.5 μm, after two additional passes, the mechanical properties in tension and compression were almost the same. It shows that grain size strengthening was completely suppressed by strong texture developed due to applied billet rotation after each pass. In contrast, sample processed by route A (no. 9), which exhibited much lower weakening due to texture produced after four passes at 250 °C, demonstrated significant yield strength increase due to grain refinement after processing at 200 °C. Moreover, it is claimed in this work that grain refinement also accounted for enhanced ductility of sample 9 due to suppression of generation of twins, which were revealed in coarse-grained specimen (Fig. 5.11) and are suspected in the literature to act as crack initiation sites (Barnett, 2007b; Al-Samman and Gottstein, 2008a). Additionally, lower twinning activity in tension arising from a grain size reduction has been already revealed by Chino et al. (2008). Tensile flow stress curve obtained for sample 9 shows that I-ECAP has a potential to improve room temperature ductility of magnesium alloys without sacrificing their strength (Fig. 5.4a).

The results of mechanical testing obtained for sample 13, which was subjected to four passes at 200 °C by route C, showed that temperature reduction is not enough to improve ductility without lowering strength. Although the grain size of that specimen (~3.5 μm) was smaller than of samples processed by routes A and B_C at 250 °C (~5.5 μm), strength and ductility were also lower. It could be attributed to the textural effects observed already for samples processed by route C at 250 °C, which exhibited lower yield stress than samples processed by the other routes. However, a very

limited ductility (true strain at fracture ~0.12) obtained for sample 13 could not be explained by microstructural and textural results. The grain size of ~3.5 μm after 4 passes at 200 °C was larger than ~2.5 μm after four passes at 250 °C followed by two passes at 200 °C (Fig. 5.10). It indicates that, in some cases, four passes are not enough to homogenise microstructure to 2.5 μm since ~8 μm grains are still observed in Fig. 5.10a. Similar grain size (~3 μm) was obtained after four passes of conventional ECAP by Xia et al. (2005)

The highest yield stress and strength, 290 MPa and 360 MPa, were achieved in this study when temperature of I-ECAP was reduced to 150 °C (sample 14 in Table 4.1). It showed that grain refinement to ~1 μm is required to increase strength of AZ31B magnesium alloy. The only route which was successful in lowering processing temperature below 200 °C without causing fracture was route A; therefore, it cannot be categorically stated if a small grain size is the only requirement for strength improvement or it is a combination of grain size and texture developed by a particular processing route. Texture measurement conducted for sample processed by route A at 250 °C (Fig. 5.14a) showed that basal planes after four passes were inclined at 13-20° to tensile direction, which did not favour deformation at low stress as it was observed for samples processed by routes B_C and C. Nevertheless, the obtained fracture strain of ~0.16 was higher than fracture strain for the extruded rod (~0.09) and only slightly lower than fracture strain for the rolled plate (~0.18).

5.6.2. Tension-compression yield stress asymmetry

Tension-compression asymmetry of yield stress observed for the extruded sample was almost suppressed for samples 4 and 5 (Fig. 5.2). This can be explained by texture development in those samples. The measured grain orientations show that *c*-axes of hexagonal cells are inclined at ~45° to ED; therefore, their strength in tension and compression along ED is almost the same due to symmetrical alignment of basal planes to both deformation directions. In the case of sample 3, basal planes are aligned similarly to the extruded sample and slip on basal plane is limited in compression. Activation of twinning leads to increase in strain hardening and lower ductility. Although the combination of grain size and texture obtained in sample 9 (processed by route A) led to improvement of strength and ductility in tension, the textural effects did not allow reducing tension-compression asymmetry. The distinctive concave shapes of compressive flow stress curves observed for the extruded rod and samples processed by route A were also reported for fine-grained samples with grain size 4 μm subjected to compression along ED by Barnett et al. (2004). It clearly shows that grain refinement is not enough to suppress the tension-compression asymmetry but generation of an appropriate texture is also required.

Anisotropic flow was also reported during compression of fine-grained samples (Fig. 5.3). However, it is not clear if the lower yield stress was observed along transverse or normal direction, therefore, this effect needs further investigation. This phenomenon was also studied by conducting a set of compression tests along three different directions of an ECAPed billet (Figueiredo et al., 2010b). Increased tendency for twinning was observed when sample was tested along through-thickness direction, comparing to testing along extrusion direction. Texture

measurement performed for sample processed by route C (sample 5) shows that basal planes are inclined at ~35° which favours basal slip along ED. However, their crystallographic orientation in through-thickness direction requires activation of different deformation mechanisms. It explains why the largest anisotropy was observed for sample 5, smaller for 3 and 4, and isotropy for the extruded sample.

5.6.3. *Deformation mechanisms in fine-grained samples subjected to tension*

Deformation mechanisms in fine-grained samples subjected to tension were tested using samples 3-5 (Table 4.1), processed by routes A, B_C, and C at 250 °C. They are referred to in this section as A, B, and C, respectively. Deformation bands were revealed in each examined fine-grained sample subjected to tension (Fig. 5.12). It was difficult to define deformation mechanism operating within a band due to high strain accumulation. However, twins as well as slip traces were identified in most of grains situated within a band. The mechanism of shear bands formation is not clear. Lapovok et al. (2009) revealed shear bands in AZ31 subjected to one pass of ECAP at 250 °C. Nevertheless, the effect of shear bands on flow behaviour during tension was not studied. In the present work shear bands were not revealed after four passes of I-ECAP, they appeared during tensile testing. There is no evidence of any relation between grain size and band formation since an average grain size within and outside a band is similar. Therefore, observed strain localization is attributed to an initial grain orientation.

It is suggested that grains within a band are deformed by twinning, which was also shown for biaxial tension by Scott et al. (2013). However, strong basal texture

reported for samples processed by routes B_C and C indicates that slip on basal plane is also an important deformation mechanism operating within and outside a band. Lower yield stress of samples B and C, compared to sample A, can be attributed to suppression of twinning activity. It is apparent from Fig. 5.12 that more twinned grains are observed in sample A than B, which gives rise to the strength improvement of the former one. The quantitative analysis of the twinned area ratio was not possible due to a high deformation level.

Texture of sample A does not favour slip on basal plane, therefore, its ductility is lower compared to the other fine-grained samples. Higher strength of sample A is attributed to increased activity of twinning. The deformation mechanism, different from those shown for samples B and C, is seen in Fig. 5.16. The following hypothesis is proposed to explain the origin of the observed microstructure: grains are firstly twinned which causes their reorientation to position which favours basal slip. Twinning behaviour resulting in grain reorientation more favourable to basal slip was identified in the literature as {10-11}-{10-12} double twinning (Barnett, 2007b). Since slip on basal plane is much easier to occur than any other deformation mechanism, remarkable local strain localisation appears. Observed strain localisation is probably the main reason for earlier failure of sample A, comparing to samples B and C. It should be emphasized that the proposed explanation is only a hypothesis and requires further verification using more sophisticated techniques than optical microscopy, e.g. *in situ* EBSD (Uota et al., 2009).
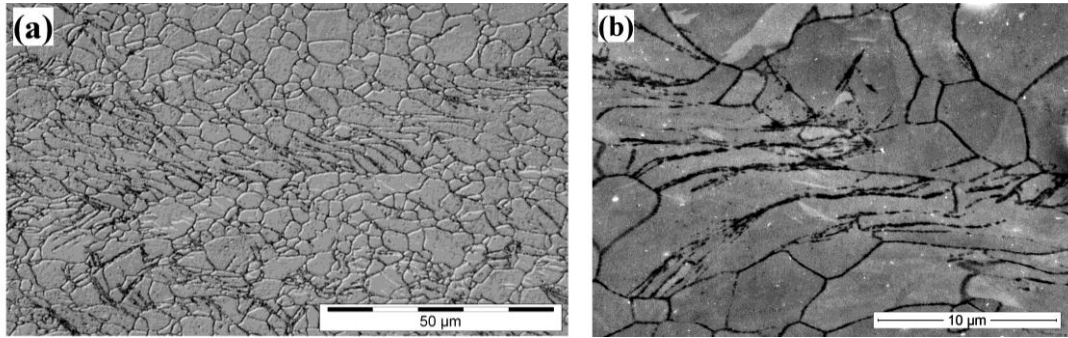
Fig. 5.16. OM image of shear band observed in tensile sample processed by route A and deformed to fracture (a) and SEM image showing twins within deformed grains (b). Tension direction is horizontal.

5.6.4. *Deformation mechanisms in fine-grained samples subjected to compression*

Deformation mechanisms in fine-grained samples subjected to compression were tested using samples 3-5 (Table 4.1), processed by routes A, B_C, and C at 250 °C. They are referred to in this section as A, B, and C, respectively. Shear failure along diagonal of cylindrical sample observed during compression of coarse- and fine-grained samples could be explained in terms of shear bands formation. It was already shown that strain localization occurs in magnesium samples subjected to compression and leads to earlier failure; this mechanism was described by Al-Samman and Gottstein (2008a). Initially twinned grains undergo secondary twinning and form double twins. They reorient parent grain to the position which favours slip on basal plane; Schmid factor for basal slip in double twinned grains was calculated to be 0.5 (Barnett, 2007b). Moreover, regions previously occupied by double twins are expected to act as sites of void formation since twin-sized voids were revealed in compressed magnesium sample using EBSD technique (Al-Samman and Gottstein, 2008a).

According to the presented fracture mechanism in compression, suppression of twinning can lead to ductility enhancement of magnesium alloys. Indeed, grain refinement obtained by I-ECAP resulted in limiting of twinning activity and led to ductility improvement in the present study. Due to texture developed during I-ECAP, most of grains could be deformed by basal and non-basal slip instead of twinning, which delayed the process of double twinning and void formation. It should be noticed that the previous statement is correct when the sample is compressed along extrusion direction; there is no experimental evidence in the current study that it is also true along other directions.

The role of grain size and its orientation in twin formation is ambiguous. Although grain size is believed to control twinning behaviour (Barnett et al., 2004), twins were observed in grains as small as 1-3 µm, as shown in Fig. 5.17. Moreover, large grains surrounding twinned regions were completely free from twins. It proves that not only grain size but also grain orientation has strong effect on twinning behaviour. Twinned grains are arranged in small colonies which can indicate that not individual grains but whole regions exhibit orientation which favours twinning. It is suggested in the present paper that those twinned colonies form shear bands where the voids are formed at the subsequent stages of deformation. It would explain why extensively twinned sample A fractured earlier than samples B and C.
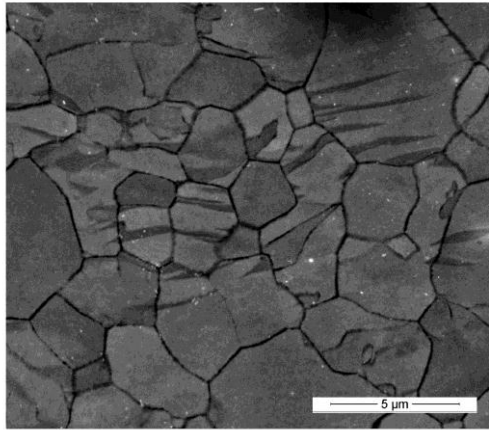
Fig. 5.17. SEM microstructure image of sample C compressed to true strain 0.1. Twins are revealed in very fine grains.

Higher twinning activity in sample A compressed to true strain of 0.1, compared to samples B and C, was confirmed by calculating the total twinned area. The results are shown in Table 5.2. It appears that the twinned area in sample A is more than two times larger than in samples B and C. These results are also supported by the distinctive concave shape of the compressive flow stress curve observed for sample A and not seen for samples B and C, as shown in Fig. 5.1b. Since the grain size is almost the same (5.45 ± 0.1 µm) for each fine-grained sample tested in this section, the increased twinning activity in sample A was attributed to the texture produced during I-ECAP.

Table 5.2. Twinned area ratio (%) in samples processed by routes: A, B_C, and C compressed to true strain of 0.1 along extrusion direction.

Sample	A	B	C
Twinned area ratio (%)	6.3	2.7	2.2

5.6.5. *Effect of heat treatment on grain size and mechanical properties*

Mechanical properties of I-ECAPed samples were significantly changed after heat treatment at 300 °C for 6 hours (Fig. 5.6). Mukai et al. (2001) have already shown that elongation to failure can exceed 40% after annealing of initially fine-grained magnesium alloy (~1 μm) for 24 hours at 300 °C. The measured ductility improvement was attributed by the authors to the grain size increase to 15 μm during heat treatment. Nevertheless, very similar elongations observed in this work cannot be attributed to grain growth since a grain size was not changed substantially (Fig. 5.14) due to the shorter annealing time. The grain size increase from 3.5 to 4.5 μm and from 5.4 to 6.2 μm in samples I-ECAPed at 200 °C and 250 °C, respectively, can be considered as negligible from the mechanical point of view. Moreover, it was shown by Agnew et al. (2004) that static recrystallisation and grain growth do not significantly change a texture produced during ECAP. Therefore, remarkable increase in true strain at fracture to 0.31 and 0.37 after heat treatment in samples I-ECAPed at 200 ° and 250 °C, respectively, can be explained only by a reduction of internal stresses rather than grain growth or texture modification.

Microstructural images taken in the deformation zone after tensile testing of the annealed sample 5 (average grain size ~6.2 μm) showed that shear bands seen previously in sample subjected to I-ECAP and tension (Fig. 5.12c) were suppressed due to the applied heat treatment. It is apparent from Fig. 5.18 that grains are not severely deformed as it was locally observed for the I-ECAPed samples but a lot of twins are present. Their occurrence can be linked with the mechanical behaviour illustrated in Fig. 5.6a. It is concluded that such a high failure strain (above 0.35) could not be accommodated only by a dislocation slip mechanism but activation of

twinning was also required. Additionally, the obtained high true stress (more than 330 MPa) can also be attributed to twinning as this deformation mechanism was already recognised as a reason of increased stress level in tension (Barnett, 2007a). A constitutive model which shows that {10-12} tensile twinning can be responsible for a high value of the work hardening exponent obtained in this work ($n = 0.45$), was also developed in the referred article. It could be explained by a lattice rotation in twinned regions to a new orientation, less favourable for slip on basal plane, which increases stress during further deformation. Moreover, the stress increase can be also explained by formation of twin boundaries, which can act as barriers for dislocation movement.
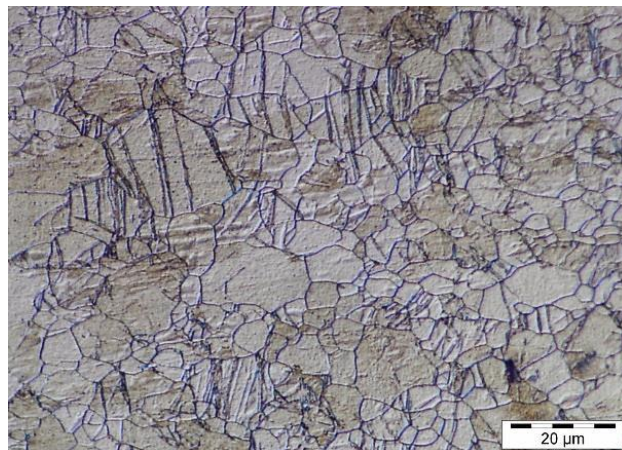
Fig. 5.18. Microstructure image (OM) of sample processed by I-ECAP at 250 °C (no. 5) followed by annealing and subjected to tensile test. The image was taken after failure in a strain gauge zone close to fracture point. Tensile direction is horizontal.

Increase of grain size from ~1 µm to ~3.7 µm induced by static recrystallisation was observed in sample 14 processed at 150 °C. It showed that microstructure with the average grain size ~1 µm is not stable at 300 °C, opposite to the grain size 3-6 µm which was not affected by heat treatment at the same temperature. As a consequence

of grain coarsening to ~3.7 μm, yield stress was lowered from 287 MPa to 165 MPa and true strain at break increased from 0.16 to 0.26. The conclusion can be drawn that the average grain size ~1 μm or smaller is required to achieve a high yield stress (290 MPa). It should be also noted that the grain size of the sample I-ECAPed by route A followed by annealing and as-processed sample after route C were almost the same (~3.7 μm and ~3.5 μm, respectively) but the flow stress curves were completely different (Fig. 5.6b an c), which proves that texture produced during I-ECAP is more relevant to obtained mechanical properties than grain size.

Sample 3 processed by four passes at 250 °C by route A was annealed for 6 hours at 300 °C, which was expected to result in a very similar grain size as observed for sample processed by route C (Fig. 5.14f) since the initial microstructures were almost the same. As it was shown in Fig. 5.7, flow stress curves obtained from compression tests showed that the distinctive concave shape of the curve after extrusion was not suppressed by I-ECAP processing using route A. Additionally, heat treatment was shown to have a very little effect on the compressive behaviour of sample 3 since the concave shape was still observed and ductility improvement could be considered as negligible. It was already discussed in Section 5.6.1 that texture produced during processing by route A is responsible for the observed shape of the flow stress curve. The conducted compression tests confirmed that the strong texture produced during I-ECAP cannot by removed by heat treatment.

5.7. Modelling microstructure evolution during ECAP and I-ECAP of magnesium alloy using cellular automata finite element (CAFE) method

5.7.1. Introduction

Figueiredo and Langdon (2010) presented a model, which states that the mechanism of grain refinement during ECAP processing of AZ31 magnesium alloy is dynamic recrystallization (DRX). This hypothesis is based on the occurrence of a bimodal microstructure after ECAP processing. They also introduced a 'critical grain size' term in order to explain that homogenous grain size distribution is possible to achieve only if the initial mean grain size is small enough. Otherwise, the newly formed recrystallized grains are not able to fully consume the initial coarse grains. Similar observations were made earlier by other researchers (Janecek et al., 2007; Lapovok et al., 2008; Ding et al., 2009).

The studies on DRX in AZ31 magnesium alloy during compression testing show that the size of recrystallized grains depends on temperature and strain. However, the relation between inverse grain size and strain is not linear and after reaching a maximum point, the size of recrystallized grains remains constant despite further deformation (Beer and Barnett, 2007; Fatemi-Varzaneh et al., 2007). Similarly in ECAP, after reaching a minimum mean grain size for a given temperature, subsequent passes do not lead to further grain refinement but only to microstructure homogenization.

In this section, a numerical model is developed to see if microstructure evolution during subsequent passes of ECAP/I-ECAP can be predicted using equations usually

used to simulate DRX. Therefore, cellular automata transition rules, which are usually used to describe DRX during hot forming of metals, are applied in the proposed model. Despite ECAP and I-ECAP of magnesium alloys sometimes being realised at low temperatures, microstructure evolution was not simulated below 200 °C. It was justified by the fact that dynamic recrystallisation is very limited below 200 °C (Agnew and Duygulu, 2005) and grain refinement in ECAP is believed to be controlled by other mechanisms.

5.7.2. *Cellular automata (CA) technique*

Cellular automata (CA) technique is used in material science to visualise digital material representation and simulate its evolution during processing (Madej et al., 2009; Hallberg et al., 2010; Svyetlichnyy, 2012). Material representation is divided into a lattice of finite cells, called the cellular automata space. The interactions between cells describe dynamics of the simulated physical phenomenon. Mathematical description of interactions is introduced by transition functions (transition rules). The current state of a cell is determined by the states of its neighbours and its own state in the previous step. Cellular automata finite element (CAFE) approach is the example of a multi scale modelling approach; it is the combination of micro scale modelling using cellular automata and finite element (FE) analysis, which is the most popular method used for metal forming simulations. The main feature of the presented technique is to exchange information between modelling scales. Therefore, results obtained from FE simulation influence microstructure evolution and microstructure characteristics could also affect FE calculations.

The advantages of using a multi scale approach are evident, especially when ultrafine-grained materials are considered. Using CA method not only a mean grain size but also microstructure homogeneity and grain size distribution can be calculated. This makes it a very useful tool since materials with the same mean grain sizes could exhibit different flow behaviour depending on their microstructure homogeneity. In this case, modelling grain size distribution is necessary for accurate prediction of mechanical properties. Another advantage of the CA approach is a possibility of describing stochastic phenomena since many real world effects have random nature.

5.7.3. *Model overview*

Microstructure evolution during ECAP and I-ECAP is modelled using a CAFE model (Fig. 5.19). The CA space plays the role of a digital material representation in meso scale, where artificial grains are composed of CA cells. Microstructure evolution is described by a transition function; parameters of this function are macro scale integration point variables obtained from FE simulation: strain, strain rate and temperature (mapped from FE nodes). Random pentagonal neighbourhood and absorbing boundary conditions were used to define the CA space and its dynamics.

The internal state variable model (Pietrzyk, 2002), which treats dislocation density as a microstructural material variable, is used to describe changes that occur in micro scale during plastic deformation. Firstly, total dislocation density is calculated using an internal state variable evolution equation. Then, total dislocation density is divided by an arbitrary number of cells so a unit dislocation density is calculated. For each one of the randomly chosen cells, its intrinsic dislocation density is increased by

the calculated unit dislocation density. The onset of nucleation during DRX is associated with the increase in intrinsic dislocation density; the critical value of this parameter in a CA cell must be reached for a new grain to occur. Further grain growth is controlled by temperature and misorientation angle between the new grain and a grain being consumed.
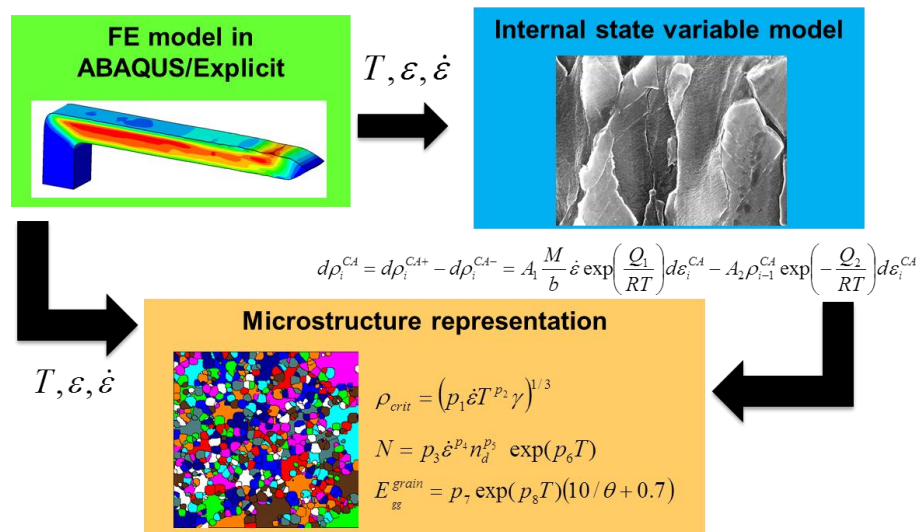
Fig. 5.19. CAFE model overview

5.7.4. *Dislocation density evolution*

Evolution of dislocation density during hot metal forming is controlled by two competing processes: strain hardening and thermal softening caused by recovery or recrystallization. Increase in dislocation density is caused by storage of dislocations while decrease in dislocation density results from annihilation of dislocations. The change of dislocation density due to strain increment is described by the following equation (Sellars and Zhu, 2000):

$$dp_i^{CA} = dp_i^{CA+} - dp_i^{CA-} = A_1 \frac{M}{b} \dot{\varepsilon} \exp\left(\frac{Q_1}{RT}\right) d\varepsilon_i^{CA} - A_2 \rho_{i-1}^{CA} \exp\left(-\frac{Q_2}{RT}\right) d\varepsilon_i^{CA}, \qquad (5.1)$$

where: M − Taylor factor, b − Burgers vector, $d\varepsilon$− effective strain increment, Q_1 − activation energy for deformation, R − gas constant, T − temperature, $\dot{\varepsilon}$ − effective strain rate, ρ_{i-1}^{CA} − dislocation density at previous strain increment, Q_2 − activation energy for self-diffusion, A_1, A_2 − fitting parameters.

The presented approach is similar to the model developed by Mecking and Kocks (1981) where dislocation density evolution is also introduced as competition between dislocations storage and annihilation. Decrease in dislocation density is dependent on temperature as dislocation annihilation is characterised as thermally activated process.

Parameters of equation (5.1) were derived from the literature (Table 5.2). Fitting coefficients were determined using Hooke-Jeeves optimization method (Kelley, 1999). Dislocation density dependence on strain at 200 °C and strain rate 0.01 s^{-1} based on these parameters, together with experimental results obtained for pure magnesium in similar conditions (Klimanek & Poetzsch, 2002; Mathis et al., 2004), are illustrated in Fig. 5.20.

Table 5.3. Parameters of dislocation density evolution equation (5.1)

A_1	A_2	Q_1, kJ/mol (Barnett, 2003)	Q_2, kJ/mol (Beer & Barnett, 2006)	M, - (Chino et al., 2006)	b, nm (Chino et al., 2006)
3.85e3	30	147	135	2.38	0.32
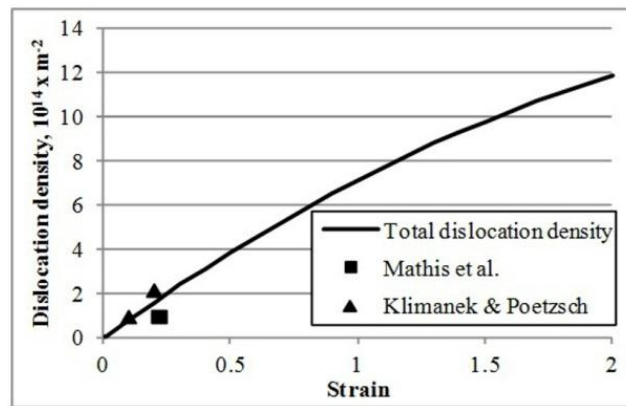
Fig. 5.20. Dislocation density evolution at 200 °C and strain rate 0.01 s^{-1}. Experimental data were taken from the works by Klimanek and Poetzsch (2002) and Mathis et al. (2004).

5.7.5. Cellular automata space evolution

Microstructure evolution during processing is modelled using transition rules, which describe how each CA cell state changes depending on its own and its neighbour state. The intrinsic dislocation density is increased in selected cells at each time increment. The cells are chosen randomly; however, a distance between the cell and the closest grain boundary significantly influences if its intrinsic dislocation density is increased or not. The likelihood of cell selection is inversely proportional to distance between the cell and the closest grain boundary. As a consequence, privileged areas for the dislocation density rise are grain boundaries and their vicinities.

The CA space dynamics can be described by the following rules:

- cell becomes the site of nucleation when its dislocation density exceeds a critical value (Galiyev et al., 2003);

- cell changes its state to recrystallized when one of its neighbours is recrystallized; grain grows until its virtual energy related to its grow potential is greater than zero; new grains cannot be consumed by other recrystallized grains.

A critical value of dislocation density in a CA cell must be reached to create a new grain nucleus in this cell. The nucleation process will be favoured at sites with increased level of stored energy. Following these arguments, equation (5.2) is used to calculate critical dislocation density. This is a simplified form of the formula introduced by Roberts and Ahlblom (1978):

$$\rho_{crit} = \left(p_1 \dot{\varepsilon} T^{p_2} \gamma\right)^{1/3}, \tag{5.2}$$

where: γ – grain boundary energy, p_1, p_2 – fitting parameters (Table 5.3).

Grain boundary energy depends on the misorientation angle between neighbouring grains. It was evaluated from the equation derived by Read and Shockley (1950) for low angle grain boundaries and for high angle grain boundaries it is kept constant. Initial orientations of grains were generated randomly and misorientation between neighbouring grains was calculated using a method presented by Zhu et al. (2000). Twinning was not taken into account since processing at elevated temperatures was simulated and twins were not revealed in the microscopic observations.

At each time step, total dislocation density increment is divided by a number of randomly chosen cells, N, which intrinsic dislocation density will be increased. N is dependent on temperature and strain rate obtained from FE simulation. Since grain boundaries are privileged areas for nucleation, more new nuclei are expected to

appear when there are more grains in the CA space. Evolution of N is given by equation:

$$N = p_3 \dot{\varepsilon}^{p_4} n_d^{p_5} \exp(p_6 T), \tag{5.3}$$

where: N – number of cells with increased extrinsic dislocation density, n_d – number of grains in CA space, p_3, p_4, p_5, p_6 – fitting parameters (Table 5.3).

The grain growth rate is associated with virtual energy assigned to each new nucleus. Since mean DRXed grain size is dependent mostly on temperature, grain growth energy is a function of temperature and misorientation angle. As the new grain grows, its energy is lowered. The process is stopped when the grain growth energy is equal to zero. In this condition, the grain has no potential for further expansion. The grain growth energy is introduced using an empirical equation:

$$E_{gg}^{grain} = p_7 \exp(p_8 T)(10/\theta + 0.7), \tag{5.4}$$

where: T – temperature, θ – misorientation angle, p_7, p_8 – fitting parameters (Table 5.3).

Table 5.4. Parameters of CA space evolution equations (5.2-5.4)

p_1	p_2	p_3	p_4	p_5	p_6	p_7	p_8
4.0756e7	-31.4176	0.6677e18	0.004261	1.06699	-0.092	1.1463	0.094

5.7.6. Model limitations

The model is based on empirical observations rather than pure mathematical description of all physical phenomena occurring during plastic deformation. Many simplifications and assumptions were made to develop the presented model; the most important of them are listed below:

1. Cellular automata cells have not underwent plastic deformation; therefore, the strain increment was introduced artificially. As a consequence, it is not possible to predict shape of particular cells, which can affect nucleation and growth of recrystallized grains. It is a general drawback of the CA method and the approach used in this work is commonly found in the literature (Ding and Guo, 2002; Madej et al., 2009; Das, 2010).

2. Mechanical shearing of grains when material is going through a channel intersection is not taken into account, only an artificial transition from the state before deformation to final microstructure is considered. One of the many difficulties when trying to develop a model of grain shearing during ECAP is lack of experimental data since it is virtually impossible to perform *in situ* observations in the deformation zone.

3. A dislocation density variable used in this work describes artificially all types of dislocations that are produced during processing. In reality, there are many types of dislocations that have different origins and effects on material behaviour.

5.7.7. Simulation details

FE simulations were run using ABAQUS/Explicit commercial software. Calculations and visualisations of CA microstructure evolution were performed using a self-developed software. CA space dimensions were 400 x 400 cells, which corresponded to 100 x 100 μm^2 area of a real material. Results obtained from I-ECAP conducted at 250 °C were used in this study. In order to investigate temperature and strain rate effect on the final mean grain size and microstructure homogeneity, additional experimental results for ECAP obtained with various processing parameters were derived from the literature (Table 5.4). Simulations were performed for temperatures: 200, 225 and 250 °C and strain rates within range 0.01-0.5 s^{-1}. Colours showed in numerical predictions of microstructures (Fig. 5.21-5.23) have no physical meaning.

Table 5.5. Simulations parameters

	Initial temperature, °C	Strain rate, s^{-1}	Channel angle, °
I-ECAP (this work)	250	0.5	90
Ding et al. (2009)	225	0.3	120
Ding et al. (2009)	200	0.3	120
Jin et al. (2006)	225	0.01	90

5.7.8. Simulations results

The initial microstructure of the material was heterogeneous; coarse grains were surrounded by smaller ones (Fig. 5.21a), which could be attributed to DRX during hot extrusion of the supplied rods. The corresponding digital representation of the as-received material was obtained by uniform grain growth and simulation of DRX (Fig. 5.21b). The mean grain size obtained after I-ECAP was ~6 μm (Fig. 5.21c),

which is similar to the results obtained by Suwas et al. (2007). However, strain rate values in both studies were significantly different, which indicates that processing temperature had a dominant effect on the final grain size. The simulated microstructure was similar to the real one and the predicted grain size was 6.3 μm (Fig. 5.21d).

Fig. 5.21. Microstructure images of as-received material (a) and after 4th pass of I-ECAP at 250 °C (c); corresponding simulation results in (b) and (d).

Ding et al. (2009) conducted ECAP of AZ31 magnesium alloy at 200 °C and 225 °C using a die with 120° channel angle. The initial microstructure and its digital material representation are shown in Fig. 5.22a and b, respectively. The initial mean grain size was 7.2 μm, the same as the average grain size of CA representation. The microstructure obtained after 4 passes at 200 °C and the corresponding results of modelling microstructure evolution are shown in Fig. 5.22c and d, respectively. After 4 passes at 200 °C the grain size was reduced to 1.8 μm while the model predicted

1.7 µm. The mean grain size after processing at 225 °C calculated using the developed model was 2.2 µm, while experimental result was 2.4 µm.
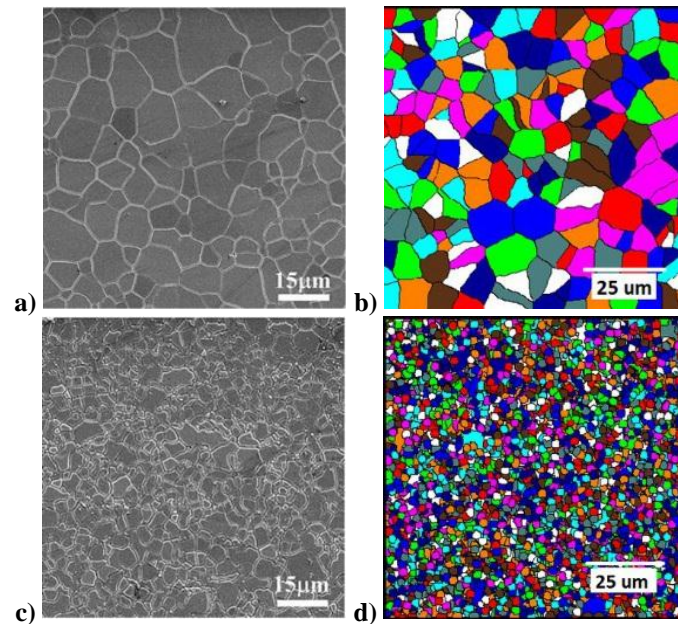
Fig. 5.22. Microstructure images of as-received material (a) and after 4th pass of ECAP at 200 °C (c); corresponding simulation results in (b) and (d). The microstructural images were taken from the work by Ding et al. (2009).

The initial mean grain size of a material processed by Jin et al. (2006) was 15.6 µm; coarse grains and few smaller grains on their grain boundaries were observed, as shown in Fig. 5.23a. A digital material representation was generated using non-uniform grain growth: 80% of grains grew slower than others and the mean grain size was 15.8 µm. After first pass at 225 °C, coarse grains were surrounded by colonies of very small ones (Fig. 5.23c). Interiors of coarse grains were not consumed during DRX process. The mean grain size after first pass was measured to be 4.1 µm while the model predicted 4.25 µm.
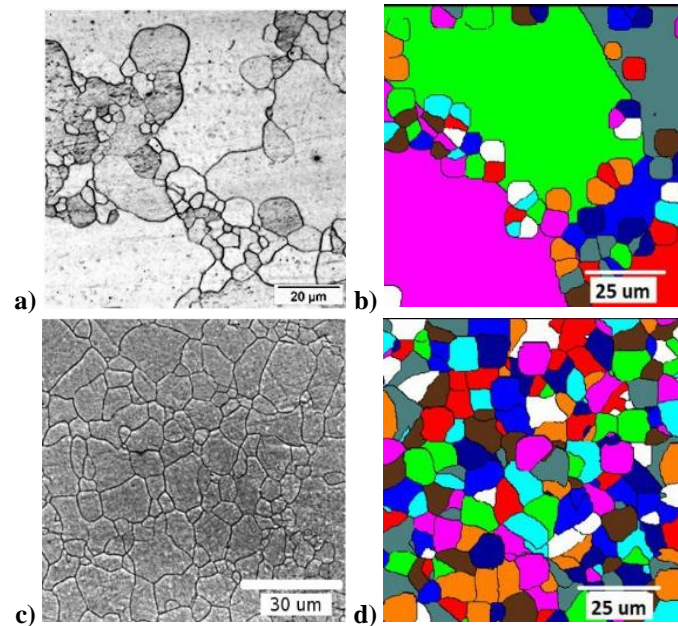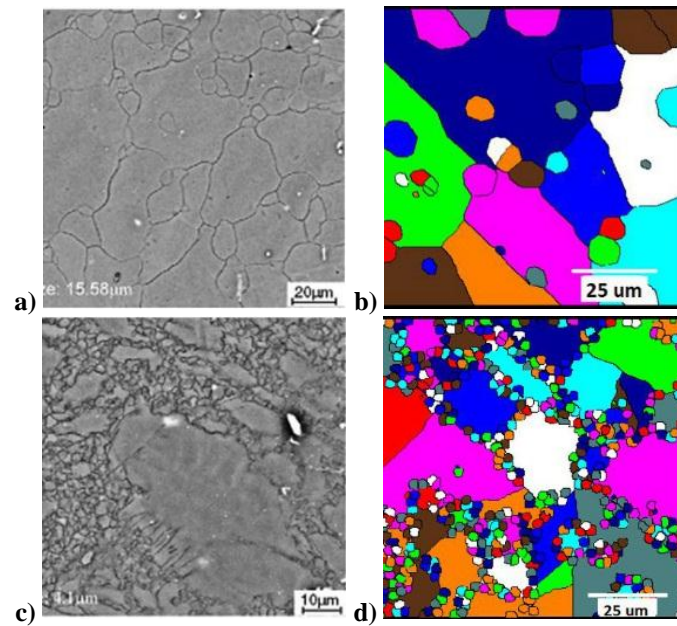
Fig. 5.23. Microstructure images of as-received material (a) and after 1st pass of ECAP at 225 °C (c); corresponding simulation results in (b) and (d). The microstructural images were taken from the work by Jin et al. (2006).

The results obtained using the developed CAFE model are in good agreement with experimental data (Fig. 5.24). The mean grain size after first pass depends strongly on the initial microstructure. A significant grain refinement is observed after first pass but it is not sufficient to refine a microstructure dominated by coarse grains. Only grains smaller than ~15 μm can be fully recrystallized during the first pass of ECAP at 200 °C. A heterogeneous grain size distribution is obtained if larger grains are found in the initial microstructure and further deformation is needed to refine and homogenize the structure. Grain refinement is controlled by temperature, it is shown that the mean grain size as small as ~2 μm can be obtained at 200 °C. This observation was also confirmed during I-ECAP experiments at 200 °C (Section 5.4.1 of this work). Although smaller grain size cannot be obtained at a given temperature, further processing leads to microstructure homogenization.
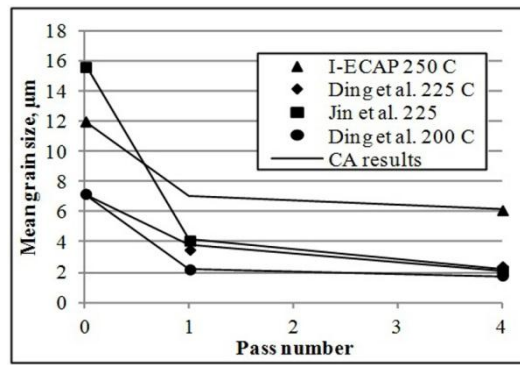
Fig. 5.24. Mean grain size obtained from the experiments and CAFE simulations.

5.7.9. *Summary of the simulation results*

A multi scale CAFE model was developed in order to simulate microstructure evolution during I-ECAP and ECAP. Computations were performed for various temperatures and strain rates which are typical for processing of magnesium alloys. Numerical results were verified using experimental data from conventional and incremental ECAP. The former were derived from the literature, the latter was obtained from I-ECAP experiments. Microstructure evolution below 200 °C was not studied as DRX is very limited below this temperature.

The model correctly predicted both the mean grain size after subsequent passes of ECAP/I-ECAP and microstructure homogeneity. In particular, a heterogeneous grain size distribution after first pass of ECAP for initially coarse-grained microstructure was predicted as well as its further homogenization. It was shown through numerical simulation that microstructure evolution during ECAP and I-ECAP can be predicted using the model based on DRX assumptions. It supports the idea that grain refinement in ECAP and I-ECAP at elevated temperatures is controlled by DRX.

5.8. Summary

The effects of temperature and processing route of I-ECAP on mechanical properties, grain size and texture of AZ31B magnesium alloy were investigated in this chapter. Selected samples were subjected to heat treatment after I-ECAP processing to improve their ductility. Moreover, microstructure characterisations of tensioned and compressed coarse- and fine-grained samples were performed to determine a dominating deformation mechanism.

It was revealed that mechanical properties of AZ31B magnesium alloy subjected to I-ECAP are controlled by texture. The obtained results showed that processing route did not influence grain size, which was dependent on billet temperature. Processing at 250 °C can be used to improve ductility of AZ31B magnesium alloy; the obtained grain size and mechanical properties are comparable to those reported for conventional ECAP. However, significant strength decrease after I-ECAP at 250 °C, reported also after conventional ECAP at the same temperature, is also observed.

Room temperature ductility of magnesium alloy AZ31B can be improved to ~0.2 of true strain without sacrificing strength by conducting four passes at 250 °C and two additional passes at 200 °C using route A. Yield strength increase to 290 MPa can be achieved by lowering processing temperature to 150 °C, which results in grain refinement to ~1 µm. The highest value of room temperature ductility (above 40%) was obtained in this study for samples annealed at 300 °C after I-ECAP. Tension-compression asymmetry, observed for the extruded rod, was suppressed by using routes B_C and C of I-ECAP in samples tested along extrusion direction. This effect

163

was attributed to the texture development and microstructure homogenization after processing.

Ex situ analysis of I-ECAPed samples subjected to tension and compression showed that increased ductility after I-ECAP was attributed to the suppression of twinning and facilitation of slip on basal and non-basal planes. Shear bands were observed in I-ECAPed samples subjected to tension. The larger amount of shear bands and smaller spacing between them were observed in samples which exhibited improved ductility.

Finally, it was shown through numerical simulation that microstructure evolution during subsequent passes of ECAP and I-ECAP can be predicted using the model based on the dynamic recrystallisation (DRX) assumptions. It supports the idea that grain refinement in ECAP and I-ECAP at elevated temperatures is controlled by DRX.

Chapter 6

Mechanical properties and microstructure of magnesium alloy sheet produced by I-ECAP followed by upsetting

6.1. Introduction

Twinning in magnesium alloys is very often observed at room temperature as this deformation mode is required to enable plastic strain due to insufficient number of slip systems on basal plane. However, recent *ex situ* studies showed that twinning can be also responsible for material fracture. Twin-sized voids were revealed in regions previously occupied by double twins in samples subjected to tension (Barnett, 2007b) and plane strain compression (Al-Samman and Gottstein, 2008a). Moreover, plate-like voids were observed on the fracture surface of AZ31 subjected to tension, which was attributed to the operation of a twinning-related mechanism of voids formation (Marya et al., 2006). However, a clear evidence of a twin evolving to a microcrack has not been presented yet. The effect of grain size on twinning activity has already been reported for uniaxial compression (Barnett et al., 2004) and tension (Chino et al., 2008), and it was shown that grain refinement led to a significant decrease in the number of twins.

The above results lead to the conclusion that reducing grain size can suppress twinning and improve ductility. Grain refinement resulting in formability improvement has been already achieved in magnesium alloy bars by I-ECAP, which was presented in Chapter 5. It was shown in the literature that I-ECAP can be used to produce not only bars but also sheets and plates. An introduction of a sheet

separating tool to the input channel of the I-ECAP rig enabled processing 2 mm thick aluminium sheets (Rosochowski et al., 2010). Another approach was used in this work; fine-grained flat products were obtained by I-ECAP followed by side upsetting. It was assumed that significant grain refinement after I-ECAP will enable remarkable cross-sectional reduction in only one operation conducted at elevated temperature.

The microstructure evolution in coarse- and fine-grained sheet samples subjected to tension was observed *in situ* in order to: (1) verify numerical and experimental results, which indicated that fracture can be initiated inside twins (Barnett, 2007b; Al-Samman and Gottstein, 2008a); (2) show twinning suppression in fine-grained samples and its effect on formability enhancement; (3) investigate a grain size effect on the fracture mechanism. Additionally, FE simulations of microstructure evolution were performed to enable interpretation of experimental results.

6.2. Experimental procedure

Material used in the present work was AZ31B wrought magnesium alloy. It was purchased in the form of hot-extruded rods with diameters of 16.8 mm, the material was characterised in Section 3.4. Square cross-section bars, with dimensions 10 mm $\times$ 10 mm $\times$ 120 mm, were machined from the rods along the extrusion direction and subjected to I-ECAP followed by side upsetting (Fig. 6.1) to reduce grain size. A double-billet variant of I-ECAP, with a 90° angle between channels, was realised using a 1 MN hydraulic servo press. Four passes with a billet rotation of 90° after each pass, known in literature as route B_C, were conducted at 250±2 °C. Plastic strain

was introduced using a punch which followed a sine wave signal defined by peak-to-peak amplitude A=2 mm and frequency f=0.5 Hz. Material feeding was realised by a motor-driven screw jack, synchronized with the reciprocating movement of the punch. Feeding stroke in each cycle was d=0.2 mm. After I-ECAP, a billet was put on its side and upset from the initial thickness of 10 mm to 2 mm, equivalent to logarithmic strain of -1.6, using a 2.5 MN hydraulic press. Upsetting was conducted at 200±5 °C using preheated and lubricated platens with a constant ram velocity 0.1 mm/s. Compression was stopped after ram displacements of ~4 mm and ~6 mm to lubricate upper and lower surfaces of the billet. Molybdenum disulphide (MoS_2) grease was used as a lubricant. The maximum force measured during compression was 1.25 MN. Three AZ31B magnesium alloy sheets were obtained using this technique.

I-ECAP

Upsetting

Temperature: 250 °C
Feeding stroke: 0.2 mm
Amplitude: 2 mm
Frequency: 0.5 Hz
Billet size: 10 x 10 x 120 mm³

Temperature: 200 °C
Initial billet height: 10 mm
Final height: 2 mm
Velocity: 0.1 mm/s
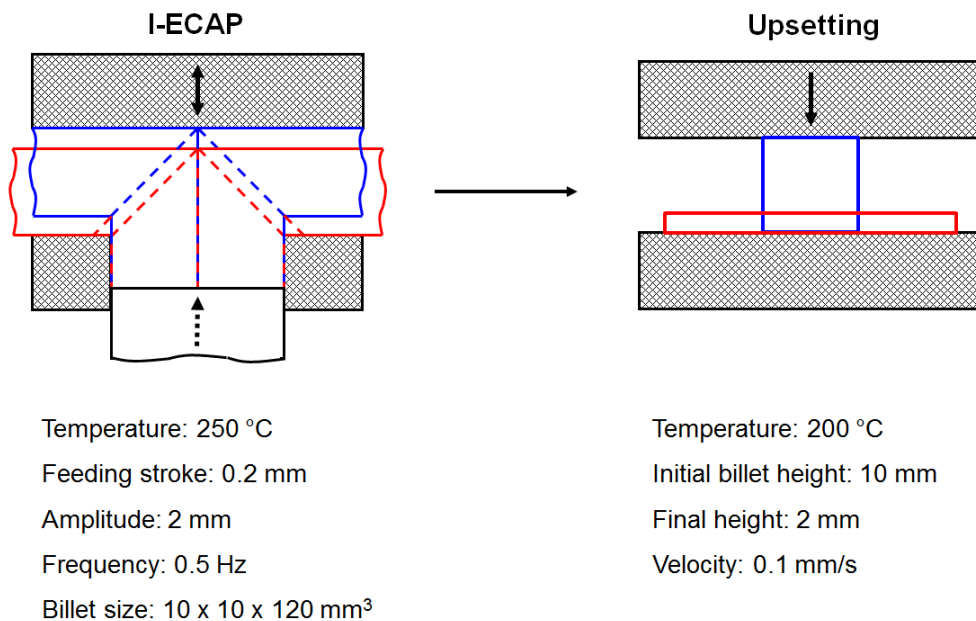
Fig. 6.1. Experimental procedure of producing fine-grained magnesium alloy sheets.

Flat tensile samples with thickness 2 mm and strain gauge dimensions of 4 mm × 15 mm were cut out along extrusion direction from both extruded (coarse-grained) and I-ECAPed and upset (fine-grained) billets. *In situ* tests were performed using a screw-driven tensile stage (Fig. 6.2a) placed inside a chamber of Jeol 7001FLV scanning electron microscope (SEM), shown in Fig. 6.2b. The experiments were performed in LEM3 Laboratory at ENSAM-Arts et Métiers ParisTech, Metz, France. Tensile testing was conducted at room temperature with a constant velocity 0.5 mm/s, which was equivalent to initial strain rate 3.3×10^{-2} s^{-1}. Cross-head displacement was measured using an LVDT displacement transducer. Since it is not an accurate method of strain measurement, additional tensile tests were conducted on Instron 5969 testing machine equipped with video-extensometer. The obtained flow stress curves were used to compare mechanical properties of investigated materials and to correct an overestimation of strain measured by the LVDT transducer. SEM images of coarse-grained samples were taken at true strains: 0.008, 0.02, 0.03, 0.06, 0.08, and 0.087 (fracture strain). In the case of fine-grained samples, testing was stopped to take pictures at true strains: 0.02, 0.03, 0.06, 0.13, and 0.19 (fracture strain).
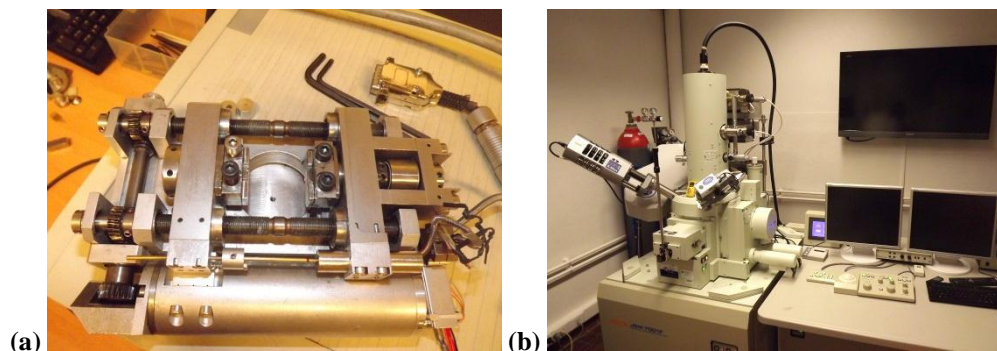
Fig. 6.2. The screw-driven tensile stage (a) and Jeol 7001FLV scanning electron microscope (b) used for experiments.

The samples were ground, polished and etched before putting into a SEM chamber. The preparation procedure included: grinding using SiC paper P600 and P1200, mechanical polishing using polycrystalline suspensions with particle sizes: 9, 3, and 1 μm, chemical treatment with nital and final polishing with 0.02 μm alumina suspension. Then, specimens were etched using acetic picral to reveal grain boundaries. The mean grain size was measured by a linear intercept method using Olympus analysis software.

The percentage of twinned area in coarse-grained samples was evaluated using ImageJ, a freeware image processing application (Fig. 6.3a). In order to estimate the twin size, each twin was framed by a polygon (Fig. 6.3b), which captured its particular shape, and the software calculated a total surface area of polygons. This approach enabled to take into account not only the increasing number of twins but also their growth. Dimensions of the examined zone were 380 μm x 280 μm and the magnification ratio was 330.

(a)

(b)
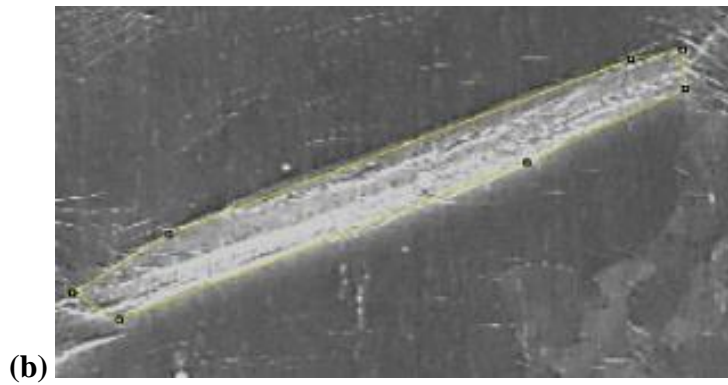
Fig. 6.3. Screenshot from ImageJ software (a) and zoomed twin, which was framed by a polygon in order to evaluate its surface area (b).

6.3. Results

6.3.1. Sample appearance

The samples were severely distorted after four passes of I-ECAP using route B_C, as shown in Fig. 6.4. This could be attributed to inhomogeneous mechanical properties in the transverse direction of such samples, which was investigated in Section 4.5 through numerical simulation. A sample after side upsetting to 2 mm is also displayed in Fig. 6.4. The irregular shape of the flat sample is caused by the billet distortion after I-ECAP. Despite a significant thickness reduction, fracture was not observed on the sample surface.

Fig. 6.4. Samples after four passes of I-ECAP (upper) and I-ECAP followed by side upsetting (lower).

6.3.2. Microstructures

Microstructure was remarkably refined and homogenised after I-ECAP. The average grain size after four passes at 250 °C was ~5.5 µm. Although the upsetting temperature was lowered to 200 °C, the average grain size was not changed significantly and was measured as ~4 µm after thickness reduction to 2 mm. A lot of grains as small as 1 µm are displayed in Fig. 6.5c; however, a few 10 µm grains are also visible. Low efficiency of grain refinement could have been caused by a very slow strain rate during compression, which could have not been changed due to technical limitations of the press.
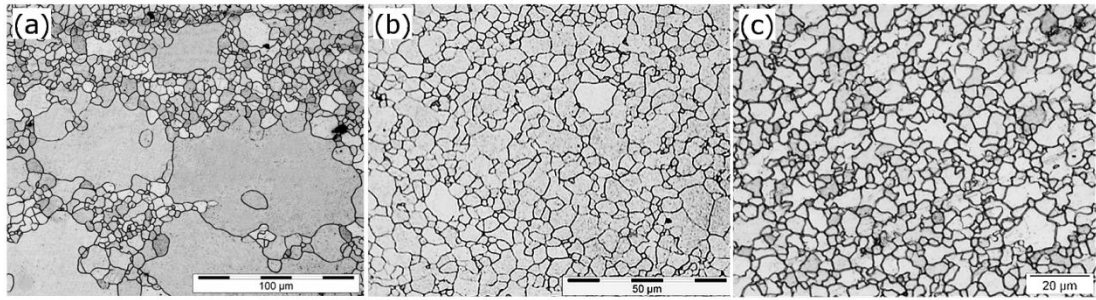
Fig. 6.5. Microstructures of extruded (a), I-ECAPed (b), and I-ECAPed and upset (c) samples.

6.3.3. Mechanical properties

Mechanical properties of the extruded rod were significantly changed after I-ECAP by route B_C (Fig. 6.6). Yield strength was lowered from 220 MPa to 80 MPa while ductility was increased from 0.09 to 0.23 of tensile true strain. The texture-related weakening of the material was already discussed in Section 5.6.1. Upsetting applied to I-ECAPed sample has changed mechanical properties of the material (Fig. 6.6). Yield stress was increased from 80 MPa to 145 MPa while true strain at fracture dropped from 0.23 to 0.19. Material strengthening can be attributed to decrease in the average grain size and to increase in dislocation density, due to a high strain (logarithmic strain of ~1.6) imposed to the billet at relatively low temperature (200 °C). It is also very likely that compressive deformation applied during upsetting has changed the alignment of basal planes to less favourable for slip, as they were tilted at ~45° after I-ECAP (Section 5.5). However, textural measurements that could confirm this suspicion have not been performed due to a high level of deformation.
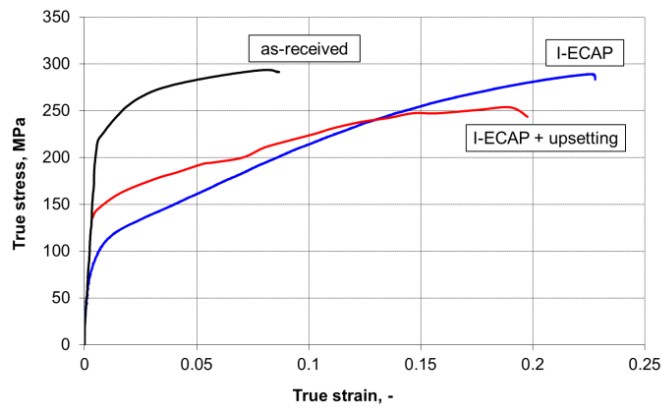
Fig. 6.6. Mechanical properties after extrusion (as-received), I-ECAP, and I-ECAP followed by side upsetting.

6.4. FE simulation of microstructure evolution in tension

A model of microstructure evolution was developed in order to interpret phenomena observed during *in situ* tensile testing of coarse- and fine-grained samples. Fracture occurrence in samples with various grain sizes subjected to tension was studied using a ductile damage model with strain and stress triaxiality as parameters. Numerical predictions were verified experimentally in Sections 6.5 and 6.6.

6.4.1. *Procedure for model development*

First, a tensile test of flat sample machined from AZ31B hot-extruded rod was conducted. Then, a macroscopic model of the test was developed in ABAQUS FE software (ver. 6.10). The results from both mechanical test and FE simulation enabled determination of the mechanical field in the sample during tensile testing. A single FE element was 'cut out' from the middle of the macroscopic model. It was meshed and used as a micro model of tensile test. Boundary conditions for micro modelling were obtained from the macroscopic results. A representative area of the

microstructure was stretched to obtain a homogeneous strain field coinciding with macroscopic results. Single inclusion, twin-like inclusion and polycrystalline structure were placed in the middle of the homogenous matrix in order to investigate their effects on strain distribution homogeneity and fracture behaviour.

6.4.2. Simulation details

Two-dimensional macro and micro models of the test were developed in ABAQUS/Explicit FE software. They were meshed using CPS4R elements, which are 4-node bilinear plane stress quadrilateral elements with reduced integration and default hourglass control. The strain gauge zone of the specimen was meshed using 3600 elements. The micro model, with dimensions 1 mm × 1 mm, was meshed using 2500 elements. In order to determine boundary conditions for the micro model, the relative change of the FE element dimensions were determined from the macro scale. An element from the centre of the sample was chosen, the total length along pulling direction (X direction) was increased to 1.08979 mm. Thus, the displacement of the micro sample side edges was set up to 0.08979 mm. Lower and upper edges were not constrained, the total decrease of the micro sample height was -0.04125 mm. Figure 6.7 shows the displacement along X direction (constrained) and Y direction (moving freely) of the right upper corner of the micro sample.
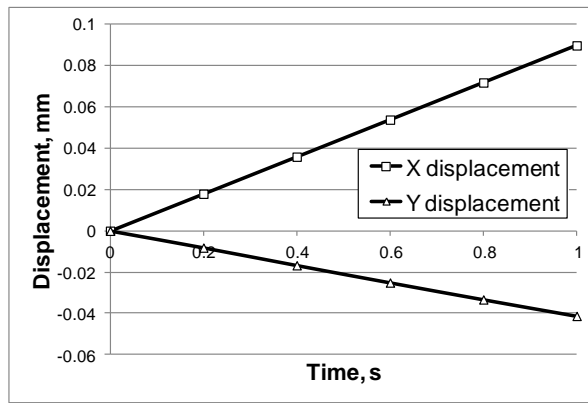
Fig. 6.7. Displacement of the right upper corner of the micro sample during pulling.

A ductile damage model available in ABAQUS was incorporated into FE micro modelling in order to investigate the fracture behaviour of the sample subjected to tension. The model is based on the concept of a critical strain that can be introduced into material without damaging it. FE elements with exceeded critical strain are removed from the model during simulation. The value of the critical strain is dependent on stress triaxiality, defined as $k = -p/\sigma_S$, where p is pressure and σ_S is effective yield stress. It was assumed that for lower stress triaxiality the fracture strain is larger and for higher triaxiality the material is more prone to fracture, the model used in the current study is shown in Fig. 6.8.
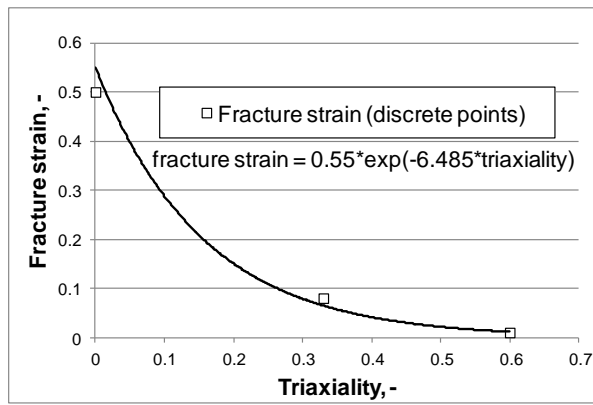
(b)

Fig. 6.8. Ductile damage model (a) and stress triaxiality distribution at the final stage of a tensile test (b).

6.4.3. Single inclusion model

A single inclusion was introduced into the homogenous matrix in order to investigate its effect on the material flow. The behaviour of matrix is defined by a flow stress curve obtained from tensile test (Fig. 6.6). The inclusion was 0.08 mm in diameter and was placed in the middle of the sample. Two different variants with hard and soft inclusion were tested. The former was defined by ideally plastic isotropic material model with yield stress defined as 80% of the matrix yield stress and the latter is 120% of the matrix yield stress. The initial state of the model is shown in Fig. 6.9a. Figures 6.9b and 6.9c show fractured samples with soft and hard inclusion, respectively.
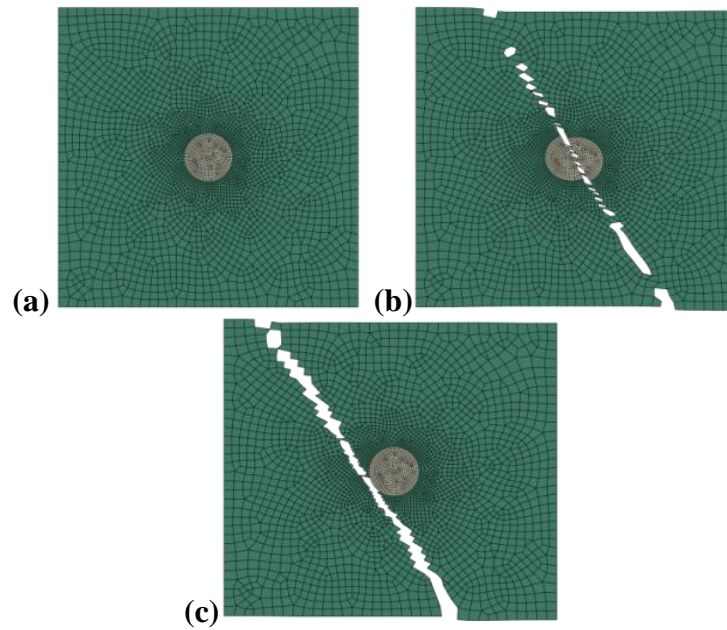
Fig. 6.9. Single inclusion model (a); model with soft inclusion after fracture (b); model with hard inclusion after fracture (c).

It is clearly shown in Fig. 6.9b and 6.9c that fracture is initiated in different areas of the sample depending on the inclusion strength. In the case of soft inclusion, strain is localised in the middle of the inclusion and then propagates to its boundary. Then, the matrix is being sheared since the inclusion cannot accommodate more strain. The harder inclusion requires higher stresses than the matrix to accommodate large strain. Therefore, strain is almost uniformly distributed along matrix surface. Finally, the strain localisation occurs on the matrix-inclusion interface due to inconsistency between stress values in the inclusion and the matrix.

6.4.4. Mechanical response of twin-like inclusion

The single inclusion model was modified by addition of a twin-like particle, as shown in Fig. 6.10a. Similarly to the previous model, the flow stress of the matrix is

described by the curve obtained from tensile test. The flow stress of the round inclusion is 120% of the matrix; isotropic material model is used. The flow behaviour of twin-like inclusion is assumed to be ideally plastic. Two different variants are tested: twin with yield stress 200 MPa and 500 MPa. The deformation zone in both cases is dominated by tensile stresses as shown in Fig. 6.10b and Fig. 6.10c. However, in the case of soft twin variant the maximum tensile stress is concentrated in the twin corners. In the hard twin variant, the maximum tensile stress occurs on the inclusion-matrix and inclusion-twin interfaces. Since the matrix is softer than the twin and inclusion, the strain is localised on its boundary and the fracture mechanism is similar to that shown in Fig. 6.9c.

The tensile stress concentration observed in twin corners leads to an earlier fracture of the sample. Figure 6.11 shows the crack initiation and propagation in the ideally plastic twin with yield stress 200 MPa, which is less than yield stress in the surrounding inclusion and the matrix. It is apparent from Fig. 6.11b that fracture is initiated in the twin corners and then propagated to its interior. It can be concluded from the FE simulation results that twins, which are softer are more prone to fracture that twins with higher yield stress.

(a)
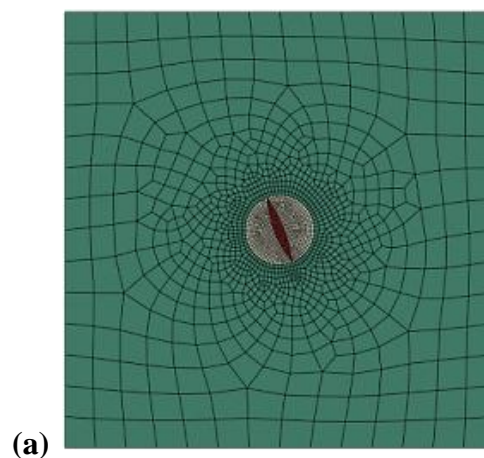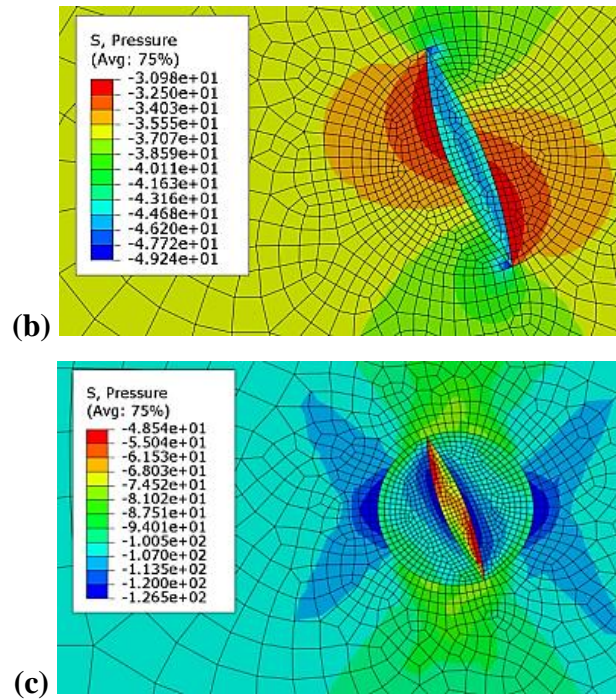
Fig. 6.10. Twin-like inclusion model (a); mean stress field in soft (b) and hard twin (c).
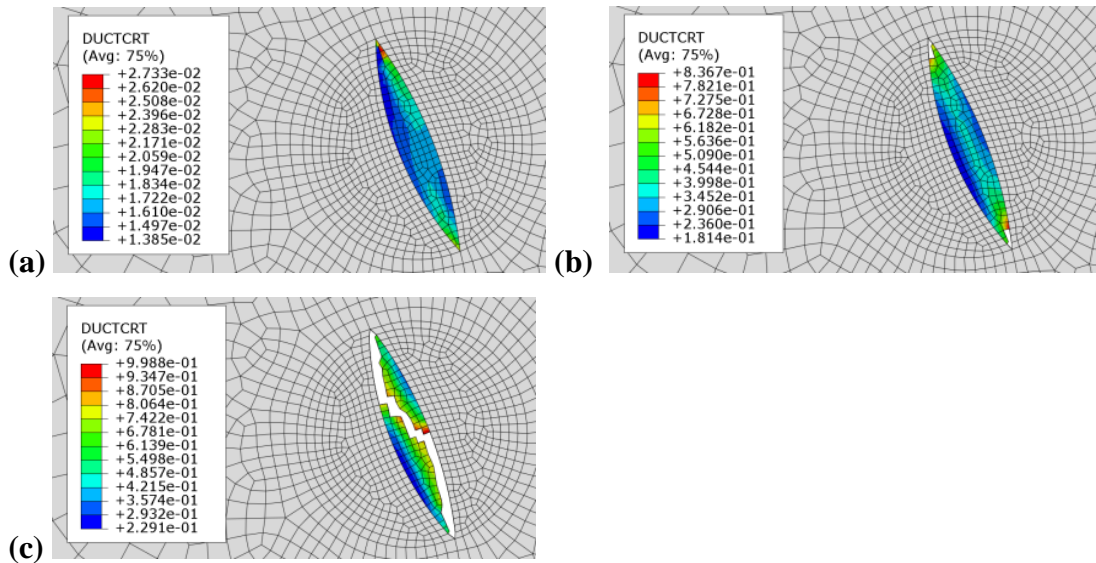
Fig. 6.11. Crack initiation (a) and propagation (b-c) within the soft twin. DUCTCRT is a ratio of the current effective strain to the critical strain, FE element is removed (equivalent to fracture occurrence) if DUCTCRT is greater than 1.

6.4.5. Polycrystalline model

The final step of the analysis was to build and run a polycrystalline model. Ten grain-like particles were placed in the same matrix as in the previous models. Different flow curves were ascribed to particular grains in order to investigate the effect of the initial grain orientation. Four grains have yield stress 80% of the matrix, another five have yield stress 120% of the matrix and one grain has the same flow stress as the matrix. The whole model was meshed using 11205 elements of the same type as in the previous models. Figure 6.12 shows a polycrystalline sample pulled to fracture. The brighter the colour of the grain the lower its yield stress. It can be seen in Fig. 6.12a that fracture is initiated in a triple junction point. The difference in the stress state in the neighbouring grains is the biggest in this case since different flow curves are ascribed to each of them. Two other fracture points, where three different grain orientations meet with each other, are shown in Fig. 6.12b. Figure 6.12c shows that crack is propagated along the grain boundary where grains with significantly different yield stresses are in contact. When this difference is not as large, a grain can be sheared due to deformation, as shown in Fig. 6.12b.
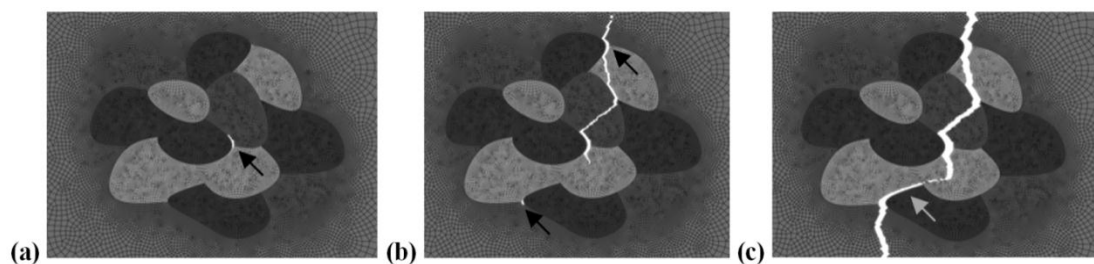
Fig. 6.12. Crack initiation and propagation in the polycrystalline sample. Arrows show crack initiation point in (a) and (b), arrow in (c) indicates fracture along grain boundary.

6.4.6. Summary of simulation results

The simulation of microstructure evolution was performed in the present work using a commercial FE software. The results showed that location of the fracture initiation point depends on the yield stress of a grain, which was modelled as a round inclusion. Twin-like inclusion was also modelled and it was observed that fracture occurs earlier in the 'softer' twin due to strain localisation. Polycrystalline model was also developed and it was shown that fracture is initiated in the triple junction points and it mainly propagates along grain boundaries.

6.5. Microstructure evolution in coarse-grained sample

First SEM images of the coarse-grained sample were taken at true strain 0.008. Reaching of the yield point became apparent as the first highlighted surface steps, arising from dislocation motion (Koike et al., 2003), occurred in both coarse and fine grains. Density of the wavy white lines, shown in Fig. 6.13a, was increasing with pulling and the lines were becoming lighter which indicated that relief on the sample surface was rising. The first twins were revealed in coarse grains when strain reached 0.03. Figures 6.13a and 6.13b show the same area observed at strain 0.02 and 0.03, respectively. It is apparent that ~70 μm long twins occurred in zones marked as 1 and 2 at strain 0.03. Moreover, one of the observed twins appeared in the grain with a large amount of slip traces (detail 1 in Fig. 6.13b), which indicated that the initial orientation of this grain allowed only limited amount of slip and further deformation must have been accommodated by twinning.
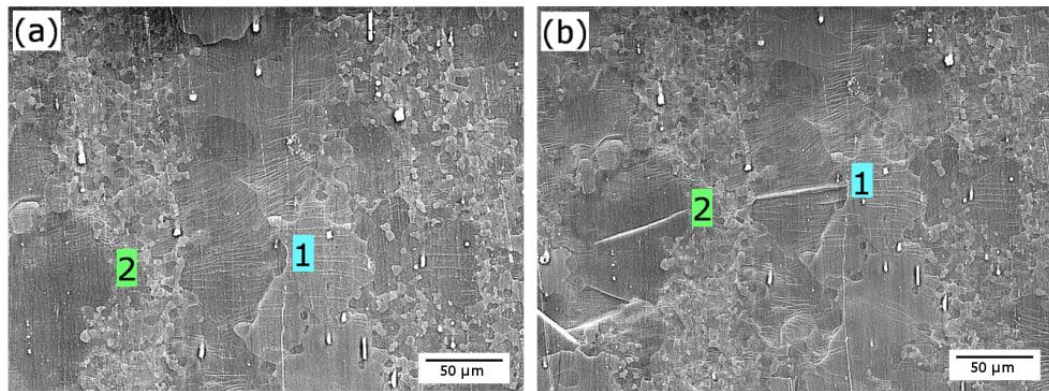
Fig. 6.13. Microstructure evolution (SEM images) in coarse-grained sample at true strains: 0.02 (a) and 0.03 (b). Tensile direction is vertical.

The number of twins rose significantly with strain increase from 0.03 to 0.09, which is shown in Fig. 6.13b and Fig. 6.14a-c. Apart from the occurrence of new twins, the 'old ones' were continuously growing, as it is observed for the twin in grain 2 in Fig. 6.13b, which has the same indication in Fig. 6.14a-c. The width of that twin rose from ~2 μm to ~8 μm with strain increasing from 0.03 to 0.06 and continued to grow as it is shown in Fig. 6.14b and 6.14c. Moreover, new twins appeared in grain 2 at strain 0.08 and they were also growing, as shown in Fig. 6.14c. Finally, the investigated grain was almost completely consumed by the twins at the last stage of deformation.
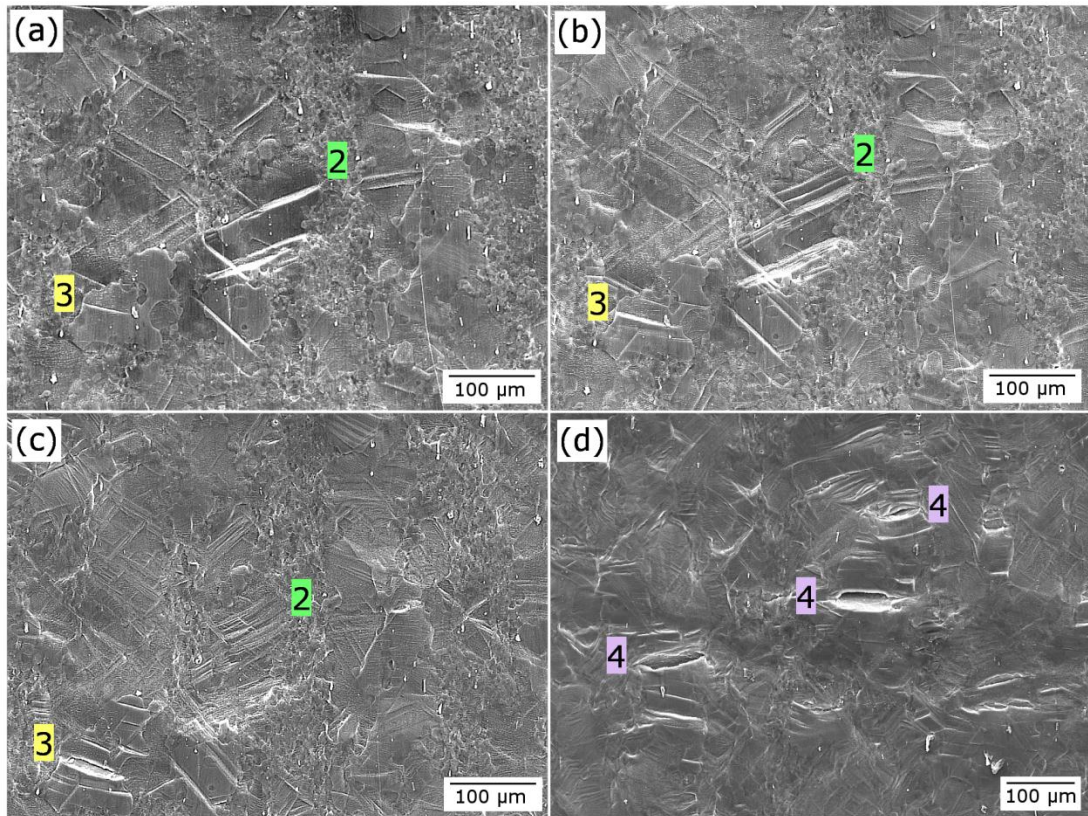
Fig. 6.14. SEM images of the same area in coarse-grained sample at true strains: 0.06 (a), 0.08 (b), 0.087 (c). Twin-sized voids at true strain 0.09 are shown in (d). Tensile direction is vertical.

The twinned area was increasing substantially as deformation continued. In the first stage of deformation, nucleation of new twins caused an increase in twinned area fraction. At subsequent stages, the fraction of twins was increasing as previously nucleated twins were growing and this process was accompanied by a continued appearance of new twins. This can be seen in Fig. 6.15 as the initially exponential relationship between strain and twinned area fraction. Relatively low elongation to failure observed in this study did not allow investigating twinning evolution at larger strains. Therefore, the current results were supplemented by experimental data obtained at strain 0.15 after tension of coarse-grained (~100 μm) AZ31 with constant strain rate 0.01 s^{-1} (Jiang et al., 2007). This changed the relation between twinned

area and strain from exponential to sigmoidal. The twinning process seemed to slow down since the generation of new twins was suppressed in the final stage of deformation due to decreasing number of available nucleation sites and, as a consequence, only twin growth contributed to further increase in twinned area fraction.
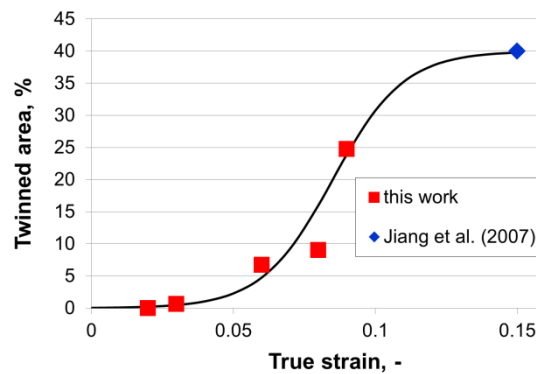
Fig. 6. 15. Evolution of twinned area fraction as a function of true strain.

Nucleation of twins and their subsequent growth was not the only microstructural feature observed in this test. For example, twin 3 in Fig. 6.14a-b was growing with strain increasing from 0.06 to 0.08. However, its growth was stopped and a 14 µm wide microcrack appeared in its place at strain 0.087, as seen in Fig. 6.14c. Other deformation zones were examined to clarify if the observed phenomenon was a common mechanism or only an incidental one. As it is shown in Fig. 6.14d, more twin-sized cracks (marked as details 4) were revealed and their number was noticeably larger in the vicinity of the fracture zone. At the same time, formation of voids was not observed at any other sites than twins.

The above observations led to the conclusion that twinning was responsible for early fracture of tested samples. Growth of some twins was suppressed, which resulted in the occurrence of microcracks. Then, growth and coalescence of the cracks led to a fracture observed at a macro-scale. The technique used in this study did not allow distinguishing between different types of twins. However, it is apparent that some twins were growing to fully consume parent grains while others were prone to fracture. Those effects can be explained by different crystallographic orientations of twins, for example, only {10-11}-{10-12} double twins are suspected to lead to early failure due to local softening (Barnett, 2007b). Simulations of the microstructure evolution performed in Section 6.4.4 have also shown that twins with softer orientations are more prone to earlier fracture that ones with higher yield stress due to the occurrence of tensile stress in the twin corners (Fig. 6.10). Those predictions were confirmed experimentally in the present study, where the twin transformation to microcrack was shown explicitly.

6.6. Microstructure evolution in fine-grained sample

Since the fracture initiation was closely related to twinning, attempts were made to suppress this deformation mechanism in order to improve ductility at room temperature. *In situ* experiments on coarse-grained samples conducted in this work showed that twins were observed only in large grains while they were hardly seen within fine grains (~12 μm). This observation and some other literature reports (Barnett et al., 2004; Chino et al., 2008) supported the idea that grain refinement can suppress twinning. Microstructure evolution of a fine-grained sample from the initial

state to strain 0.13 is shown in Fig. 6.16a-b. It is apparent that grains are significantly elongated, e.g. grain 1 is stretched along tensile direction from 11.7 μm to 13 μm (~11%). At the same time, some small grains (~1-2 μm) are virtually not deformed; therefore, a different mechanism must have been activated to ensure stress compatibility on grain boundaries, e.g. grain boundary sliding (GBS). This conclusion is supported by the results obtained by Koike et al. (2003), where GBS was shown to operate at room temperature in fine-grained AZ31.
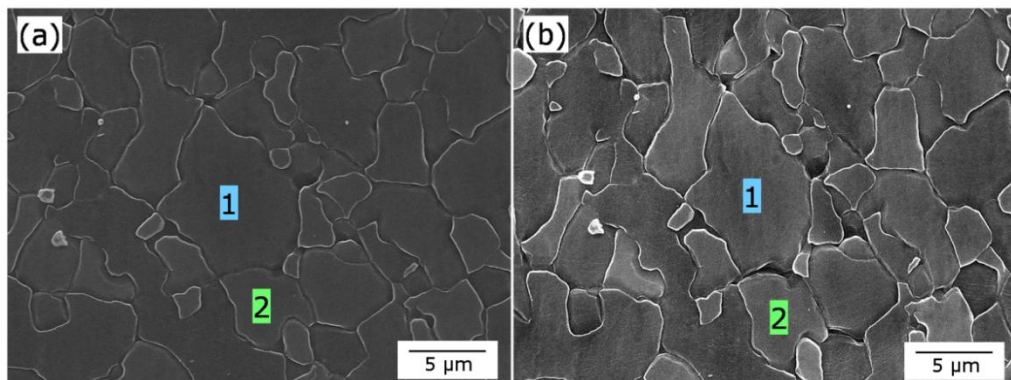
Fig. 6.16. Microstructure evolution (SEM images) in fine-grained sample from initial state (a) to true strain 0.13 (b). Tensile direction is vertical.

Fracture mechanism observed in fine-grained samples was completely different from that in coarse-grained ones. The first microcracks were revealed on grain boundaries at strain 0.13, as shown between grains 1 and 2 in Fig. 6.16b. Their occurrence can be attributed to stress incompatibilities on grain boundaries arising from different crystallographic orientations of neighbouring grains, which was predicted in simulations performed in Section 6.4.5 and in the literature (Milenin et al., 2011). Growth and coalescence of the generated voids was much slower than in the case of a coarse-grained sample, as it enabled further deformation to strain of 0.19. Large

voids observed near the fracture zone are shown in Fig. 6.17a. Although the earlier stages of test indicated that the only failure mechanism is intergranular fracture (Fig. 6.16b), the images taken in the deformation zone reveal that mechanical shearing of grains has also contributed to material damage, as shown in Fig. 6.17b. This effect was also captured by FE simulation in Section 6.4.5, where mechanical shearing of grains was predicted in regions with grains exhibiting similar yield strengths (equivalent to similar crystallographic orientations).
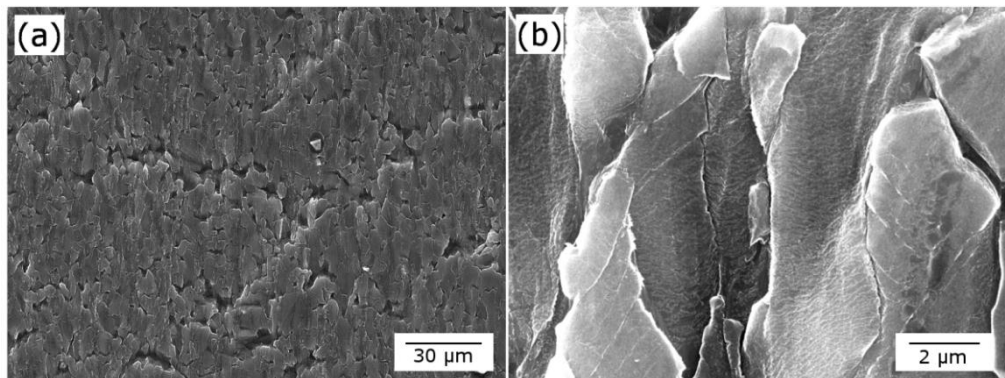
Fig. 6.17. Regions near the fracture zone of fine-grained sample (SEM images). Tensile direction is vertical.

6.7. Summary

A magnesium alloy bar processed by four passes of I-ECAP at 250 °C by route B_C was successfully subjected to upsetting at 200 °C with a significant height reduction from 10 mm to 2 mm. Fracture was not observed despite a high deformation level (logarithmic strain ~1.6), which confirmed that formability of fine-grained AZ31B at elevated temperature was reasonably high. It was shown that upsetting increased the room temperature yield strength from 80 to 145 MPa but lowered ductility, measured by tensile true strain, from 0.23 to 0.19.

FE simulations and *in situ* tensile tests in a SEM chamber were carried out to study microstructure evolution in coarse- and fine-grained samples. Twinning in AZ31B magnesium alloy was found to be strongly related to grain size and its occurrence in the coarse grained material led to an early material fracture resulting from transformation of twins to microcracks. According to simulation results, fracture initiation was predicted within twins with lower yield stress, recognised in the literature as contraction and double twins.

Grain refinement achieved by I-ECAP resulted in suppression of twinning and the associated twin-based microcracks. Cracking was initiated on grain boundaries due to stress incompatibilities arising from different crystallographic orientations of neighbouring grains, which was shown through numerical simulation. Grain boundary sliding is suspected to operate in fine-grained regions (1-2 µm) to ensure stress compatibility on grain boundaries.

Chapter 7

Conclusions, contribution of the thesis and recommendations for the future work

7.1. Conclusions

The effects of temperature, initial grain size and processing route on formability of AZ31B magnesium alloy during I-ECAP were investigated in Chapter 4. The conducted experiments and performed FE simulations allowed the following conclusions to be drawn:

1. The minimum allowable I-ECAP temperature for magnesium alloy depends on initial grain size and processing route. I-ECAP temperature for AZ31B magnesium alloy can be reduced to 200 °C and 150 °C when the average initial grain size is as small as ~8 µm and ~1.5 µm, respectively.

2. Experiments with various routes of I-ECAP showed that billet rotation by 90° (route B_C) and 180° (route C) after each pass lead to an earlier fracture than processing without rotation (route A). FE simulations showed that incomplete filling of the exit channel during processing by routes B_C and C increases tensile stress and leads to material damage.

3. The asymmetrical shape of a billet processed by route B_C, not reported before for ECAP was displayed in this work. FE simulations confirmed that the observed distortion can be explained by inhomogeneous strain rate sensitivity arising from a non-uniform strain distribution during the preceding pressing. The developed numerical model was able to predict a location of fracture initiation zone.

In Chapter 5, effects of temperature and processing route of I-ECAP on mechanical properties, grain size and texture of an AZ31B magnesium alloy were investigated. Microstructure characterisation of tensile and compression coarse- and fine-grained samples was performed in order to determine a dominating deformation mechanism. The following conclusions were drawn from this study:

4. Grain size after I-ECAP depends on processing temperature. Grain refinement to 6, 3, and 1 µm was achieved by processing at 250, 200, and 150 °C, irrespectively of the route used.

5. I-ECAP at 250 °C can be used to improve ductility of AZ31B magnesium alloy; the obtained grain size and mechanical properties are comparable to those reported after conventional ECAP. However, significant strength decrease after I-ECAP at 250 °C, reported also after conventional ECAP at the same temperature, is also observed.

6. Room temperature ductility of magnesium alloy AZ31B can be improved without sacrificing strength by conducting four passes at 250 °C and two additional passes at 200 °C using route A. Nevertheless, tension-compression yield stress asymmetry observed for extruded rod was not suppressed by processing by route A.

7. Yield strength of the examined alloy can be increased to 290 MPa along with sustaining a reasonable ductility, expressed as 0.16 of true strain, when temperature of I-ECAP is reduced to 150 °C.

8. Texture controls mechanical properties of AZ31B magnesium alloy subjected to I-ECAP at 250 °C. The obtained results showed that processing route did not influence the grain size but significantly changed mechanical properties.

The EBSD measurements confirmed the effect of texture on flow behaviour of I-ECAPed magnesium alloy.

9. Tension-compression asymmetry is suppressed by using routes B_C and C of I-ECAP in samples tested along extrusion direction. This effect was attributed to texture development and microstructure homogenization after processing.

10. Increased ductility after I-ECAP was attributed to suppression of double twinning and facilitation of slip on basal and non-basal planes. Shear bands were observed in I-ECAPed samples subjected to tension. A larger amount of shear bands and smaller spacing between them were observed in samples, which exhibited improved ductility.

11. Twinning activity in compression is higher for samples processed by route A than B_C and C. This conclusion is supported by the concave shape of flow stress curve and quantitative analysis of microstructural images. Since the average grain size was almost the same for samples processed by various routes at 250 °C, this effect was attributed to the texture produced during I-ECAP.

12. Heat treatment after I-ECAP can improve room temperature ductility (elongation to failure above 40%) without strength decrease. It was concluded that this effect is attributed to the reduction of internal stresses rather than grain growth or texture modification.

13. It was shown through numerical simulation that microstructure evolution during subsequent passes of ECAP and I-ECAP can be predicted using the model based on dynamic recrystallisation (DRX) assumptions. It supports the

idea that grain refinement in ECAP and I-ECAP at elevated temperatures (≥200 °C) is controlled by DRX.

Combination of I-ECAP and upsetting was used in Chapter 6 to produce 2 mm thick fine-grained AZ31B magnesium alloy sheet. *In situ* observations were performed in a SEM chamber during tensile testing using samples which were cut out from coarse-grained rod and fine-grained sheet. The conclusions drawn from this study are listed below:

14. Fine-grained AZ31B magnesium alloy exhibits high formability at elevated temperatures, which was proved through successful upsetting at 200 °C with deformation level of -1.6 of logarithmic strain.

15. Side upsetting of I-ECAPed bar can increase room temperature yield strength from 80 to 140 MPa but decreases ductility since tensile true strain at fracture dropped from 0.23 to 0.19.

16. Twinning in AZ31B magnesium alloy is related to grain size and its occurrence in the coarse-grained material led to an early material fracture resulting from transformation of twins to microcracks. According to FE simulation results, fracture initiation was predicted within twins with lower yield stress, recognised in the literature as contraction and double twins.

17. Grain refinement achieved by I-ECAP followed by upsetting resulted in suppression of twinning and the associated twin-based microcracks. Cracking in fine-grained sample is initiated on grain boundaries due to stress incompatibilities arising from different crystallographic orientations of neighbouring grains, which was shown through numerical simulation.

7.2. Thesis contributions

Most of the findings presented in the thesis were revealed for the first time since no results on I-ECAP of magnesium alloy were published before by other researchers. In order to select processing parameters for AZ31B, formability of the alloy during I-ECAP has been studied in terms of billet temperature, initial grain size, and processing route. The established relation between grain size and the minimum I-ECAP temperature can be also useful for conventional ECAP as it was shown that the obtained results are consistent with the literature data. Moreover, the effect of processing route on billet shape and fracture occurrence was shown for the first time for ECAP/I-ECAP. The results from this study were published in peer-reviewed journal *Key Engineering Materials* (Gzyl et al., 2013a; Gzyl et al., 2014a) and presented at international conferences ESAFORM 2013 and ESAFORM 2014.

The study dedicated to the effect of processing route on mechanical properties and microstructure was published in peer-reviewed journal from Thomson Reuters Master Journal List *Metallurgical and Materials Transactions A* (Gzyl et al., 2014b). The occurrence of shear bands in I-ECAPed samples subjected to tension was reported for the first time in this article. Moreover, multi scale CAFE simulation of microstructure evolution during ECAP/I-ECAP was performed to confirm that grain refinement in those processes is controlled by dynamic recrystallisation. The numerical results were presented at an international conference Komplastech 2013 and published in *Computer Methods in Materials Science* (Gzyl et al., 2013b).

Fine-grained magnesium alloy sheet was obtained in this work for the first time by I-ECAP of a square bar followed by side upsetting. It was revealed through *in situ*

tensile testing in a SEM chamber that fracture mechanisms in coarse- and fine-grained samples are different. The transformation of a twin to microcrack was shown explicitly, which proved that twinning was responsible for earlier fracture of coarse-grained samples. The performed FE simulations predicted fracture within twin with lower yield stress. The numerical results were presented at an international conference Numisheet 2014 and published in the conference proceedings (Gzyl and Rosochowski, 2013). The paper which gathers the experimental and numerical results was submitted to a peer-reviewed journal and it is currently under review.

The list of publications accompanying this thesis:

Gzyl, M. and Rosochowski, A. (2013) 'FE simulation of magnesium alloy microstructure evolution in tension', *AIP Conference Proceedings 1567*, pp. 776-79.

Gzyl, M., Rosochowski, A., Yakushina, E., Wood, P., and Olejnik, L. (2013a) 'Route effects in I-ECAP of AZ31B magnesium alloy', *Key Engineering Materials*, vols. 554-557, pp. 876-84.

Gzyl, M., Rosochowski, A., Milenin, A., Olejnik, L. (2013b) 'Modelling microstructure evolution during equal channel angular pressing of magnesium alloys using cellular automata finite element method', *Computer Methods in Materials Science*, vol. 13, pp. 357-63.

Gzyl, M., Rosochowski, A., Olejnik, L., Reshetov, A. (2014a) 'The effect of initial grain size on formability of AZ31B magnesium alloy during I-ECAP', *Key Engineering Materials* – in press.

Gzyl, M., Rosochowski, A., Pesci, R., Olejnik, L., Yakushina, E., and Wood, P. (2014b) 'Mechanical properties and microstructure of AZ31B magnesium alloy processed by I-ECAP', *Metallurgical and Materials Transactions A*, vol. 45, pp. 1609-20.

7.3. Recommendations for the future work

The billet shape distortion and the occurrence of fracture in billets processed by route B_C are intriguing since such results were not reported before for ECAP. It should be verified experimentally whether the distinctive billet shape obtained in this work occurs only after I-ECAP or after conventional ECAP too. Therefore, it should be investigated in the future if I-ECAP has the same effect on billet shape and fracture occurrence as ECAP. Moreover, an effect of strain rate and die angle on formability during I-ECAP should be also studied in the future since this work was focused only on the initial grain size and the processing route. It was already shown in the literature that processing at a very low strain rate (Bryla et al., 2009) as well as increase of die angle (Figueiredo et al., 2007) led to a successful lowering of ECAP temperature. Recently, ECAP of AZ31 magnesium alloy was successfully conducted at room temperature with a low strain rate and a very large back-pressure (400 MPa) by Gu et al. (2013). It is a very promising result and further experiments should be also focus on finding a possible ways to carry out I-ECAP at room temperature.

Mechanical tests conducted in this work proved that I-ECAP can be successful in improving strength or ductility of AZ31B magnesium alloy. Nevertheless, more experimental research should be done to reveal a relation between grain size, texture and mechanical properties. Most of samples processed by I-ECAP were subjected to four passes; however, increased number of passes can result in homogenisation of the structure and generation of high angle grain boundaries. A comprehensive experimental plan for I-ECAP of magnesium alloy covering temperature range 150-

250 °C and the three main processing routes should be realised to establish how the obtained grain size and texture affect mechanical properties.

It was shown in this work that heat treatment after I-ECAP can significantly improve room temperature ductility of AZ31B alloy. However, only one combination of annealing temperature and time was used; therefore, another recommendation for the future work is to investigate an effect of annealing temperature and time on the microstructure and mechanical properties of billets processed by I-ECAP. A thermal stability of fine- and ultrafine-grained structures in magnesium alloys should be also studied in the future.

Most of ECAP experiments, including this work, are conducted using popular wrought magnesium alloys (AZ31, ZK60, AZ91), with the main alloying elements being aluminium, zinc, and zirconium. Nowadays, emphasis is put on producing lightweight alloys with improved strength and ductility. For example, addition of rare-earth elements, e.g. yttrium, neodymium and gadolinium, is one of the currently used approaches to improve mechanical properties. Combination of alloying solid solution strengthening and severe plastic deformation appears like an interesting technique of producing advanced magnesium alloys; however, a research in this field is still very limited (Kutniy et al., 2009; Pachla et al., 2012). The successful preliminary trials of I-ECAP on Magnesium Elektron alloys with additions of rare-earth elements were already conducted; the future work will be continued with those alloys.

References

Agnew, S.R. and Duygulu, O. (2005) 'Plastic anisotropy and the role of non-basal slip in magnesium alloy AZ31B', *International Journal of Plasticity*, vol. 21, pp. 1161-93.

Agnew, S.R., Horton, J. A., Lillo T. M., and Brown, D. W. (2004) 'Enhanced ductility in strongly textured magnesium produced by equal channel angular processing', *Scripta Materialia*, vol. 50, pp. 377-81.

Agnew, S.R., Mehrotra, P., Lillo, T.M., Stoica, G.M., and Liaw, P.K. (2005) 'Crystallographic texture evolution of three wrought magnesium alloys during equal channel angular extrusion', *Materials Science and Engineering A*, vol. 408, pp. 72–78.

Al-Samman, T. and Gottstein, G. (2008a) 'Room temperature formability of a magnesium AZ31 alloy: Examining the role of texture on the deformation mechanisms', *Materials Science and Engineering A*, vol. 488, pp. 406-14.

Al-Samman, T. and Gottstein, G. (2008b) 'Dynamic recrystallization during high temperature deformation of magnesium', *Materials Science and Engineering A*, vol. 490, pp. 411-20.

Al-Samman, T. and Gottstein, G. (2010) 'Orientation dependent slip and twinning during compression and tension of strongly textured magnesium AZ31 alloy', *Materials Science and Engineering A*, vol. 527, pp. 3450-63.

Barnett, M.R. (2003a) 'A Taylor model based description of the proof stress of magnesium AZ31 during hot working', *Metallurgical and Materials Transactions A*, vol. 34, pp. 1799-1806.

Barnett, M.R. (2003b) 'Recrystallization during and following hot working of magnesium alloy AZ31', *Materials Science Forum*, vols. 419-422, pp. 503-8.

Barnett, M.R. (2007a) 'Twinning and the ductility of magnesium alloys Part I: Tension twins', *Materials Science and Engineering A*, vol. 464, pp. 1-7.

Barnett, M.R. (2007b) 'Twinning and the ductility of magnesium alloys. Part II. Contraction twins', *Materials Science and Engineering A*, vol. 464, pp. 8-16.

Barnett, M.R., Keshavarz, Z., Beer, A.G., and Atwell, D. (2004) 'Influence of grain size on the compressive deformation of wrought Mg–3Al–1Zn', *Acta Materialia*, vol. 52, pp. 5093-5103.

Beer, A.G. and Barnett, M.R. (2006) 'Influence of initial microstructure on the hot working flow stress of Mg–3Al–1Zn', *Materials Science and Engineering A*, vol. 423, pp. 292–99.

Beer, A.G. and Barnett, M.R. (2007) 'Microstructural development during hot working of Mg-3Al-1Zn', *Metallurgical and Materials Transactions A*, vol. 38, pp. 1856-67.

Beer, A.G., and Barnett, M.R. (2009) 'The post-deformation recrystallization behaviour of magnesium alloy Mg–3Al–1Zn', *Scripta Materialia*, vol. 61, pp. 1097-1100.

Beygelzimer, Y., Orlov, D., and Varyukhin, V. (2002) 'A new severe plastic deformation method: twist extrusion', in Zhu, Y.T., Langdon, T.G., Mishra, R.S., Semiatin, S.L., Saran, M.J., and Lowe, T.C. (eds) *Ultrafine Grained Materials II, Proceedings of a symposium held during the 2002 TMS Annual Meeting in Seattle,* Washington, 17-21 February 2002, The Minerals, Metals, and Materials Society, Warrendale, PA, pp. 297-304.

Biswas, S., Dhinwal, S.S., and Suwas, S. (2010) 'Room-temperature equal channel angular extrusion of pure magnesium', *Acta Materialia*, vol. 58, pp. 3247-61.

Bridgman, P.W. (1935) 'Effects of high shearing stress combined with high hydrostatic pressure', *Physical Review*, vol. 48, pp. 825-47.

Bryla, K., Dutkiewicz, J., and Malczewski, P. (2009) 'Grain refinement in AZ31 alloy processed by equal channel angular pressing', *Archives of Materials Science and Engineering*, vol. 40, pp. 17-22.

Charit, I. and Mishra, R.S. (2005) 'Low temperature superplasticity in a friction-stir-processed ultrafine grained Al–Zn–Mg–Sc alloy', *Acta Materialia*, vol. 53, pp. 4211-23.

Cheng, S., Spencer, J.A., and Milligan, W.W. (2003) 'Strength and tension/compression asymmetry in nanostructured and ultrafine-grain metals', *Acta Materialia*, vol. 51, pp. 4505-18.

Chino, Y., Hoshika, T., and Lee, J.-S. (2006) 'Mechanical properties of AZ31 Mg alloy recycled by severe deformation', *Journal of Materials Research*, vol. 21, pp. 754-60.

Chino, Y., Kimura, K., and Mabuchi, M. (2008) 'Twinning behavior and deformation mechanisms of extruded AZ31 Mg alloy', *Materials Science and Engineering A*, vol. 486, pp. 481-88.

Cockcroft, M. and Latham, D. (1968) 'Ductility and the workability of metals', *Journal of the Institute of Metals*, vol. 96, pp. 33–39.

Comley, P.N. (2004) 'Manufacturing advantages of superplastically formed fine-grain Ti-6Al-4V alloy', *Journal of Materials Engineering and Performance*, vol. 13, pp. 660-64.

Cyganek, Z., and Tkocz, M. (2012) 'The effect of AZ31 alloy flow stress description on the accuracy of forward extrusion FE simulation results', *Archives of Metallurgy and Materials*, vol. 57, pp. 199-204.

Das, S. (2010) 'Modelling mixed microstructures using a multi-level cellular automata finite element framework', *Computational Materials Science*, vol. 47, pp. 705-11.

Ding, R., and Guo, Z.X. (2002) 'Microstructural modelling of dynamic recrystallisation using an extended cellular automaton approach', *Computational Materials Science*, vol. 23, pp. 209-18.

Ding, S.X., Chang, C.P., and Kao, P.W. (2009) 'Effects of processing parameters on the grain refinement of magnesium alloy by equal-channel angular extrusion', *Metallurgical and Materials Transactions A*, vol. 40, pp. 415-25.

Ding, S.X., Lee, W.T., Chang, C.P., Chang, L.W., and Kao, P.W. (2008) 'Improvement of strength of magnesium alloy processed by equal channel angular extrusion', *Scripta Materialia*, vol. 59, pp. 1006–9.

Dobrzanski, L.A. (2002) 'Podstawy nauki o materialach i metaloznawastwo. Materialy inzynierskie z podstawami projektowania materialowego', WNT, Warszawa, ISBN: 83-20427-93-2.

El Mehtedi, M., Balloni, L., Spigarelli, S., Evangelista, E., Rosen, G., Lee, B.H., and Lee, C.S. (2007) 'Comparative study of high temperature workability of ZM21 and AZ31 magnesium alloys', *Metallurgical Science and Technology*, vol.25, pp. 23-30.

Erb, U. (1995) 'Electrodeposited nanocrystals: Synthesis, properties and industrial applications', *Nanostructured Materials*, vol. 6, pp. 533-38.

Estrin, Y., Kim, H.-E., Lapovok, R., Ng, H.P., and Jo, J.-H. (2013) 'Mechanical strength and biocompatibility of ultrafine-grained commercial purity titanium', *BioMed Research International*, Available at http://www.hindawi.com/journals/ bmri/2013/914764 (Accessed 21 March 2014).

Faghihi, S., Azari, F., Zhilyaev, A.P., Szpunar, J.A., Vali, H., Tabrizian, M. (2007) 'Cellular and molecular interactions between MC3T3-E1 pre-osteoblasts and nanostructured titanium produced by high-pressure torsion', *Biomaterials*, vol. 28, pp. 3887-95.

Fatemi-Varzaneh, S.M., Zarei-Hanzaki, A., and Beladi, H. (2007) 'Dynamic recrystallization in AZ31 magnesium alloy', *Materials Science and Engineering A*, vol. 456, pp. 52-57.

Figueiredo, R.B. and Langdon, T.G. (2009a) 'Principles of grain refinement and superplastic flow in magnesium alloys processed by ECAP', *Materials Science and Engineering A*, vol. 501, pp. 105-14.

Figueiredo, R.B. and Langdon, T.G. (2009b) 'Principles of grain refinement in magnesium alloys processed by equal-channel angular pressing', *Journal of Material Science*, vol. 44, pp. 4758-62.

Figueiredo, R.B., Cetlin, P.R., and Langdon, T.G. (2007) 'The processing of difficult-to-work alloys by ECAP with an emphasis on magnesium alloys', *Acta Materialia*, vol. 55, pp. 4769-79.

Figueiredo, R.B., Cetlin, P.R., and Langdon, T.G. (2010a) 'Stable and unstable flow in materials processed by equal-channel angular pressing with an emphasis on magnesium alloys', *Metallurgical and Materials Transactions A*, vol. 41, pp. 778-86.

Figueiredo, R.B., Szaraz, Z., Trojanova, Z., Lukac, P., and Langdon, T.G. (2010b) 'Significance of twinning in the anisotropic behavior of a magnesium alloy processed by equal-channel angular pressing', *Scripta Materialia*, vol. 63, pp. 504-7.

Friedrich, H.E. and Mordike, B.L. (2006) 'Preface/Foreword', in Friedrich, H.E. and Mordike, B.L. (eds) *Magnesium technology: metallurgy, design data, applications*, Springer-Verlag, Heidelberg, pp. 5-6.

Froes, F.H., Eliezer, D., and Aghion, E. (2006) 'Magnesium aerospace', in Friedrich, H.E. and Mordike, B.L. (eds) *Magnesium technology: metallurgy, design data, applications*, Springer-Verlag, Heidelberg, pp. 603-619.

Fujita, T., Horita, Z., and Langdon, T.G. (2004) 'Using grain boundary engineering to evaluate the diffusion characteristics in ultrafine-grained Al–Mg and Al–Zn alloys', *Materials Science and Engineering A*, vol. 371, pp. 241-50.

Furui, M., Kitamura, H., Anada, H., and Langdon, T.G. (2007) 'Influence of preliminary extrusion conditions on the superplastic properties of a magnesium alloy processed by ECAP', *Acta Materialia* 55, pp. 1083-91.

Galiyev, A., Kaibyshev, R., and Sakai T. (2003) 'Continuous dynamic recrystallization in magnesium alloy', *Materials Science Forum*, vols. 419-422 pp. 509-14.

Ghosh, A.K. and Huang, W. (2000) 'Severe deformation based process for grain subdivision and resulting microstructures', in Lowe, T.C. and Valiev, R.Z. (eds) *Investigations and applications of severe plastic deformation*, Kluwer Academic Publishers, Dordrecht, pp. 29-36. Available at http://link.springer.com/book/10.1007%2F978-94-011-4062-1 (accessed 21 March 2014).

Gu, C.F., Toth, L.S., Field, D.P., Fundenberger, J.J., and Zhang, Y.D. (2013) 'Room temperature equal-channel angular pressing of a magnesium alloy', *Acta Materialia*, vol. 61, pp. 3027-36.

Hall, E.O. (1951) 'The deformation and ageing of mild steel: III discussion of results', *Proceedings of the Physical Society of London Section B*, vol. 64, pp. 747-53.

Hallberg, H., Wallin, M., and Ristinmaa, M.(2010) 'Simulation of discontinuous dynamic recrystallization in pure Cu using a probabilistic cellular automaton', *Computational Materials Science*, vol. 49, pp. 25-34.

Horita, Z., Fujinami, T., Nemoto, M., and Langdon, T.G. (2001) 'Improvement of mechanical properties for Al alloys using equal-channel angular pressing', *Journal of Materials Processing Technology*, vol. 117, pp. 288-92.

Horita, Z., Komura, S., Berbon, P.B., Utsunomiya, A., Furukawa, M., Nemoto, M., and Langdon, T.G. (1999) 'Superplasticity of ultrafine-grained aluminum alloys processed by equal-channel angular pressing', *Materials Science Forum*, vols. 304-306, pp. 91-96.

Huang, J., Zhu, Y.T., Alexander, D.J., Liao, X., Lowe, T.C., and Asaro, R.J. (2004) 'Development of repetitive corrugation and straightening', *Materials Science and Engineering A*, vol. 371, pp. 35-39.

Huang, J.Y., Zhu, Y.T., Jiang, H., and Lowe, T.C. (2001) 'Microstructures and dislocation configurations in nanostructured Cu processed by repetitive corrugation and straightening', *Acta Materialia*, vol. 49, pp. 1497-1505.

Hutchinson, W.B. and Barnett, M.R. (2010) 'Effective values of critical resolved shear stress for slip in polycrystalline magnesium and other hcp metals', *Scripta Materialia*, vol. 63, pp. 737-40.

Iwahashi, Y., Horita, Z., Nemoto, M., and Langdon, T.G. (1998) 'The process of grain refinement in equal-channel angular pressing', *Acta Materialia*, vol. 46, pp. 3317-31.

Iwahashi, Y., Wang, J., Horita, Z., Nemoto, M., and Langdon, T.G. (1996) 'Principle of equal-channel angular pressing for the processing of ultra-fine grained materials', *Scripta Materialia*, vol. 35, pp. 143-46.

Janecek, M., Popov, M., Krieger, M.G., Hellmig, R.J., and Estrin, Y. (2007) 'Mechanical properties and microstructure of a Mg alloy AZ31prepared by equal-channel angular pressing', *Materials Science and Engineering A*, vol. 462, pp. 116-20.

Jiang, J. and Ma, A. (2011) 'Bulk ultrafine-grained magnesium alloys by SPD processing: technique, microstructures and properties', in Czerwinski, F. (ed) *Magnesium alloys - design, processing and properties*. InTech. Available at http://www.intechopen.com/books/ magnesium-alloys-design-processing-and-properties (accessed 21 March 2014).

Jiang, J., Ma, A., Saito, N., Shen, Z., Song, D., Lu, F., Nishida, Y., Yang, D., and Lin, P. (2009) 'Improving corrosion resistance of RE-containing magnesium alloy ZE41A through ECAP', *Journal of Rare Earths*, vol. 27, pp. 848-52.

Jiang, L., Jonas, J.J., Mishra, R.K., Luo, A.A., Sachdev, A.K., and Godet, S. (2007) 'Twinning and texture development in two Mg alloys subjected to loading along three different strain paths', *Acta Materialia*, vol.. 55, pp. 3899-910.

Jin, L., Lin, D., Mao, D., Zeng, X., Chen, B., and Ding, W. (2006) 'Microstructure evolution of AZ31 Mg alloy during equal channel angular extrusion', *Materials Science and Engineering A,* vol. 423, pp. 247-52.

Johnson, G.R., and Cook, W.H. (1983) 'A constitutive model and data for metals subjected to large strains, high strain rates and high temperatures', *Proceedings of 7th International Symposium on Ballistics*, The Hague, The Netherlands, April, 1983, pp. 541-47.

Kang, F., Wang, J.T., and Peng, Y. (2008) 'Deformation and fracture during equal channel angular pressing of AZ31 magnesium alloy', *Materials Science and Engineering A*, vol. 487, pp. 68-73.

Kelley, C.T. (1999) *Iterative methods for optimization*, Society for Industrial and Applied Mathematics, Philadelphia, USA, 1999, p. 145.

Kelley, E.W. and Hosford, W.F. (1968) 'Deformation characteristics of textured magnesium', *Transactions of the Metallurgical Society of AIME,* vol. 242, pp. 5-13.

Kim, H.S. (2002) 'Evaluation of strain rate during equal-channel angular pressing', *Journal of Materials Research*, vol. 17, pp. 172-79.

Kim, W.J., An, C.W., Kim, Y.S., and Hong, S.I. (2002) 'Mechanical properties and microstructures of an AZ61 Mg Alloy produced by equal channel angular pressing', *Scripta Materialia*, vol. 47, pp. 39-44.

Kleiner, S. and Uggowitzer, P.J. (2004) 'Mechanical anisotropy of extruded Mg–6% Al–1% Zn alloy', *Materials Science and Engineering A*, vol. 379, pp. 258-63.

Klimanek, P. and Poetzsch, A. (2002) 'Microstructure evolution under compressive plastic deformation of magnesium at different temperatures and strain rates', *Materials Science and Engineering A*, vol. 324, pp. 145-50.

Koch, C.C. (2009) 'Nanostructured materials: An overview', in Zehetbauer, M.J. and Zhu, Y.T. (eds) *Bulk nanostructured materials*, WILEY-VCH Verlag GmbH & Co. KGaA, Weinheim.

Koike, J., Ohyama, R., Kobayashi, T., Suzuki, M., and Maruyama, K. (2003) 'Grain-boundary sliding in AZ31 magnesium alloys at room temperature to 523 K', *Materials Transactions*, vol. 44, pp. 445-51.

Korbel, A., Richert, M., and Richert, J. (1981) 'The effects of very high cumulative deformation on structure and mechanical properties of aluminium', in Hansen, N., Horsewell, A., Leffers, T., and Lilholt, H. (eds) *Proceedings of the 2nd Risø International Symposium on Metallurgy and Material Science*, Roskilde, Denmark, 14-18 September 1981, Risø National Laboratory, pp. 445-50.

Kutniy, K.V., Papirov, I.I., Tikhonovsky, M.A., Pikalov, A.I., Sivtzov, S.V., Pirozhenko, L.A., Shokurov, V.S., and Shkuropatenko, V.A. (2009) 'Influence of grain size on mechanical and corrosion properties of magnesium alloy for medical implants', *Materialwissenschaft und Werkstofftechnik*, vol. 40, pp. 242-46.

Langdon, T.G. (2007) 'The principles of grain refinement in equal-channel angular pressing', *Materials Science and Engineering A*, vol. 462, pp. 3-11.

Langdon, T.G. (2013) 'Achieving superplasticity in ultrafine-grained metals', *Mechanics of Materials*, vol. 67, pp. 2-8.

Lapovok, R. (2005) 'The role of back-pressure in equal channel angular extrusion', *Journal of Materials Science*, vol. 40, pp. 341-46.

Lapovok, R., Estrin, Y., Popov, M.V., and Langdon, T.G. (2008) 'Enhanced superplasticity in a magnesium alloy processed by equal-channel angular pressing with a back-pressure', *Advanced Engineering Materials*, vol. 10, pp. 429-33.

Lapovok, R., Toth, L., Molinari, A., and Estrin, Y. (2009) 'Strain localisation patterns under equal-channel angular pressing', *Journal of the Mechanics and Physics of Solids*, vol. 57, pp. 122-36.

Lee, J.C., Seok, H.K., Han, J.H., and Chung, Y.H. (2001) 'Controlling the textures of the metal strips via the continuous confined strip shearing (C2S2) process', *Materials Research Bulletin*, vol. 36, pp. 997-1004.

Li, Y.J., Zeng, X.H., and Blum, W. (2004) 'Transition from strengthening to softening by grain boundaries in ultrafine-grained Cu', *Acta Materialia*, vol. 52, pp. 5009-18.

Lin, H.K. and Huang, J.C. (2002) 'High strain rate and/or low temperature superplasticity in AZ31 Mg alloys processed by simple high-ratio extrusion methods', *Materials Transactions*, vol. 43, pp. 2424-32.

Madej, L., Hodgson, P.D., and Pietrzyk, M. (2009) 'Development of the multi-scale analysis model to simulate strain localization occurring during material processing', *Archives of Computational Methods in Engineering*, vol. 16, pp. 287-318.

Marya, M., Hector, L.G., Verma, R., and Tong, W. (2006) 'Microstructural effects of AZ31 magnesium alloy on its tensile deformation and failure behaviors', *Materials Science and Engineering A*, vol. 418, pp. 341-56.

Masoudpanah, S.M. and Mahmudi, R. (2010) 'The microstructure, tensile, and shear deformation behavior of an AZ31magnesium alloy after extrusion and equal channel angular pressing', *Materials and Design*, vol. 31, pp 3512–17.

Masumura, R.A., Hazzledine, P.M., and Pande, C.S. (1995) 'Yield stress of fine grained materials', *Acta Materialia*, vol. 46, pp. 4527-34.

Mathis, K., Nyilas, K., Axt, A., Dragomir-Cernatescu, I., Ungar, T., and Lukac ,P. (2004) 'The evolution of non-basal dislocations as a function of deformation temperature in pure magnesium determined by X-ray diffraction', *Acta Materialia*, vol. 52, pp. 2889-94.

Matsubara, K., Miyahara, Y., Horita, Z., and Langdon, T.G. (2003) 'Developing superplasticity in a magnesium alloy through a combination of extrusion and ECAP', *Acta Materialia*, vol. 51, pp. 3073-84.

May, J., Hoeppel, H.W., and Goeken, M. (2005) 'Strain rate sensitivity of ultrafine-grained aluminium processed by severe plastic deformation', *Scripta Materialia*, vol. 53, 189-94.

Mayama, T., Noda, M., Chiba, R., Kuroda, M. (2011) 'Crystal plasticity analysis of texture development in magnesium alloy during extrusion', *International Journal of Plasticity*, vol. 27, pp.1916-35.

McCandlish, L.E., Kear, B.H., and Kim, B.K. (1992) 'Processing and properties of nanostructured WC–Co', *Nanostructured Materials*, vol. 1, pp. 119-24.

Mecking, H. and Kocks, U.F. (1981) 'Kinetics of flow and strain-hardening', *Acta Metallurgica*, vol. 29, pp. 1865-75.

Milenin, A., Byrska, D.J., and Grydin, O. (2011) 'The multi-scale physical and numerical modeling of fracture phenomena in the MgCa0.8 alloy', *Computers and Structures*, vol. 89, pp. 1038-49

Mises, R.V. (1928) 'Mechanik der plastischen formänderung von kristallen', *Zeitschrift für Angewandte Mathematik und Mechanik*, vol. 8, pp. 161-85.

Mishin, O.V., Juul Jensen, D., and Hansen, N. (2003) 'Microstructures and boundary populations in materials produced by equal channel angular extrusion', *Materials Science and Engineering A*, vol. 342, pp. 320-28.

Mukai, T., Somekawa, H., Inoue, T., and Singh, A. (2010) 'Strengthening Mg–Al–Zn alloy by repetitive oblique shear strain with caliber roll', *Scripta Materialia*, vol. 62, pp. 113-16.

Mukai, T., Yamanoi, M., Watanabe, H., and Higashi, K. (2001) 'Ductility enhancement in AZ31 magnesium alloy by controlling its grain structure', *Scripta Materialia*, vol. 45, pp. 89-94.

Nakashima, K., Horita, Z., Nemoto, M., and Langdon, T.G. (2000) 'Development of a muti-pass facility for equal-channel angular pressing to high total strains', *Materials Science and Engineering A*, vol. 281, pp. 82-87.

Orlov, D., Ralston, K.D., Birbilis, N., and Estrin, Y. (2011) 'Enhanced corrosion resistance of Mg alloy ZK60 after processing by integrated extrusion and equal channel angular pressing', *Acta Materialia*, vol. 59, pp. 6176-86.

Osmer, J., Riemer, O., Brinksmeier, E., Rosochowski, A., Olejnik, L., and Richert, M., 'Diamond turning of ultrafine grained aluminium alloys', *Proceedings of the 7th euspen International Conference*, Bremen, Germany, May 20-24 2007, pp. 316-19.

Ostrovsky, I. (2006) 'Composite coatings – the newest surface treatment technology for magnesium', in Kainer, K.U. (ed) *Magnesium: Proceedings of the 7th International Conference on Magnesium Alloys and Their Applications*, Wiley-VCH, Frankfurt, pp. 834-41.

Ota, S., Akamatsu, H., Neishi, K., Furukawa, M., Horita, Z., and Langdon, T.G. (2002) 'Low-temperature superplasticity in Al alloys processed by equal-channel angular pressing', *Materials Transactions*, vol. 43, pp. 2364-69.

Pachla, W., Mazur, A., Skiba, J.,Kulczyk, M., and Przybysz S. (2012) 'Wrought magnesium alloys ZM21, ZW3 and WE43 processed by hydrostatic extrusion with back pressure', *Archives of Metallurgy and Materials*, vol. 57, 485-93.

Panicker, M.R.R. and Chokshi, A.H. (2011) 'Influence of grain size on high temperature fracture in a Mg AZ31 alloy', *Materials Science and Engineering A*, vol. 528, pp. 3031-36.

Petch, N.J. (1953) 'The cleavage strength of polycrystals', *Journal of the Iron and Steel Institute*, vol. 174, pp. 25-28.

Pietrzyk, M. (2002) 'Through-process modeling of microstructure evolution in hot forming of steels', *Journal of Materials Processing Technology*, vols. 125-126, pp. 53-62.

Popov, K.B., Dimov, S.S., Pham, D.T., Minev, R.M., Rosochowski, A., and Olejnik, L. (2006) 'Micromilling: material microstructure effects', *Proceedings of IMechE Part B: Journal of Engineering Manufacture*, vol. 220, pp. 1807-13.

Qiao, X.G., Gao, N., Moktadir, Z., Kraft, M., and Starink, M.J. (2010) 'Fabrication of MEMS components using ultra fine grained aluminium alloys', *Journal of Micromechanics and Microengineering*, vol. 20. Available at http://iopscience.iop.org/0960-1317/20/4/045029/ pdf/0960-1317_20_4_045029.pdf (accessed 21 March 2014).

Quang, P., Krishnaiah, A., Hong, S.I., and Kim, H.S. (2009) 'Coupled analysis of heat transfer and deformation in Equal Channel Angular Pressing of Al and steel', *Materials Transactions*, vol. 50, pp. 40-43.

Raab, G.J., Valiev, R.Z., Lowe, T.C., and Zhu, Y.T. (2004) 'Continuous processing of ultrafine grained Al by ECAP-Conform', *Material Science and Engineering A*, vol. 382, pp. 30-34.

Read, W.T. and Shockley, W. (1950) 'Dislocation models of crystal grain boundaries', *Physical Reviews*, vol. 78, pp. 275-89.

Roberts, W. and Ahlblom, B. (1978) 'A nucleation criterion for dynamic recrystallization during hot working', *Acta Metallurgica*, vol. 26, pp. 801-13.

Rosochowski, A. and Olejnik, L. (2007) 'FEM simulation of incremental shear', in Cueto, E. and Chinesta, F. (eds), *Proceedings of the 10th International Conference on Material Forming, Esaform 2007*, April 18-20, 2007, Zaragoza, Spain, American Institute of Physics, vol. 907, pp. 653-58.

Rosochowski, A. and Olejnik, L. (2012) 'Severe plastic deformation for grain refinement and enhancement of properties', in Lin, J., Balint, D., Pietrzyk, M.

(eds) *Microstructure evolution in metal forming processes*, Woodhead Publishing, Cornwall, pp. 114-41.

Rosochowski, A., Olejnik, L. (2011) 'Incremental equal channel angular pressing for grain refinement', *Materials Science Forum*, vol. 674, pp. 19-28.

Rosochowski, A., Olejnik, L., and Richert, M. (2007) '3D-ECAP of square aluminium billets', in Banabic, D. (ed) *Advanced methods in material forming*, Springer-Verlag, Berlin Heidelberg, pp. 215-32.

Rosochowski, A., Olejnik, L., and Richert, M. (2008a) 'Double-billet incremental ECAP', *Materials Science Forum,* vols. 584-586, pp. 139-44.

Rosochowski, A., Olejnik, L., and Richert, M. (2008b) 'Incremental ECAP of plates', *Materials Science Forum*, vols. 584-586, pp. 108-13.

Rosochowski, A., Olejnik, L., Gagne, J., Ladeveze, N., and Rosochowska, M. (2006) 'Compression behaviour of UFG aluminium', in Juster, N. and Rosochowski, A. (eds) *Proceedings of the 9th International Conference on Material Forming ESAFORM 2006*, Glasgow, United Kingdom, April 26-28, 2006, Scientific Publishing House, Akapit, Krakow, pp. 543-46.

Rosochowski, A., Presz, W., Olejnik, L., and Richert, M. (2007) 'Micro-extrusion of ultra-fine grained aluminium', *The International Journal of Advanced Manufacturing Technology*, vol. 33, pp. 137-46.

Rosochowski, A., Rosochowska, M., Olejnik, L., and Verlinden, B. (2010) 'Incremental equal channel angular pressing of sheets', *Steel Research International*, vol. 81, pp. 470-73.

Saito, Y., Tsuji, N., Utsunomiya, H., Sakai, T., and Hong, R.G. (1998) 'Ultra-fine grained bulk aluminium produced by accumulative roll-bonding (ARB) process', *Scripta Materialia*, vol. 39, pp. 1221-27.

Sanders, P.G., Eastman, J.A., and Weertman, J.R. (1997) 'Elastic and tensile behaviour of nanocrystalline copper and palladium', *Acta Materialia*, vol. 45, pp. 4019-25.

Sato, Y.S., Urata, M., Kokawa, H., and Ikeda, K. (2003) 'Hall-Petch relationship in friction stir welds of equal channel angular-pressed aluminium alloys', *Materials Science and Engineering A*, vol. 354, pp. 298-305.

Schumann, S. and Friedrich, H.E. (2006) 'Automotive applications in Europe', in Friedrich, H.E. and Mordike, B.L. (eds) *Magnesium technology: metallurgy, design data, applications*, Springer-Verlag, Heidelberg, pp. 499-568.

Scott, J., Miles, M., Fullwood, D., Adams, B., Khosravani, A., and Mishra, R.K. (2013) 'Room temperature shear band development in highly twinned wrought magnesium AZ31B sheet', *Metallurgical and Materials Transactions A*. vol. 44, pp. 512-16.

Segal, V.M. (1995) 'Materials processing by simple shear', *Materials Science and Engineering A*, vol. 197, pp. 157-64.

Segal, V.M. (2002) 'Severe plastic deformation: simple shear versus pure shear', *Materials Science and Engineering A*, vol. 338, pp. 331-44.

Segal, V.M. (2008) 'Equal channel angular extrusion of flat products', *Materials Science and Engineering A*, vol. 476, pp. 178-85.

Segal, V.M. (2010) 'Mechanics of continuous equal-channel angular extrusion', *Journal of Materials Processing Technology*, vol. 210, pp. 542-49.

Segal, V.M., Reznikov, V.I., Drobyshevskiy, A.E., and Kopylov, V.I. (1981) 'Plastic working of metals by simple shear', *Russian Metallurgy (Metally)*, vol.1, pp. 99-105.

Seipp, S., Wagner, M. F.-X., Hockauf, K., Schneider, I., Meyer, L.W., and Hockauf, M. (2012) 'Microstructure, crystallographic texture and mechanical properties of

the magnesium alloy AZ31B after different routes of thermo-mechanical processing', *International Journal of Plasticity*, vol. 35, pp. 155-66.

Sellars, C.M. and Zhu, Q. (2000) 'Microstructural modelling of aluminium alloys during thermomechanical processing', *Materials Science and Engineering A*, vol. 280, pp. 1-7.

Sieniawski, J. and Motyka, M. (2007) 'Superplasticity in titanium alloys', *Journal of Achievements in Materials and Manufacturing Engineering*, vol. 24, pp. 123-30.

Srinivasan, R., Chaudhury, P.K., Cherukuri, B., Han, Q., Swenson, D., and Gros, P. (2006) 'Continuous severe plastic deformation processing of aluminum alloys', Wright State University. Available at http://www.osti.gov/bridge/purl.cover.jsp?purl= /885079-37CRhi (accessed 21 March 2014).

Staiger, M.P., Pietak, A.M., Huadmai, J., and Dias, G. (2006) 'Magnesium and its alloys as orthopedic biomaterials: A review', *Biomaterials*, vol. 27, pp. 1728-34.

Stolyarov, V.V., Zhu, Y.T., Lowe, T.C., and Valiev, R.Z. (2001) 'Microstructure and properties of pure Ti processed by ECAP and cold extrusion', *Materials Science and Engineering A*, vol. 303, pp. 82-89.

Su, C.W., Lu, L., and Lai, M.O. (2006) 'A model for the grain refinement mechanism in equal channel angular pressing of Mg alloy from microstructural studies', *Materials Science and Engineering A*, vol. 434, pp. 227-36.

Suwas, S., Gottstein, G., and Kumar, R. (2007) 'Evolution of crystallographic texture during equal channel angular extrusion (ECAE) and its effects on secondary processing of magnesium', *Materials Science and Engineering A*, vol. 471, pp. 1-14.

Svyetlichnyy, D.S. (2012) 'Reorganization of cellular space during the modeling of the microstructure evolution by frontal cellular automata', *Computational Materials Science*, vol. 60, pp. 153-62.

Uota, T., Suzu, T., Fukumoto, S., and Yamamoto, A. (2009) 'EBSD observation for reversible behavior of deformation twins in AZ31B magnesium alloy', *Materials Transactions*, vol. 50, pp. 2118-20.

Utsunomiya, H., Saito, Y., Suzuki, H., and Sakai, T. (2001) 'Development of the continuous shear deformation process', *Proceedings of the Institution of Mechanical Engineers, Part B: Journal of Engineering Manufacture*, vol. 215, pp. 947-57.

Valiev, R.Z. and Langdon, T.G. (2006) 'Principles of equal-channel angular pressing as a processing tool for grain refinement', *Progress in Materials Science*, vol. 51, pp. 881-981.

Valiev, R.Z., Alexandrov, I.V., Zhu, Y.T., and Lowe, T.C. (2002) 'Paradox of strength and ductility in metals processed by severe plastic deformation', *Journal of Materials Research*, vol. 17, pp. 5-8.

Valiev, R.Z., Islamgaliev, R.K., Alexandrov, I.V. (2000) 'Bulk nanostructured materials from severe plastic deformation', *Progress in Materials Science*, vol. 45, pp. 103-189.

Valiev, R.Z., Krasilnikov, N.A., and Tsenev, N.K. (1991) 'Plastic deformation of alloys with submicro-grained structure', *Materials Science and Engineering A*, vol. 137, pp. 35-40.

Valiev, R.Z., Semenova, I.P., Latysh, V.V., Rack, H., Lowe, T.C., Petruzelka, J., Dluhos, L., Hrusak, D., and Sochova, J. (2008) 'Nanostructured titanium for biomedical applications', *Advanced Engineering Materials*, vol. 10, pp. 15-17.

Wang, K.Y., Shen, T.D., Quan, X., Wei, W.D. (1993) 'HalI-Petch relationship in nanocrystalline titanium produced by ball-milling', *Journal of Materials Science Letters*, vol. 12, pp. 1818-20.

Watanabe, H., Mukai, T., Ishikawa, K., Okanda, Y., and Higashi, K. (1999) 'Superplastic characteristics in an extruded AZ31 magnesium alloy', *Journal of Japan Institute of Light Metals*, vol. 49, pp. 401-4.

Watanabe, H., Tsutsui, H., Mukai, T., Kunio, I., Okanda, Y., Kohzu, M., and Higashi, K. (2000) 'Superplastic behavior in commercial wrought magnesium alloys', *Materials Science Forum*, vols. 350-351, pp. 171-76.

Wonsiewicz, B.C. and Backofen, W.A. (1967) 'Plasticity of magnesium crystals', *Transactions of the Metallurgical Society of AIME*, vol. 239, pp.1422-31.

Wu, B.L., Wan, G., Zhang, Y.D., Du, X.H., Wagner, F., and Esling, C. (2010) 'Fragmentation of large grains in AZ31 magnesium alloy during ECAE via route A', *Materials Science and Engineering A*, vol. 527, pp. 3365-72.

Xia, K., Wang, J.T., Wu, X., Chen, G., and Gurvan, M. (2005) 'Equal channel angular pressing of magnesium alloy AZ31', *Materials Science and Engineering A*. vols. 410–411, pp. 324–27.

Xing, J., Soda, H., Yang, X., Miura, H., and Sakai, T. (2005) 'Ultra-fine grain development in an AZ31 magnesium alloy during multi-directional forging under decreasing temperature conditions', *Materials Transactions*, vol. 46, pp. 1646-50.

Xu, C., Furukawa, M., Horita, Z., and Langdon, T.G. (2003) 'Using ECAP to achieve grain refinement, precipitate fragmentation and high strain rate superplasticity in a spray-cast aluminum alloy', *Acta Materialia*, vol. 51, pp. 6139-49.

Yoshinaga, F. and Horiuchi, R. (1963) 'Deformation mechanisms in magnesium single crystals compressed in the direction parallel to hexagonal axis', *Transactions of the Japan Institute of Metals*, vol. 4, pp.1-8.

Zartner, P., Cesnjevar, R., Singer, H., and Weyand, M. (2005) 'First successful implantation of a biodegradable metal stent into the left pulmonary artery of a preterm baby', *Catheterization and Cardiovascular Interventions*, vol. 66, 590-94.

Zhu, G., Mao, W., and Yu, Y. (2000) 'Calculation of misorientation distribution between recrystallized grains and deformed matrix', *Scripta Materialia*, vol. 42, pp. 37-41.